



Politecnico  
di Torino

ScuDo  
Scuola di Dottorato ~ Doctoral School  
WHAT YOU ARE, TAKES YOU FAR

Doctoral Dissertation  
Doctoral Program in Chemical Engineering (33<sup>rd</sup> cycle)

# Measurement methods of gas-solid interactions

**Bilal Alam Khan**

\* \* \* \* \*

## **Supervisors**

Prof. Guido Sassi, Supervisor

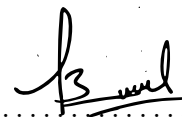
## **Doctoral Examination Committee:**

Prof. Mustafa Anwar, National University of Science and Technology, Islamabad, Pakistan  
Prof. Michela Segal, Istituto Nazionale di Ricerca Metrologica (INRiM), Torino, Italy

Politecnico di Torino  
September 22, 2021

This thesis is licensed under a Creative Commons License, Attribution - Noncommercial-NoDerivative Works 4.0 International: see [www.creativecommons.org](http://www.creativecommons.org). The text may be reproduced for non-commercial purposes, provided that credit is given to the original author.

I hereby declare that, the contents and organisation of this dissertation constitute my own original work and does not compromise in any way the rights of third parties, including those relating to the security of personal data.



.....  
Bilal Alam Khan  
Turin, September 22, 2021

# Summary

This dissertation develops a quantitative method for the measurements of interactions of Volatile Organic Compounds (VOCs) and surfaces of commercially available pipes usually used for VOC's sampling. VOCs are widely measured at ppb and ppt level in many fields of life, from therapy monitoring to climate change monitoring and to indoor air quality. The need for accuracy has always been stressed in all these fields. The interactions between gas mixtures and solid surfaces in the sampling lines and instruments play an essential role in calculating the total uncertainty of VOC concentration. The amount of substances in the gas mixture is affected by its reversible and irreversible interactions with the wall of the sampling line. These interactions between VOCs and different surfaces are of different nature, from sorption to chemical reactions or permeation depending upon the nature and thermodynamic properties of the VOC, the properties of the wall, the VOC concentration, temperature, humidity, and air velocity. There was a need of a specific study to quantify the interactions since not enough data are available in the literature. An equilibrium constant ( $K_e$ ) is measured as the ratio of the maximum amount of substance per unit area segregated during equilibrium ( $C_{A,e}$ ) on the test pipe's internal surface to the gas concentration. The  $C_{A,e}$  and  $K_e$  are estimated for different materials at different conditions. The characteristic time ( $t_c$ ) of the dynamic in which the phenomenon occurs is measured, which is particularly important to define whether the phenomenon should be considered or neglected with respect to the time in which the process of interest takes place. The dynamic of the phenomenon can be analyzed based on the rate of reaction at which equilibrium occurs. In polymeric materials, the irreversible losses due to permeation is significant and can be measured as mass per unit area per unit time ( $J$ ) is measured to quantify these losses. The pipe's memory effect plays a role in the repeated use of sampling and is estimated as a mass release from unit area per unit time i.e., release rate ( $M$ ). This research proposes and discusses the methods to quantify maximum surface concentration ( $C_{A,e}$ ), Equilibrium constant ( $K_e$ ), irreversibly reaction rate ( $J$ ), and release rate due to memory ( $M$ ). The sensibility of the methods on residence time, surface area, gas velocity, temperature, and pressure has been evaluated to identify the main influence quantities and biases for correction of the results and the limits of the applicability of the method. An experimental set-up

has been designed in which a mixture containing a single VOC was flushed inside a clean test pipe. A fast response detector (Flame Ionization Detector (*FID*)) was used to retrieve the signal of VOC concentration. The amount of VOC that interacted to the wall from the mixture was calculated from the depletion of the signal. Air-Acetone ( $C_3H_6O$ ) mixture at the ppm level with certified uncertainty that has a high response on the detector is used for the experimentation as a representative VOC mixture. Four different common materials were tested with two different internal diameters at different lengths having the same surface area.

The proposed methodologies were applied to 4 different materials. As expected, the interactions with Sulfinert® treated stainless steel were the lowest, followed by Copper, and the highest for electropolished Stainless steel followed by Perfluoroalkoxy (PFA). An attempt to quantify the Kinetic constant  $k_{kin}$  was made, and regression to the experimental data for all materials was performed, but the model was not fitted to any of the data, which indicates these interactions are not simple and can be the sum of different phenomena. The irreversible losses due to permeation or reaction were negligible for Sulfinert®, and these were pretty measurable for PFA and Stainless steel. The release amount due to memory was following the same order of magnitude as that of irreversible reacted mass flux. The effect of temperature and pressure was evident and considered as bias to the measurements and the results were corrected accordingly to a reference temperature and pressure. The effects of fluid dynamics and residence time were investigated and were found negligible for all the tested pipes. and The methodology for estimation of losses can be extended to lower concentration, different applications and used in comparing the response of different materials that are usually used for sampling at lower concentration.



# Acknowledgements

First, I would like to express my sincere gratitude to my supervisor Professor Guido Sassi for his continuous support, supervision and guidance throughout the research. I am very grateful to him for providing me valuable platform which I found very useful in developing my career, and research. I really appreciate for their sincere efforts of delivering the knowledge, his guidance and patience to answer my questions during the research.

I would also like to thank Maricarmen Iecuna (PoliTo) on her support and guidance throughout the research.

I thank to my dear friend Dr Abeer Irfan, without his support and guidance it was not even possible to accomplish this research. I am grateful for his cooperation and acceptance.

I want to thank Dr Asad Ullah (BUIITEMS) for his needful support and Dr Asif Hussain Khoja (NUST) for his continuous guidance and encouragement.

Last but not the least; I would like to give my heartfelt thanks to my Friends especially Muhammad Awais (PoliTo) for their wonderful company and help throughout my degree.

I want to thank my friends and family members especially Gabina Khan, for their continues patience and bearing my absence of attention during my research. This study would not be accomplished without their continued love, encouragement and appreciation.

## *Dedication*

*I would like to dedicate. this thesis to my infant daughter (Gabina Khan) and my loving Wife (Hina Bilal) who stood with me in every up and down.*

# Contents

<b>List of Tables</b>	XI
<b>List of Figures</b>	XIII
<b>1 Introduction</b>	<b>3</b>
1.1 Importance of metrology of VOCs and efforts . . . . .	3
1.2 Challenges in measurements . . . . .	7
1.3 Gas-wall interactions . . . . .	10
1.3.1 Chemical passivation . . . . .	13
1.3.2 Electropolishing . . . . .	14
1.3.3 Coating . . . . .	15
1.4 Research objective . . . . .	16
1.5 Scope of the work . . . . .	16
1.6 Thesis outline . . . . .	17
<b>2 Experimentation</b>	<b>19</b>
2.1 Experimental set-up . . . . .	19
2.2 Materials . . . . .	22
2.3 Quantification of leakages . . . . .	23
2.3.1 Injection test for volume estimation . . . . .	24
2.4 Pressure measurements and validation . . . . .	25
2.5 Flowrate measurements and validation . . . . .	27
2.6 Temperature measurements . . . . .	28
2.7 Diameter measurements . . . . .	29
<b>3 Methodology</b>	<b>31</b>
3.1 Definition of system . . . . .	33
3.2 Amount of VOC adsorbed and equilibrium constant . . . . .	34
3.3 Determination of irreversible losses . . . . .	38
3.3.1 Procedure for irreversible losses . . . . .	40
3.4 Determination of mass release due to memory effect . . . . .	41
3.4.1 Procedure for memory release . . . . .	43



3.5	Bias corrections . . . . .	44
3.5.1	Bias correction for air inside the pipe . . . . .	44
3.6	Experimental biases . . . . .	47
3.6.1	Instability of FID and system saturation . . . . .	48
3.6.2	Instability of flowrate . . . . .	51
3.6.3	Interactions in system . . . . .	52
3.6.4	Pressure fluctuation during experiment . . . . .	54
3.6.5	Irreversible losses in equilibrium . . . . .	55
3.6.6	Equilibrium not established . . . . .	55
3.6.7	Temperature variation during measurement . . . . .	56
3.6.8	Artifacts during measurement . . . . .	57
3.7	Measurement uncertainty . . . . .	57
<b>4</b>	<b>Losses during equilibrium</b>	<b>59</b>
4.1	Comparison of two different approaches . . . . .	59
4.2	Adsorption and desorption with Sulfinert <sup>®</sup> treated stainless steel pipe . . . . .	60
4.2.1	Sensitivity with temperature and correction . . . . .	62
4.2.2	Sensitivity with pressure . . . . .	64
4.2.3	Reproducibility and accuracy for Sulfinert <sup>®</sup> . . . . .	73
4.3	Adsorption and desorption with Copper pipe . . . . .	74
4.3.1	Sensitivity with temperature . . . . .	74
4.3.2	Sensitivity with pressure . . . . .	76
4.3.3	Reproducibility and accuracy with Copper pipe . . . . .	81
4.4	Adsorption and desorption measured with electropolished Stainless steel pipe . . . . .	83
4.4.1	Sensitivity with temperature . . . . .	83
4.4.2	Sensitivity with pressure . . . . .	85
4.4.3	Reproducibility and accuracy with Stainless steel pipe . . . . .	90
4.5	Adsorption and desorption measured with PFA pipe . . . . .	91
4.5.1	Sensitivity with temperature . . . . .	91
4.5.2	Sensitivity with pressure . . . . .	93
4.5.3	Reproducibility and accuracy with PFA pipe . . . . .	98
4.6	Comparison and discussion . . . . .	99
<b>5</b>	<b>Estimation of irreversible losses and memory effect</b>	<b>103</b>
5.1	Irreversible losses $J$ . . . . .	103
5.1.1	Sensitivity of reacted mass flux with temperature . . . . .	106
5.1.2	Sensitivity of irreversibly reacted mass flux on pressure . . . . .	107
5.2	Release flux due to memory effect . . . . .	108
5.2.1	Sensitivity of released mass flux with temperature . . . . .	110
5.2.2	Sensitivity of released mass flux with Pressure . . . . .	111

<b>6 Conclusion</b>	113
<b>Bibliography</b>	115

# List of Tables

2.1	List of materials with specifications . . . . .	22
2.2	Uncertainty budget of the diameter of PFA . . . . .	30
3.1	The sequence of configurations on measurement. . . . .	36
3.2	Correspondence of signal times with residence/contact times, box refers to figure 3.2 . . . . .	38
3.3	Sequence of scenarios during irreversible losses estimation . . . . .	41
3.4	Sequence of scenarios during memory release flux ( $M$ ) estimation . . . . .	43
3.5	Sequences of mass balance over a test pipe and bypass . . . . .	53
3.6	Template for uncertainty budget using GUM procedure . . . . .	58
4.1	Number of experiments on Sulfinert® , pipe length, and test condition ranges (residence time, temperature, pressure, and Reynolds number . . . . .	61
4.2	Areic amount adsorbed per unit area of Sulfinert® ( $C_{A,e}$ ), Raw data and data corrected at 20 °C 1 bar with experimental standard deviations for a single sample and all data aggregated considering adsorption and desorption as a unique population. . . . .	67
4.3	Equilibrium constant $K_e$ with Sulfinert®; Raw data and data corrected at 20 °C 1 bar with experimental standard deviations for a single sample and all data aggregated considering adsorption and desorption as a unique population . . . . .	67
4.4	Areic amount adsorbed per unit area of Sulfinert® ( $C_{A,e}$ ), Raw data and data corrected at 20 °C 1 bar with experimental standard deviations for a single sample considering adsorption and desorption as separate population. . . . .	68
4.5	Equilibrium constant ( $K_e$ ) with Sulfinert®; Raw data and data corrected at 20 °C 1 bar with experimental standard deviations for a single sample considering adsorption and desorption as separate population . . . . .	69
4.6	Uncertainty budget for $C_{A,e}$ for most conservative experiment on Sulfinert® Sample D . . . . .	73
4.7	Uncertainty budget for $K_e$ for the most conservative experiment of Sulfinert® Sample D . . . . .	73

4.8	Number of experiments on Copper pipe, pipe length and test condition ranges (residence time, temperature, pressure, and Reynolds number).	74
4.9	Areic amount adsorbed and desorbed per unit area ( $C_{A,e}$ ) and Equilibrium constant with Copper pipe	78
4.10	Uncertainty budget for $C_{A,e}$ for most conservative experiment on Copper pipe.	82
4.11	Uncertainty budget for $K_e$ for most conservative experiment on Copper pipe	82
4.12	Number of experiments on Stainless steel, pipe lengths and test condition ranges (residence time, temperature, pressure, and Reynolds number).	83
4.13	Areic amount adsorbed and desorbed per unit area ( $C_{A,e}$ ) and $K_e$ with Stainless steel pipe	87
4.14	Uncertainty budget for $C_{A,e}$ for most conservative experiment on Stainless steel pipe	90
4.15	Uncertainty budget for $K_e$ for most conservative experiment on Stainless steel pipe	90
4.16	Number of experiments with PFA, pipe lengths and test condition ranges (residence time, temperature, pressure, and Reynolds number).	91
4.17	Areic amount adsorbed and desorbed per unit area ( $C_{A,e}$ ) and $K_e$ with PFA pipe	94
4.18	Uncertainty budget for $C_{A,e}$ for most conservative experiment on PFA pipe	98
4.19	Uncertainty budget for $K_e$ for most conservative experiment on PFA pipe	98
4.20	Areic amount adsorbed and desorbed ( $C_{A,e}$ ) and Equilibrium constant ( $K_e$ ) with reproducibility	101
5.1	Number of experiments and test condition ranges (temperature, pressure, and residence time).	103
5.2	Irreversible reacted flux (J) for different materials raw data and corrected.	105
5.3	Release flux ( $M$ ) for different materials raw data and corrected.	110

# List of Figures

2.1	Scheme of the experimental setup. . . . .	20
2.2	Device connections for monitoring the VOC mixture and zero air in bypass and test pipe. The dotted line represents the zero air and solid line shows the VOC mixture. . . . .	21
2.3	List of commercially available pipes of different materials. . . . .	23
2.4	Schematic view of injection test and 3-way valve. . . . .	25
2.5	Scheme for pressure monitor validation. . . . .	26
2.6	Comparison of measurements of flowrate with three different devices. . . . .	27
2.7	Temperature correlation model for Pt-100. . . . .	28
2.8	Daily temperature fluctuation measured by both sensors placed in the air. . . . .	29
3.1	Scheme of mass balance over a test pipe. . . . .	33
3.2	FID signal during measurement, spike times of events from Table 3.2 are reported at the boxes which zoom on the signal. Experimental raw data for the sample Sulfinert®A at 100 Sml/min, 6 repeated experiments . . . . .	37
3.3	Model for irreversible losses in pipes, PFA 100Sml·min <sup>-1</sup> . . . . .	40
3.4	Model for memory effect in pipes, PFA 100Sml·min <sup>-1</sup> . . . . .	42
3.5	Approach A for bias correction: Lined area represents residence time, while black area represents net integral. . . . .	45
3.6	Method B for calculating the integral: Red area represents the desorption of bypass, and black represents the adsorption over the test pipe. . . . .	46
3.7	Stability analysis of signal with zero air and VOC mixture during an experiment on sulfinert® at 32Sml·min <sup>-1</sup> flowrate. . . . .	49
3.8	Signal for zero air and VOC mixture in bypass during 100Sml·min <sup>-1</sup> flowrate (shown in black) and 9 Sml·min <sup>-1</sup> shown in (blue). The intensity represents the distance from the saturation point. . . . .	49
3.9	Stability of signal for VOC mixture for ten experiments at flowrate 35 Sml·min <sup>-1</sup> . . . . .	50
3.10	FID response signal against different flowrate for air flowing internally in the GC and externally (left) and VOC mixture (right). . . . .	52

3.11	Scheme of sequences for mass balance over a test pipe and bypass. . . . .	52
3.12	Effect on signal with different pressure drops for flowrate $35\text{Sml}\cdot\text{min}^{-1}$ . . . . .	55
3.13	Temperature and flowrate profile over time. . . . .	57
4.1	Comparing the results of $C_{A,e}$ plotted against residence time $t_R$ for Sulfinert <sup>®</sup> with two different approaches. . . . .	60
4.2	Comparative analysis of reproducibility of Raw- $C_{A,e}$ over two different lengths– Sulfinert <sup>®</sup> Sample A (26m) and Sample B, C, D (8.5m). . . . .	61
4.3	Sensitivity of adsorbed amount per unit area of Sulfinert <sup>®</sup> , on temperature. . . . .	63
4.4	Sensitivity of equilibrium constant $K_e$ [ $\mu\text{m}$ ] on temperature. . . . .	64
4.5	Sensitivity of adsorbed amount per unit area $C_{A,e}$ of sulfinert <sup>®</sup> on pressure. The data set was corrected for temperature bias at 20 °C. . . . .	65
4.6	Sensitivity of equilibrium constant $K_e$ area on pressure. The data set was corrected for temperature bias at 20 °C. . . . .	66
4.7	Sensitivity of adsorbed amount per unit area $C_{A,e}$ on Reynolds number. Values corrected at 20 °C, 1bar, and grouped on $Re$ . . . . .	70
4.8	Sensitivity of equilibrium constant on Reynolds number. Values corrected at 20 °C, 1bar, and grouped on $Re$ . . . . .	70
4.9	Sensitivity of adsorbed amount per unit area on residence time. Values corrected at 20 °C, 1bar and grouped on $\tau_R$ . . . . .	72
4.10	Sensitivity of equilibrium constant $K_e$ on residence time. Values corrected at 20 °C, 1bar and grouped on $\tau_R$ . . . . .	72
4.11	Sensitivity of adsorbed and desorbed amount per unit area of the Copper pipe on temperature. . . . .	75
4.12	Sensitivity of equilibrium constant $K_e$ with Copper pipe on temperature. . . . .	76
4.13	Sensitivity of adsorbed amount per unit area of the Copper pipe on pressure. The data set was corrected for temperature bias at 23 °C. . . . .	77
4.14	Sensitivity of equilibrium constant $K_e$ with Copper pipe on pressure. The data set was corrected for temperature bias at 23 °C. . . . .	77
4.15	Sensitivity of adsorbed and desorbed amount per unit area of Copper on Reynolds number. Values corrected at 23 °C, 1 bar, and grouped on $Re$ . . . . .	79
4.16	Sensitivity of Equilibrium constant with Copper pipe on Reynolds number. Values corrected at 23 °C, 1bar, and grouped on $Re$ . . . . .	79
4.17	Sensitivity of adsorbed amount per unit area of Copper on residence time. Values corrected at 20 °C, 1bar and grouped on $\tau_R$ . . . . .	80
4.18	Sensitivity of Equilibrium constant with Copper pipe on residence time. Values corrected at 23 °C, 1bar and grouped on $\tau_R$ . . . . .	81
4.19	Sensitivity of adsorbed amount per unit area $C_{A,e}$ with Stainless steel pipe on temperature. . . . .	84

4.20	Sensitivity of Equilibrium constant $K_e$ with Stainless steel pipe on temperature. . . . .	84
4.21	Sensitivity of adsorbed amount per unit area ( $C_{A,e}$ ) of Stainless steel pipe on pressure. . . . .	85
4.22	Sensitivity of Equilibrium constant $K_e$ with Stainless steel pipe on pressure. . . . .	86
4.23	Sensitivity of adsorbed amount per unit area of Stainless steel pipe on Reynolds number. . . . .	87
4.24	Sensitivity of Equilibrium with Stainless steel pipe on Reynolds number. . . . .	88
4.25	Sensitivity of adsorbed amount per unit area of Stainless steel pipe on residence time. . . . .	89
4.26	Sensitivity of Equilibrium constant with Stainless steel pipe on residence time. . . . .	89
4.27	Sensitivity of adsorbed amount per unit area of PFA pipe on temperature. . . . .	92
4.28	Sensitivity of Equilibrium constant with PFA pipe on temperature. . . . .	92
4.29	Sensitivity of adsorbed amount per unit area with PFA pipe on pressure. . . . .	93
4.30	Sensitivity of Equilibrium constant $K_e$ with PFA pipe on pressure. . . . .	94
4.31	Sensitivity of adsorbed amount per unit area of PFA pipe on Reynolds number. . . . .	95
4.32	Sensitivity of Equilibrium constant with PFA pipe on Reynolds number. . . . .	96
4.33	Sensitivity of adsorbed amount per unit area $C_{A,e}$ of PFA pipe on residence time. . . . .	97
4.34	Sensitivity of Equilibrium constant $K_e$ with PFA pipe on residence time. . . . .	97
4.35	Comparing the concentration curves for different materials during adsorption and desorption test. The dim color represents the desorption. . . . .	100
5.1	Signal of VOC in bypass and test pipe (PFA) at different saturation times. Red color shows less saturation while black shows more saturation time. . . . .	104
5.2	PFA, Sensitivity of irreversible reacted amount per unit area per unit time on saturation time. . . . .	105
5.3	Signal of VOC in bypass and saturated test pipe during measurements for irreversible losses. . . . .	106
5.4	Sensitivity of irreversibly reacted mass flux on temperature for different materials. . . . .	107
5.5	Sensitivity of irreversibly reacted mass flux on temperature for different materials. . . . .	108

5.6	Signal of VOC in bypass and test pipe (PFA) at different cleaning time ( $t_{sat}$ ). Red colour shows less cleaning while black and blue shows more cleaning time. . . . .	109
5.7	Sensitivity of release amount from unit area of PFA per unit time ( $M$ ) on saturation time. . . . .	110
5.8	Sensitivity of release mass flux ( $M$ ) on temperature for different materials. . . . .	111
5.9	Sensitivity of released mass flux ( $M$ ) on pressure for different materials.	112



## GLOSSARY

Symbol	Description	units
$A$	Pipe wall area	$\text{m}^2$
$C$	Volumetric concentration	$\text{mol} \cdot \text{m}^3$
$C_{A,e}$	Superficial molar concentration	$\text{mol} \cdot \text{m}^{-2}$
$D$	Inside diameter	mm
$q_v$	Volumetric flow rate	$\text{l} \cdot \text{min}^{-1}$
$q$	Mass flow rate	$\text{mol} \cdot \text{min}^{-1}$
$K_e$	Equilibrium constant	$\mu\text{m}$
$L$	Length of the pipe	m
$dL$	Length of length or step size in length	m
$m$	Mass	mol
$P$	pressure	Pa
$S$	FID signal	mV
$t$	Time	min
$T$	Temperature	$^{\circ}\text{C}$ or K
$v$	Velocity of gas	$\text{m} \cdot \text{s}^{-1}$
$V$	Volume	L or $\text{m}^3$
$\zeta$	Dimensionless concentration	—
$\tau$	Characteristic time, residence time	min
$\chi$	Molar fraction	—
$I$	Integral of curve	min
$J$	Mass flux	$\text{mol} \cdot \text{min}^{-1} \cdot \text{m}^{-2}$
$Dj$	Diffusivity constant	m
$d\varphi/dx$	Pressure gradient across pipe wall	$\text{Pa} \cdot \text{m}^{-1}$
$M$	Release flux rate	$\text{mol} \cdot \text{min}^{-1} \cdot \text{m}^{-2}$
$^{\circ}$	Standard conditions	—



# Chapter 1

## Introduction

Volatile organic compounds (VOCs) are a group of chemical compounds that entails numerous substances, including various hydrocarbons, organic acids, a range of alcohols, and aldehydes. These compounds are distinguished based on their volatility under normal room temperature and pressure. One of the biggest sources of VOCs is biological processes or living organisms followed by anthropogenic origins, which include the production and combustion of fuels, in particular, due to incomplete combustion phenomena in automobiles and in industrial combustion chambers. Emissions of the anthropogenic sources primarily occur in densely populated, heavily industrialized zones and evaporation from landfill sites. The real and prevalent consequence of releasing VOCs into the atmosphere is the generation of low-level ozone. Although ozone is very beneficial for humans in the upper atmosphere as it blocks the ultraviolet rays, at a lower level, it is hazardous as it constitutes a primary component of smog. VOCs can cause sensory irritation indoor and are a great source of concern in air quality and atmosphere. VOCs are undoubtedly critical environmental pollutants because they are moving, persistent and harmful. Therefore, the need for accurate measurement of different VOCs with the maximum accuracy is indispensable for proper monitoring and thus controlling to safe limits. Measurement of VOCs in the air is challenging because of the availability of a number of compounds, diversity of techniques for sampling and analysis, and lack of uniform and consistent methods. The mechanism of precisely measuring VOCs is the primary concern for the researchers, industry, and regulatory authorities that arises from improving uncertainty estimation.

### 1.1 Importance of metrology of VOCs and efforts

The measurements of volatile organic compounds (VOCs) at trace level have a significant role in atmospheric chemistry, health, ultra-clean industrial processes, indoor air quality, and metrology [89, 106]. In all these applications, measurements

of VOCs amount of substance require a challenging target accuracy at the level of  $\text{pmol}\cdot\text{mol}^{-1}$  (ppt) and  $\text{nmol}\cdot\text{mol}^{-1}$  (ppb) [89]. VOCs' monitoring within 1-1000 ppb range is required for the atmosphere and indoor air quality, at an uncertainty of 5% for different VOCs and 3% for different fluorinate volatile compounds [71, 74, 88]

## Atmosphere and environment

Measuring VOCs at ppb level in the atmosphere is imperative due to their role in ozone precursors. In the presence of sunlight and oxides of nitrogen, VOCs form ozone, and other products, that are hazardous pollutants at a lower altitude [78]. VOCs are more reactive due to the presence of C=C double bonds, and upon oxidation, produces a large variety of particle-phase compounds that are more hazardous than the original one. Oxidation of complex organic compounds results in dissolution, which gives a number of free radicals and more stable molecules such as aldehydes [82]. VOCs are the cause of concern mainly because of their role in creating ground-level ozone and smog [90].

In monitoring the ambient air quality for health impacts and effects on ecology, the knowledge of types of VOCs, their concentration, dispersion routes, their fate in the environment, kind of VOCs in relation to photochemical ozone creating potential and their health endpoints is a prerequisite. Lack of a defined approach to ascertain the toxic compounds requires the development of own monitoring method, sampling plan, analysis logistics, calibration, quality control, and averaging time. The choice of monitoring method depends on the fundamental purpose of data, including regulatory purpose, health impact, impact on climate, and impact on ecology.

In 1989 the Global Atmosphere Watch (GAW) Program was created, and the members of the World Meteorological Organization (WMO) recognized the importance of atmospheric chemistry in their weather, climate, and air quality and activities [105]. The first VOC inter comparison exercise was held in 2003 under the GAW/WMO programme which raised the need for stable and uniform calibration standards [74]. Data quality objectives (DQO) were defined for different VOCs with accuracy ranging from 10-20% and precision 5-15% depending on type of VOC [71]. One of the areas of interest in recent years is the monitoring and control of reactive gases. This group includes surface ozone, carbon monoxide, volatile organic compounds (VOCs), oxidized nitrogen compounds, hydrogen, and sulphur dioxide. USEPA has provided a compendium of available methods for monitoring the toxics in the ambient air [77].

## Industry

VOCs are also disturbing many of the commercial, industrial manufacturing facilities and causing a great deal of concern and research to counter the problems posed by these chemical entities. Airborne Molecular Contaminants (AMCs) comprise a range of chemical compounds, including volatile organic compounds that are a potential threat to the yield of ultra-sensitive manufacturing processes, including semiconductors, nanotechnology, and photovoltaics that demand accurate information measurements at ppb level [25, 102, 41]. Microfabrication or even smaller centers face the environmental challenges caused by these VOCs, especially concerning cleanliness and environmental control aspects [41].

These chemicals are causing the losses of yield at a minor level that affect the consistency of products in industries [102]. It is established that airborne amines or ammonia cause a decrease in the resolution of photoresists that are chemically enhanced.

In the semiconductor industry, we can say that room is ultra clean in the sense of the absence of particles of the size of particulate matter, but we cannot say this in absolute terms because of the presence of other contaminants [42]. Moisture and the presence of different compounds in the air could cause the deterioration of or even collapse of semiconductor devices [41]. Unintentional hydrophobization and the generation of haze on the silicon wafers are the leading problems due to volatile organic compounds even in traces [27, 41]. VOCs pollutants are also reported to have a damaging effect on changing the thickness of film due to variable time of incubation during chemical vapor deposition (CVD) [85]. The need for accurate measurement with the lowest possible uncertainty is vital to consider VOCs' effect and devise the approaches to handle them even at the ppb level effectively.

## Indoor air quality (IAQ)

Indoor air quality is of paramount importance when discussed from the perspective of human health. The presence of certain chemical compounds beyond the safe level could result in different health-related problems. Indoor VOC concentrations are higher than outdoor ones [2], and human exposure to these VOCs can have short and long-term adverse effects on their health. Organic compounds can cause sensory effects such as irritation or problem of odor [12]. In most developed nations, the urban lifestyle is predominant and has compelled people to spend their time indoors rather than outside. This has made the concern of indoor air quality very pertinent and crucial very justified. Furthermore, a most susceptible chunk of the population, such as physically challenged persons suffering from some serious chronic diseases and even infants, consumes most of their time indoors. The concentration of the VOCs indoors is higher than that of outdoor air [18, 24, 2]. There are few VOCs present in the flooring materials that are potentially carcinogenic [5].

Till present, no global standards are in place for VOC concentration there according to the region and country. These limits vary. However, there is some minimum concentration above which these compounds become dangerous, and below that level, no adverse consequences are expected. This limit is known as the Lowest concentration of Interest (LCI).

LCI is the criterion that guides us whether the emission level in indoor air is acceptable or not; therefore, serves as a standard. Based on the exposure to the VOCs indoor for a certain period (8 hours) about their health risk based on toxicology is defined as Chronic Reference Exposure Level (CREL) by California Environment Protection Agency (CalEPA).

The level of concentration is measured using different techniques and methodology, but the main challenge encountered is accurate measurement. Accuracy in the indoor VOCs measurement is paramount because knowing the exact quantity accurately with the lowest uncertainty at ppb and ppt level would enable us to devise some mechanism to control the dangerous concentrations.

## Health

Our human body is continuously emitting the number of VOCs from different parts. Most of these compounds are emitted through the breath, skin, sweat, feces, and urine. The use of VOCs as a biomarker for the diagnosis of different diseases requires monitoring at the ppb level. Therefore, the good estimation of emitted VOCs from different parts of the human body is vital. At the different conditions of human health, different sort of VOCs are generated like some VOCs are generated into lungs and come out through the exhaling process while others are just released into the bloodstream and ultimately find their way out of the body. This exit of these VOCs from the body gives us the opportunity to detect and quantify them by using some sophisticated procedures. Upon detection and quantification, interpretation of this data lead us to diagnose the inherent cause or disease present in the body. First of this sort of detection and measurement was performed in 1985 by using chromatography/mass spectroscopy [17, 3, 24].

A nanoscale artificial nose named NA-NOSE has been developed to detect the cancer of the neck and head through breath analysis which is built by an array of cross-reactive gas sensors having monolayer capped metallic nanoparticles. This device can separately identify the different VOCs at the concentration of  $\text{nmol} \cdot \text{mol}^{-1}$  [39]. The same compound at a certain concentration at different constituents triggers different responses in the sensors. In the breath sample, the signal from the sensors is cumulative for a mixture of compounds. Typical signal for the cancer biomarkers for a sensor ranges between 10-100  $\text{nmol} \cdot \text{mol}^{-1}$ . Hence, the signal is less likely to be disturbed by the noise and allows less uncertainty in Gas Chromatography (GC)/Mass Spectroscopy (MS) /Solid Phase Microextraction (SPME) analysis [39]. Detection of cancer is very crucial because around 1.59 million people

die and many of them due to late diagnosis. [84] have investigated that 1-propanol and 2-butanone are the most associable biomarkers for this disease. Other research groups have also identified ethylbenzene, hexanal, isoprene, and styrene as biomarkers for the said cancer. For the development of novel methods of detection and calibration of instruments used for breath sampling, a project under the European Union with the name EURAMET was initiated in 2015 and they stressed on the need of accurate sampling and instrumentation for reactive VOCs [50]. Accuracy in the measurement of interactions and quantification with the lowest possible uncertainty is key to trusted diagnosis.

## 1.2 Challenges in measurements

Measurement of VOCs in the air is generally difficult, owing to a large number of VOCs present of our concern, a wide array of available techniques for sampling and analysis, and inadequacy of standard and documented procedures [95]. The choice of suitable method for VOC analysis depends on number of factors ranging from type of VOC, range of concentration, humidity and temperature while sampling, type of sample, accuracy, sensitivity, procedure, interference, and also on the cost of the methods [65, 104]. A number of techniques are employed for the analysis of VOCs for example where greater sensitivity is required mass spectrometry (MS) detectors are used because of their good suitability for environmental analysis [83]. Field effect transistors of carbon nanotubes and detectors made of optical fiber with polymeric film are used as VOC detector owing to their sensing capability [92, 91]. Among the number of techniques used for VOC analysis as discussed in [64], commonly used technique is GC with either FID, Photoionization or electron capture detector.

VOCs monitoring, regardless of the applications and techniques, requires the use of pipes, fittings, liners, cylinders, joints, pressure regulators, environmental chambers, generation devices, and measurement instruments, all built using solid materials of different nature. In all these applications, the gas-wall interactions affect the mole fraction of VOCs [76, 14, 69, 109, 52, 108, 45, 6, 58].

VOCs pose a serious challenge in measurement due to their presence in a wide range. Therefore, their precise and consistent quantification is a real task to work on. Quantification of VOCs can be divided mainly in two categories, namely, source emission and ambient air.

In source emission, three major mechanisms are employed for the evaluation of VOCs, which are material balance, emission factors, and emission testing. Realistic determination of VOCs depends upon different factors; among them is the 'purpose of data is of foremost importance. If the evaluation is being performed for regulatory purposes, the agencies concerned would be more interested in knowing the total VOC emissions, concentration limits, and control efficiencies of different control

equipment. Gas chromatograph equipped with FID detector is used to separate the VOCs compounds from different interference and from each other. The detector must be calibrated for each individual VOC compound which makes it cumbersome and lengthy. In another method FID is used to quantify the TGNMO (total-gaseous non-methane organic) by first extracting the VOC from methane, carbon dioxide, and carbon monoxide. This method gives the estimation of VOC in terms of carbon content. The detection limit of this method is 50 ppm, and it cannot be used in many instances where concentration is way less than that [94].

Therefore, there is a need for the development of new measurement techniques to have the ability of uniform evaluation of different VOCs, especially hazardous air pollutants.

### **Instability of reference gas mixture**

Reference gas mixtures are normally used for (a) validation of proper analytical procedures and (b) calibration of control and measurement devices [31]. The instability of the reference mixture poses a serious threat to the accuracy of VOC measurements. During calibration, the response of the instrument to the standard material or process is reported with the uncertainties associated. Calibration is comparison with the values or indications between standard things and measured things. Calibration makes sure the consistency between different instrument performing the same task and help in minimizing the uncertainty. In the presence of a number of analytes of different types, an investigator might even need to maintain as many as 24 different cylinders of the reference material. Having such a number of cylinders is not only expensive in the first place but also very difficult to maintain due to the issue of instability. The problem of stability is further underlined when having reacting gases such as VOCs. As these standard mixtures are used for performing very critical measurements, there no compromise should be made on the quality of these measurements. In order to assure this, a shelf life is reported on the certificate of the gas analysis cylinder. The stability of a reference gas mixture with a concentration under  $1000 \text{ nmol}\cdot\text{mol}^{-1}$  greatly depends on the techniques employed by the supplier companies. Some of the vendors only give their certification based on weighed into the cylinder only. However, it should be kept in mind that gravimetric certifications do have certain limitations, such as [35]:

- Due to surface absorption, the loss of minor and most reactive compounds. For example, loss of chlorine in the steel cylinders.
- Occurrence of impurities in the multi-component mixtures.
- Impurities may react with the minor reactive component.
- By mistake, the addition of wrong and undesired component.



Two available techniques are being used for the preparation of the gas mixture, namely, static and dynamic. These techniques help us improve the accuracy for estimating the molar fraction of mixtures and their stability. The gas-wall interactions affect the molar fraction of the standard gas mixture at trace level, mostly produced statically by using the calibrated gas cylinders [89] and dynamic preparation as defined by ISO 6145 standards [86]. For climate change and indoor air quality, the expanded uncertainty for the reference gas standards is required to be lower than 5% [71]. Commercially available calibrated gas cylinders are stable for the short term (months); however, for the long term (years) the stability of cylinders within the required uncertainty is not guaranteed [32, 71, 86], as the long-term stability is affected by the gas-wall interactions [89, 76, 14, 56, 55]. The losses due to gas-wall interactions in cylinders had been previously investigated in [98, 49, 38, 51, 101, 15, 57]. Recently [56] has proposed a method for the estimation of these losses in cylinders. The dynamic method gives the advantage of having less gas-wall interactions and provides a stable amount of substance fractions [89]. However, losses due to gas-wall interactions contribute as a source of uncertainty combined with other sources such as leakages, pressure, and temperature instability.

### **Detection of VOCs concentration ppb or ppt level**

Detection of VOCs at the trace level has become increasingly pertinent due to their hazardous effects in most cases, even in very low concentrations. Therefore, a number of major environmental safety agencies have set the minimum limits to save the human from the exposure in order to save from adverse effects even at low concentration of ppb and ppt level [53]. There is great demand for detecting such VOCs with sensitivity and selectivity. Accordingly, these requirements demand the availability of portable sensors that can be used on the spot to detect such a lower level of concentration. In work performed by [29] response of the sensing layer was enhanced by the addition of gold nanoparticles on the surface of tin-oxide. This gold catalytic enhancement induces the capability of the sensor to detect as low as ppb with reproducible responses. Micro-machining is used by coupling with pre-concentration selective material to fabricate the portable sub-ppb sensors for the detection of aromatic VOCs. The sensitivity of metal oxide (MOX) gas sensors is associated with the supramolecular concentration unit to lower down the detection limits [110].

### **Accuracy of sampling**

For monitoring of gaseous mixtures at ppb and ppt level requires accurate and representative sampling. A sampling of gases mixture is greatly affected by interactions of the gas mixture with the wall of the sampling line, leaks, and human artifact. A sampling of analytes is prone to positive and/or negative artifacts,

which tend to either overestimate or underestimate our desired gaseous mixtures measurement and subsequently quantification [100]. The losses due to interaction with the wall of the sampling tool are significant in the case of the reactive analyte. In particular, for oxygenated VOCs (OVOCs) like ethanol and methanol, significant losses can occur as these OVOCs strongly interact with various metal surfaces, including stainless steel (found in, e.g., sampling lines or pressure regulators) and aluminum (e.g., gas cylinders). The lower the OVOC mole fraction that needs to be prepared or monitored, the more important it is to use suitable materials to reduce losses. In the Standard operating procedure (SOP), the use of materials other than stainless steel (heated), glass, silicon-coated stainless steel (inner surfaces are coated with amorphous silicon), PFA, and Polytetrafluoroethylene (PTFE) is discouraged for the measurement of non-methane hydrocarbons in air samples [75]. In particular, polymers other than PFA and PTFE shall not be used to prevent memory effects. For an on-line sampling of OVOCs, the SOP recommends inlet lines of either silicon-coated stainless steel or PFA (perfluoroalkoxy alkanes), but not stainless steel. Silicon coated steel should be humidified before the first usage (e.g., by-passing ambient air). The line has to be as short as possible, and the diameter should not be larger than 1/8 inch to minimize the dead volume of the sampling line unless it is permanently flushed. The residence time in the inlet should not exceed a few seconds.

### 1.3 Gas-wall interactions

Gases, when coming into contact with solid surfaces, during standard gas preparation, sampling, storage, transport, and analysis; interact through adsorption, desorption: permeation, diffusion, electrostatic forces, and gravitational settling [63].

The gas-wall interactions cause reversible and irreversible losses; that depends on the different parameters such as contact time, contact area, and thermodynamic conditions [111]. The characteristics of the analyte, e.g., polarities and molecular mass, are crucial in determining the nature and intensity of interactions [36]. The reversible losses are for a short period but with a high rate and very important for sampling purposes, while the irreversible losses are important for long stays as they are continuous losses.

The adsorption and desorption of gases over the surfaces are the sum of collective phenomena in series and/or parallel [62]. In adsorption, molecules, upon leaving the bulk fluid and reach towards the surface, would move over the surface and even into the material owing to the porosity of the material. Whereas desorption is just the opposite phenomenon. Every phenomenon occurs depending upon the difference in the energy. When this gradient of energy is zero, then these phenomena are said to be at equilibrium. However, this equilibrium state is time dependent. Relaxation time controls these phenomena, such as if the relaxation time is greater than the

contact time between mixture and surface, then the phenomenon is explained by the equilibrium model, which is independent of time. On the other hand, if the relaxation time is shorter than the contact time between mixture and surface, then the phenomenon is explained by the equilibrium model, which is time-dependent; however, if both the relaxation and contact time are of the same magnitude, then it will be described by the kinetic model which is time-dependent [79].

Gas-wall partitioning is a relatively recent phenomenon under consideration that causes the underestimation in the measurement of our desired analyte for different purposes especially concerning environmental monitoring and human health [52]. Smog chambers are very helpful for performing experiments relating to atmospheric chemistry in a controlled fashion. Many of the experiments involved in such types of investigations count on the measurement of particle mass variations. A serious hurdle that hinders the accurate analysis is the loss of particles to the surface of the wall during the experiment [22]. The effect on measurements in the environmental chambers is quantified as the delay time in measurements by [69, 26].

The effect of gas-wall interaction in the formation of secondary organic aerosols (SOA) from the oxidation of organic compounds draws significant attention; the however mass of SOA that produced remained questionable due to uncertainties involved because of such interactions [73]. Particles of gas interact with the walls. The rate at the wall loss is dependent on the size of the particle, turbulence in the passage and presence of any electric field, and the geometry of the passageway [22]. Difficulty in accounting for the mass interacted of vapor wall losses results in incorrect estimation of SOA that results in the skewed prediction of ambient SOA mass [19]. Loss at the walls is smaller when the chemistry of the moving compound is rapid [73].

Sampling pipes that convey the air from the atmosphere to the detectors can potentially disturb the measurement of the amount of the analyte segregating on or releasing from the wall surfaces, i.e., these interactions challenge the accuracy of the measurement [50]. The gas mixtures interact by adsorption, desorption, and reactions with the available surfaces, both at the wall or, by permeation, inside of it [63].

Gas-phase organic compounds undergo wall losses. Not only quantification but also identification becomes difficult in the case when reaction products are formed [61]. Considerable interactions of an organic compound have been observed [61, 109, 113] in the Teflon chamber where the organic compound is reversibly partitioned to the wall of the chamber, having the equilibrium reaching a time in few multiples of ten. Researchers also found that semi-volatile organic compounds can partition in a reversible manner to the chamber of Teflon [61, 109]. [69] concluded that these tubings were very much similar to the chromatography column in response to dealing with the material being transported. The effect was not only limited to change the time profile but, more importantly, also changed the concentrations. It was further found that if the walls or the particles are charged, then the rate of loss

increases as a result of interaction [63, 73]. Particles of organic compounds with relatively smaller sizes interact and deposit more efficiently to the wall than those of particles with larger sizes due to the larger Brownian diffusion and charge to mass ratio. [109] investigated that many atmospherically relevant hydrocarbons, when undergoing oxidation, could result in the compounds that have tangible partitioning to the chamber of Teflon, which leads to their loss from further chemical reaction making the analysis hard to interpret; this underlines the need for close monitoring and quantification [13].

In the study [69], delays of VOCs and intermediate volatility-compounds (VOCs) were studied in perfluoroalkoxy alkane (PFA) Teflon tubing. It was observed that the delay increased significantly as the concentration of compounds decreased. In similarly conducted studies, environmental chambers and Teflon walls were considered as equivalent absorbing mass. The results from both materials were consistent. However, tubing proved to be a far better option for the determination of gas-surface interaction owing to the minimal effect of variations in buoyancy and turbulence in the transport, which is more common in chambers that cause more uncertainty in the measured values [52]. In the continuation of these studies, [69] have tested different tubing of Teflon, polymeric material, coated and uncoated steel, glass, and aluminum. All used tubing of polymeric material proved pretty consistent with the absorptive partitioning, and Teflon PFA proved to be the best when it comes to delaying handling at the concentration ranges of  $10^4$  to  $10^7$   $\text{mg}\cdot\text{m}^{-3}$ . PFA and FEP (fluorinated ethylene propylene) materials are recommended for sampling lines with aided special design amendments or even heating to reduce the delays [58, 68, 67]. On the other hand, uncoated and coated glass and metals proved consistent with the adsorptive partitioning. [26] displayed that among stainless steel and Silonite (metal coated with ceramic to give smooth surface and minimum adsorption/absorption), stainless steel is preferred for having a fast response time. It was observed that the passivation of metal tubing with ketone mixtures imparts a peculiar behavior where less-volatile compounds were displacing the more volatile compounds from the surface sites. Therefore, it is safe to say that in the less concentrated species and in the atmosphere, this behavior of displacement might occur.

Presence of a finite number of adsorptive sites resulted in the memory effect, a phenomenon where the surface of the walls is contaminated by the gas flowing through it and thus decreasing the detection limit of the chamber or tubing [21]. Moreover, the responses depends on concentration also make the analytical modeling difficult, As the finding shows that the delays continuously increases as the concentration of the compounds decreases [52]. Since the gases with lower volatility mostly remain in the equilibrium with the system, this causes the disturbance of gas-particle owing to the delays in transport which leads to aerosol evaporation. In order to measure the aerosol mass, oxidation-flow reactor or other systems need the inlets. Hence the measurements can greatly be perturbed due to tubing delays

because aerosol mass has the major chunk of lower volatility compounds [47, 58]. This partitioning phenomenon in tubing influences both aerosol and gas quantification, stipulating the better mechanism to have representative quantification with minimum uncertainty.

Apart from the semivolatile and intermediate volatility organic compounds (S/IVOCs, some smaller molecules like  $\text{NO}_3$  or  $\text{HNO}_3$  also adsorb and absorb on the surfaces, so special attention is needed for their rapid response time [46, 68, 58]. Chemical ionization mass spectrometry (CIMS) is a technique for forming ions of the compound of interest [66] and the measurements with it can be improved to get less delay times by adjusting the design [58, 93]. Chemical composition and structural design of transporting tube determine how the interaction will take place between tube and sample being transported. The chemical inclination of the sample decides the type of chemical reaction (e.g., rate of corrosion) and binding energy of the sample with the surface of the wall as a result of the interaction. The surface area of the tube dictates the availability of the space for the chemical reaction site. Smoother and mirror-like surfaces offer less area for the reactions as compared to coarse or rough surfaces, which provide a greater area for reaction. Different methods that affect the surface chemistry and roughness of the tube are being used in the fabrication process of stainless-steel tubes that are used for sample transport. The inner surface of such tubes is depended on the initial material used for fabrication, type of processing technique, and post-fabrication processes [40]. Many of the manufactured tubes have surface free iron, which is a serious problem due to its high reactivity [103]. The presence of iron and iron oxide readily invites rapid attack and facilitates the process of corrosion and surface activity. Moreover, the very presence of iron oxides is very friendly towards adsorption and strongly absorbs hydrogen sulfide and water [48, 11].

For the redressing of such problems and in order to enhance the performance of the tubing in a real-world application, these are subjected to a variety of post-treatment. These treatments include:

- Chemical passivation.
- Electropolishing.
- Coating.

### 1.3.1 Chemical passivation

Passivation is a metal-finishing technique in which a thin layer is coated over the material surface to make it more resistant to corrosion. For manufacturers and industry standards, the ASTM A976 [96] defines the passivation of stainless steel as: the chemical treatment of stainless steel with a mild oxidant, such as a nitric acid solution, for the removal of free iron or other foreign matter. Chemical

passivation and cleaning are very pertinent processes in the backdrop of surfaces involved in corrosive or critical environments [8, 40]. Initially, this was prompted due to the need for repairing activated areas of the welds [7].

The primary goal of this technique is to build and deposit the inert layer over the surface of the material that maximizes the corrosion resistance, which would act as a shield against any untoward chemical interaction to the minimum possible level. Passivation and cleaning actually expunge the adsorbed contaminants, which facilitate the sites for corrosion that progressively turns into rough formation. The formation of the Cr/Fe layer with the higher chromium lowers the rate of iron oxide formation. Anodic oxide film, which is coated over the surface, is very thin in the order of 10-50 Å [81]. There is a number of physical parameters which are considered for measuring corrosion-resistant surfaces, such as oxide layer depth, Cr/Fe ratio, surface contaminant inclusions, and the surface area or roughness. Chemical passivation enhances the ratio of chromium oxide to iron oxide to a greater extent. Acid interaction has more impact with the sharp peaks and high points than smooth surfaces. The process of passivation of the tube significantly reduces the surface roughness. The measurement of roughness average (Ra) is carried out as a measure of mean deviation from the mean height expressed in microns ( $\mu\text{m}$ ) [40].

### 1.3.2 Electropolishing

Electropolishing is an electrochemical process that removes the material from the surface in order to polish, trim and passivate to get a smoother surface of the metallic parts. It is the reverse of the process of electroplating [107]. This is a specific type of process in which metallic pieces are passed in the electrolytic cell through electrolyte where the subjected metallic piece serves as an anode and attached to the positive terminal of DC current source while the negative terminal is linked to the cathode. Afterward, the piece to be electropolished is dipped in the special electrolytic solution under the controlled temperature conditions [107, 23]. Generally, the electrolytes used are concentrated acid solutions having elevated viscosity, e.g., phosphoric acid and sulphuric acid.

Electropolishing has a wide range of applicability in the metal finishing industry due to its process simplicity and ability to accommodate the parts and equipment of complex geometry and shape [43]. This technique has the capacity of producing high-quality surface finished work pieces. Even plastic or press and wire-drawing die, electrical and optical parts can take benefit from this process [72]. In order to improve the dimensional accuracy and to relieve the surface layer stressing, electrochemical honing of tubular holes play a pivotal role [16]. Manufacturing of thin metal samples for the transmission of an Electron microscope also entails the use of electropolishing due to the fact that this process does not deform the surface layers. Ultra-high vacuum components, in order to have improved pumping speed, vacuum pressures, and out gassing rates, use electropolishing for smoother surfaces

[70]. Apart from the point of view of appearance, the following are the additional advantages of electropolishing:

- A highly smooth surface having minimized adherence of particles of gas and liquid.
- Removing oil and iron from the surfaces.
- Corrosion resistance due to increased Cr/Fe ratio and reducing the reactivity to a greater extent.
- Creating the passive chromium oxide, which is free of iron contaminants .
- Minimization of surface stresses that leads to improved mechanical properties.

### 1.3.3 Coating

The coating is adding inert coating material like silicon to protect, preserve, and enhance the performance of the material. The chemical deposition process is employed to deposit the layer of amorphous silicon onto or into the steel surface at temperature  $400\text{ }^{\circ}\text{C}$ . This process also helps in the reduction of moisture hold-up and inertness of the surface [9]. The coating can be prepared from different materials like polymers, ceramics and glasses, and metals. However, the use of polymers has advantages, especially in terms of lower processing and material costs and convenient deposition techniques. Polymeric-based coatings have the problem of relatively lower hardness and reduced thermal and chemical stability. In the case of metallic coatings, the cost of processing and material is high. Moreover, resistance to oxidation and corrosion is way less than that of polymers. Although ceramic-based coatings have higher temperature and wear resistance and hardness, having oxidation and corrosion stability yet these types of coatings require more processing costs and as compared to polymeric and metallic coatings. Considering all the factors discussed, silicon-based polymers appear to be the best choice in most of the cases [10].

Deposition of coatings in the liquid state can be carried out by a number of techniques depending upon the suitability of the method for a specific system. These techniques include; spraying, spinning, dipping, screen printing, roll coating, and brushing, etc. Liquid state deposition is greatly influenced by the rheology of coating material and suspension. Therefore, rheology must be carefully controlled to get high-quality coatings [28]. Although the depositing of silicon-based coating in gaseous or solid form is possible yet very uncommon because processing tends to be very costly and complicated. Plasma-assisted chemical vapor deposition (CVD) and other types of CVD processes can be used for this type of coatings [4].

## 1.4 Research objective

The objective of this work is development of methods for the quantification of gas-wall interactions in sampling lines. Different post-treatment methods greatly improve the performance of the tubing in terms of minimizing the effects of interactions and other disturbances, however; there still exist some sort of interactions and loss of material as a result of these interactions. When it comes to considering the detection and quantification of these interactions at trace levels like ppb and ppt, these smaller interactions cannot be ignored and overlooked. Therefore, an efficient and reliable quantification mechanism with the lowest uncertainty is vital while dealing with such a minuscule level measurement.

A quantification of equilibrium amount segregated on the material surface is available from theoretical insight and models for few types of wall materials [36]. Equilibrium between gas mixtures and pipe walls is expected to be at a constant ratio between potentials on the two phases expressed as an amount per unit volume of mixture and amount per unit active surface of pipe wall [36]. Experimental methods have been proposed in research projects [32, 88], the preliminary results showed a very large uncertainty in theoretical previsions and a low reproducibility in experimental data [32]. The purpose is to investigate interaction at a very low level [88], but the risk of working at a low level is to have instability of sources that do not allow to have reliable data on the material properties. This work is aimed to fix a starting point of a quantitative method for the measurement of reversible interactions, irreversible interactions, and memory effect before applying the method to the low amount of substance. The novelty of the work is the proposal of a quantitative method for reproducible measurement of interactions in sampling lines to offer reliable data to calculate the biases affecting VOC measurements.

## 1.5 Scope of the work

This dissertation develops a quantitative method for the measurements of interactions of VOCs and surfaces of commercially available pipes usually used for sampling. Simplified conservative quantification of the losses due to gas-wall interactions in the sampling lines has been proposed; it is based on the value of an equilibrium amount of VOC adsorbed on the pipe wall.

The novelty of this work is the proposal of a quantitative method for reproducible measurement of interactions in sampling lines to offer reliable data to calculate the biases affecting VOC measurements. These interactions are reversible losses during equilibrium, irreversible losses due to reaction or permeation, and release due to memory effect.

An experimental set-up has been designed for the quantification of the gas-wall interaction. A mixture containing a single VOC was flushed inside a clean test pipe.



A fast response detector was used to retrieve the signal of VOC concentration. The amount of VOC that interacted to the wall from the mixture was calculated from the depletion of the signal. The maximum amount of VOC interacted per unit area was considered as surface concentration and equilibrium constant ( $K_e$ ) of VOC adsorption on the internal surface of the test pipe, while the irreversible losses due to reaction are calculated as mass flux  $J$  ( $\text{mol}\cdot\text{m}^{-2}\cdot\text{min}^{-1}$ ) from the signal of VOC in the saturated test pipe and in the bypass of the system. The released amount of VOCs due to the memory effect of the pipe is calculated from the signal of air in the bypass and test pipe after a memory effect.

The acetone ( $\text{CH}_3\text{-CO-CH}_3$ ) mixture in the air at the ppm level with certified uncertainty is used for the experiments due to the stability of acetone, its high response on the detector, and its importance in applications. Four different common materials were tested with two different internal diameters at different lengths having the same surface area. The sensitivity of  $K_e$  and  $K_{\text{kin}}$  to the residence time in the test pipe has been analyzed by controlling the flow rate and length of the test pipe. The sensitivity of the method on residence time, surface area, gas velocity, temperature, and pressure has been evaluated to identify the main influencing quantities and the limits of the applicability of the methods.

## 1.6 Thesis outline

Chapter 2 addresses the experimentation process and metrological characterization of the primary system. The details about the measurements of all parameters and devices and their working principle are explained here.

In Chapter 3, the generation process of the model is described, and the methodology including the definition of concepts and methods necessary for the development of this work. A model based on the mass balance of the pipe was developed that leads to measurand equations for mass adsorbed and desorbed and equilibrium constant, irreversible losses, and memory release.

Chapter 4 . The results for adsorbed and desorbed amount during equilibrium ( $C_{A,e}$ ) and the equilibrium constant ( $K_e$ ) with four different materials are discussed. The sensitivity of the method on different parameters such as temperature pressure records and contact time has been carried out, and corrections were made where necessary to a reference point. The reproducibility of the method and associated uncertainty have been calculated. A comparison of the applicability of the methods on different materials has been discussed.

Chapter 5 shows the calculations for irreversible losses and memory effects. The results with two different approaches for estimating the irreversible losses and memory has been compared. The biases due to saturation have been analyzed, and data were corrected. The effect of temperature and pressure has been discussed.

Finally, The conclusion of the work as a summary is presented, with the contributions from this research and the opportunities for the future.

# Chapter 2

## Experimentation

### 2.1 Experimental set-up

An experimental set-up for the quantification of the gas-wall interaction has been developed. Two sources of gases have been flushed in a test pipe or in the bypass and analyzed in a fast response detector; the schematic drawing is shown in Figure 2.1. The dry air, obtained from the commercial air cylinder (A), is considered as zero air (having a negligible amount of hydrocarbons). A certified VOC mixture in the air is supplied from the cylinder (M). The flow rates of zero-air and VOC mixture are controlled by sonic nozzles  $S_{N1}$  and  $S_{N2}$  and regulated by the pressure reducing valves  $V_{R1}$  and  $V_{R2}$ , respectively. A 4-way valve  $V_{S1}$ , with reduced surface and reduced dead volume, is used to switch the stream flowing to the detector between zero air and VOC mixture. The change in the position of this valve also allows measuring the pressure and flow rate of the two streams.  $V_{S2}$  has the same specifications as  $V_{S1}$ , and it is used to insert or removes the test pipe from the line on which the gas is flowing to the detector.

The flame ionization detector (FID) of a gas chromatograph (Bruker GC-450) is used for the detection of VOC in the mixture, which is leaving the setup. The mass flow rate is measured by 100  $\text{Sml}\cdot\text{min}^{-1}$  Bronkhorst mass flow meter (FI). For high flow, two flowmeters are placed in parallel, of which one works as a flow controller and the other as a flowmeter. The test pipes are insulated by polystyrene sheet and kept at controlled room temperature ranging from 18°C to 30 °C. The temperature of the test pipe is estimated from the measurement of resistivity of calibrated temperature sensor Pt-100.

Pressure drop in every branch is different that causes pressure spikes while switching. This effect could be reduced by keeping the same pressure drop on the vent and FID line using capillary tubes  $pd_1$  and  $pd_2$ . Capillary tubes are used as pressure drop devices which have a pressure drop much higher than pressure drop in the pipe due to its small diameter. Pressure drop is measured by MT-110 as differential pressure from the atmospheric room pressure.

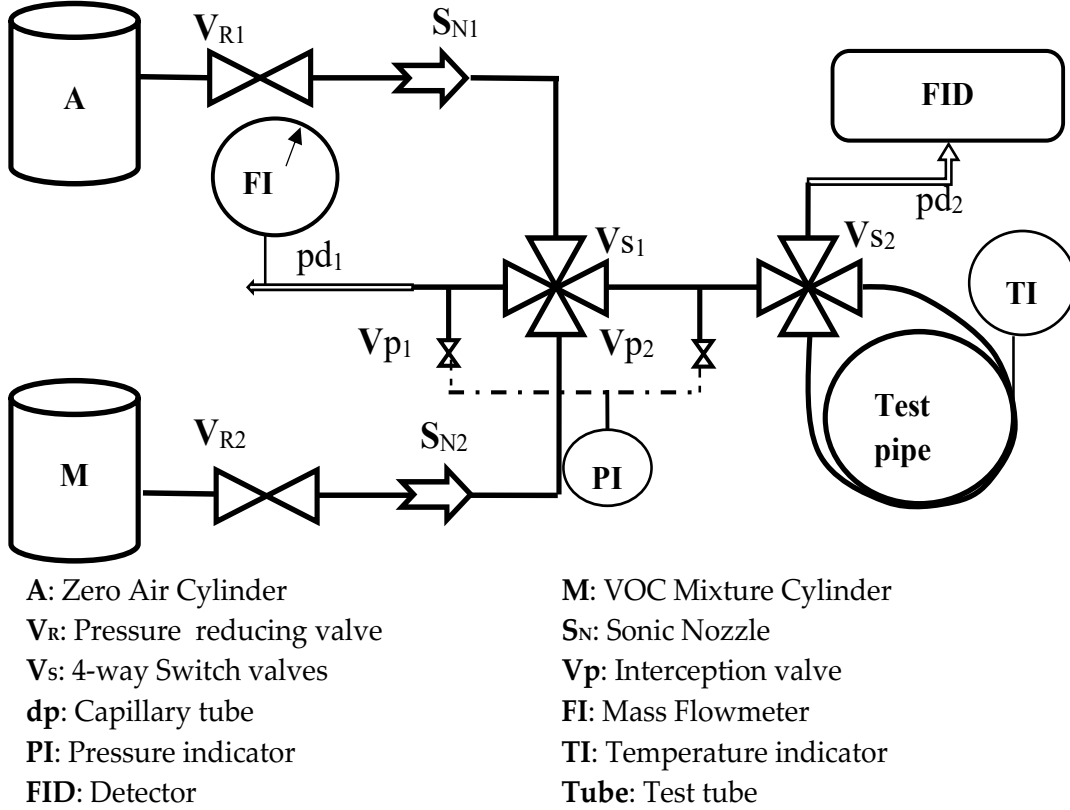


Figure 2.1: Scheme of the experimental setup.

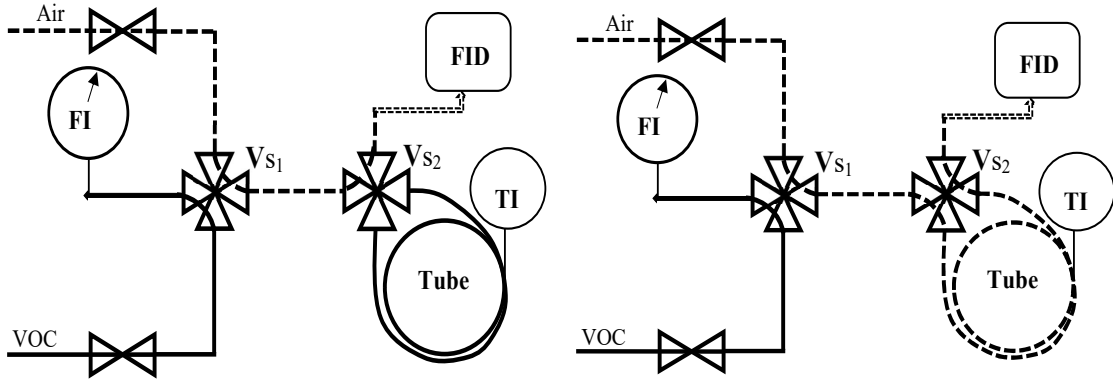
The system is checked periodically for leakages using the procedure described in [89]. GC is switched ON for more than an hour to stabilize the FID signal and temperature of the system.

At very short contact time, interactions are limited, and FID response sharply changes from zero to VOC mixture concentration. At prolonged contact time, the phenomenon of the interaction completes, and the system reaches equilibrium, the solid surface is saturated by the mixture, and the FID response changes from zero to mixture concentration with time. There is an optimal contact time corresponding to the relaxation times of the observable phenomena. Working within the same window of time of the interaction process maximizes the effect of the wall interaction phenomena. At the optimal contact time, the FID response change has a minimal slope. The presence of multiple slopes indicates multiple controlling phenomena. The contact time between the pipe and the mixture is equal to the residence time  $\tau_R$  of each experiment. The residence time  $\tau_R$  of the gas stream in the test pipe is regulated by flow rate and is considered as the ratio between internal test pipe volume and volumetric flow rate. The uncertainty of residence time and effect of influence quantities were calculated using the equation 2.1

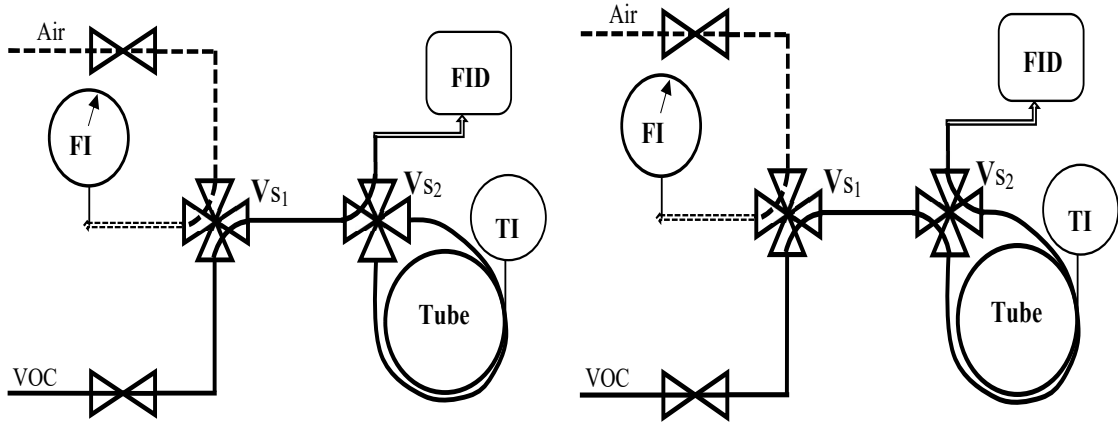
$$\tau_R = \frac{V_{testtube}}{q_{v,g}} = \frac{\frac{\pi D^2 L}{4}}{q_{v,g} \frac{P^0 T_{wc}}{P_{atm} + dP_{wc} T^0}} \quad (2.1)$$

Where  $D$  and  $L$  are the diameter and length of the test pipe, respectively.  $T$  and  $P$  are temperature and pressure respectively; Superscript  $o$  accounts for standard condition subscript  $atm$  for atmospheric conditions (retrieved from [99]), subscript  $wc$  for working condition,  $dP_{wc}$  is the pressure drop.

$q_{v,g}$  is the mass flow rate expressed as volumetric flow rate at standard condition measured by the mass flow meter.



Configuration A: Zero air flowing in bypass, VOC mixture flowing to vent  
 Configuration B: Zero air flowing in the test pipe, VOC mixture flowing to vent



Configuration C: VOC mixture flowing in bypass, zero air flowing to vent  
 Configuration D: VOC mixture flowing in test pipe, zero air flowing to vent

Figure 2.2: Device connections for monitoring the VOC mixture and zero air in bypass and test pipe. The dotted line represents the zero air and solid line shows the VOC mixture.

Four different configurations have been designed for the experimentation based

on the position of Valves  $V_{S1}$  and  $V_{S2}$ ; they are presented in Figure 2.2

**Configuration A:** The detector monitors the zero-air flowing through the bypass while the VOC mixture is sent to the vent, where the flow rate of the VOC mixture is measured by the flowmeter.

**Configuration B:** The detector monitors the zero-air flowing through the test pipe while the VOC mixture is sent to the vent, where the flow rate of Zero-air is measured.

**Configuration C:** The detector monitors the VOC mixture flowing through the bypass while zero air is sent to the vent.

**Configuration D:** The detector monitors the VOC mixtures flowing through the test pipe while zero air is sent to the vent.

## 2.2 Materials

Experiments were performed on commercial pipes 1/8" and 1/4" nominal diameter as listed in Table 2.1; The internal diameter was measured by weighing pipes empty and filled by water on 1m pipe length with 2cm uncertainty. As normally, manufacturers declare the value of internal diameters without guaranteeing the uncertainty that arises the need of proper measurement of diameter and estimation of uncertainty. Sulfinert® coated stainless, and Copper with 1/8" diameters were tested while electropolished stainless steel and perfluoroalkoxy alkanes (PFA) with diameter 1/4" were tested that are shown in Figure 2.3.

Table 2.1: List of materials with specifications

Materials	Length (m)	$u(L)$ (m)	$OD$ (in.)	$ID$ (cm)	$u(ID)$ (cm)
Sulfinert®	26	0.13			
	8.5	0.05	0.13	0.216	0.001
Copper	11.1	0.17	0.13	0.165	0.003
PFA	4.7	0.2	0.25	0.39	0.001
Stainless steel	3	0.2	0.25	0.457	0.009

VOC mixture of acetone was chosen because of its high response and stability on FID [97] and owing to its importance in different applications [1, 89]. Acetone has a higher molecular response and stability to FID as compared to ethanol due to a high number of effective carbons [97]. VOC mixture of Acetone in air at 10ppm with 10% uncertainty is obtained from a cylinder containing certified gas



Figure 2.3: List of commercially available pipes of different materials.

mixture. Acetone is an oxygenated hydrocarbon that is present in the atmosphere in significant amounts. It is a key source of  $\text{HO}_x$  radicals while being transported to the mid and upper troposphere. It is included in the list of Global Atmospheric Watch (GAW) monitoring programs [1]. Acetone is the main VOC for silicon deposition for electronic and photovoltaic industrial applications [89]. Acetone at a nominal supply of 10 ppm in the air was supplied as a VOC mixture from a certified gas cylinder with 10% uncertainty. Experiments were performed from two cylinders of the same concentration ( $10 \pm 0.1$  ppm). The results were compared for both cylinders; the effect on repeatability was negligible.

## 2.3 Quantification of leakages

Leakages have both direct and indirect effects on our measurements. This phenomenon causes fluctuations in flow rate, which means changing the residence time which we intend to calculate. Thus, it leads to errors in our final measurand. Indirect leakages change the pressure of the system and consequently cause different

thermodynamic conditions. Besides these leakages, these spur change in response to our signal in the sensor. For all these reasons, the leakages must be controlled properly by measuring accurate values and performing leakage-test repeatedly over every small change (installation of new equipment) in the system. To achieve this, pressure decay over a known time and volume are monitored, and by  $dP/dt$  for a known volume, we can calculate the volume losses as explained in [89].

The measure of leaks can be performed to quantify the mass loss from the volume per unit time. Considering that the gas behaves ideally for a known volume  $V$  with initial conditions  $P_0, T$  and  $n_0$ .

$$P_0V = n_0RT$$

Assuming negligible temperature losses after some time, the pressure and number of moles will reduce to  $P_1, T$  and  $n_1$  respectively due to leakages.

$$P_1V = n_1RT$$

As the volume of the system remains the same so

$$\begin{aligned} n_L &= n_0 - n_1 = V \frac{(P_0 - P_1)}{RT} \\ V_L &= V \frac{dP_{leaks}}{P_{atm}} \\ Q_L &= \frac{V_L}{t} = \frac{V}{P_{atm}} \frac{(P_0 - P_1)}{t} = \frac{V}{P_{atm}} \frac{dP_{leaks}}{t} \end{aligned} \quad (2.2)$$

$dP$  due leaks are measured for a known time and known volume. If the leaks are higher, the volume of the system is split into small segments to investigate the leaking joints. For a known volume, the system is left for some time for stabilization of pressure because during switching, the heat is transferred from the body of the operator to the stored gas inside the system.

### 2.3.1 Injection test for volume estimation

Usually, the system is split into small segments as the actual volume of those segments is unknown. While the volume of the segment/system is important to estimate as it is important to calculate leakages. For this purpose, an injection test is performed in which a known volume is injected with the help of an injection device to the unknown volume of the system. The unknown volume of the system of interest, i.e., a small segment of the whole set-up, is disconnected from the rest of the system and connected to a three-way valve, as shown in Figure 2.4. One-way it is connected to the system; second-way it is related to pressure monitoring device PI, and third-way it is connected to an injection device. The medical syringe of 50 ml volume is used as an injection device.



Initially, both the pressure in the system and syringe will have atmospheric conditions. After the injection, the pressure and temperature of the system will rise. The measurements are repeated for injection of different volumes of air repeatedly, and from the rise of pressure in the system, the volume of the system is calculated.

As the number of moles before and after injection will remain the same. Applying ideal gas law, we get equation 2.3:

$$V_s = \frac{P_i V_i}{T_i} \left( \frac{T_{sf} T_{si}}{P_{sf} T_{si} - P_{si} T_{sf}} \right) - V_d \quad (2.3)$$

$V$  is the amount of air in the system volume at initial system conditions  $T_{si}$  and  $P_{si}$ ,  $V_i$  is the injected volume at initial syringe conditions  $T_i$  and  $P_i$ .  $T_{sf}$  and  $P_{sf}$  represent the system's final conditions.  $V_d$  is dead volume considered for the connection among the volume under measurement, the pressure gauge, and the syringe.

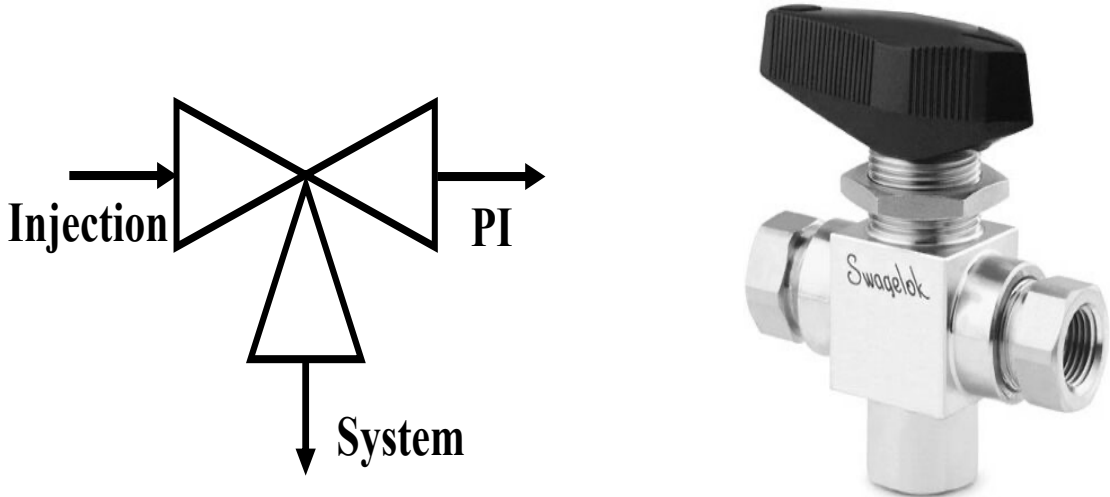


Figure 2.4: Schematic view of injection test and 3-way valve.

## 2.4 Pressure measurements and validation

The measurement of pressure is important for its role in affecting other parameters such as flowrate residence time and also affecting the measurements of leakages. For this reason, a pressure measurement device monometer Yokogawa MT-110 is used. The differential pressure in the system related to the atmosphere (room pressure) is measured. While the data for atmospheric pressure is retrieved from [99], assuming the same atmospheric pressure throughout the city.

The validation of the measurements is important to increase the degree of trust on measurements. The validation of measurements can be done by:

- Measurement of a known a physical quantity.
- Comparison with measurement by another device.

For the validation, the pressure inserted due to a known height of the water column is measured. The device is connected to a long pipe filled with water, as shown in Figure 2.5. The other end of the pipe is closed from the atmosphere, leading to a difference in water level. The pressure measured in the device will be double of pressure calculated from the difference of water level as:

$$P_{PI} = 2 \cdot \rho g(dh)$$

The pressure measured in the system was higher than the pressure calculated for all the flowrate due to joints/valves and bending. A detailed study was performed to understand the pressure drop in every part of the system and factors affecting the pressure in the system.

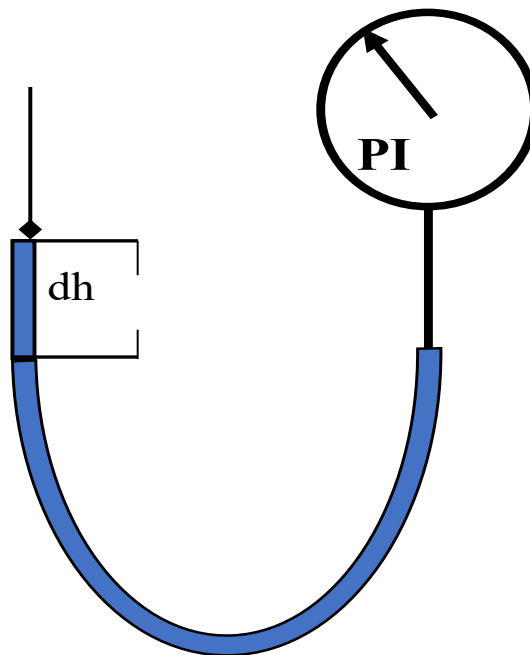


Figure 2.5: Scheme for pressure monitor validation.

## 2.5 Flowrate measurements and validation

Measurement of flow rate is important for two reasons. Firstly, it affects the residence time, and secondly, it affects the response of the FID signal. Brooks and Bronkhorst flowmeters with high-pressure drop and lower pressure drop are used with a maximum flow rate of 100 sml/min. For higher flow rates, both were used in parallel, in which one acts as a flow controller and the other as a flowmeter.

For validation of the measurements, all the three devices are interconnected by measuring flowrate arranging them in series and in parallel. The measured value of flowrates was also compared with flowrates estimated from sonic nozzles as at sonic condition; sonic nozzle allows a certain flow at known supplied pressures. Figure 2.6 shows measurements with all the three devices connected in parallel to each other and connected in series to the sonic nozzle. The relative differences are plotted against the average values of the flow rates measured with all the three devices. Since Brooks and low pressure Bronkhorst (Bronkhorst LP) both have almost the same pressure drop; both devices have almost the same measurement with some variation and quite different with the High pressure Bronkhorst (Bronkhorst HP) flowrater. The relative difference decreases from 27% for Brooks and 8.5% for Bronkhorst HP to 7% and <1% respectively with 50 Sml·min<sup>-1</sup> rise in flow rate.

A comparison of flowmeters was performed by connecting all the flowmeters in series; It was noticed that Brooks and Bronkhorst (LP) have a 0.5-1% difference at different flow rates while Bronkhorst (HP) always measures lowers by 1-2%.

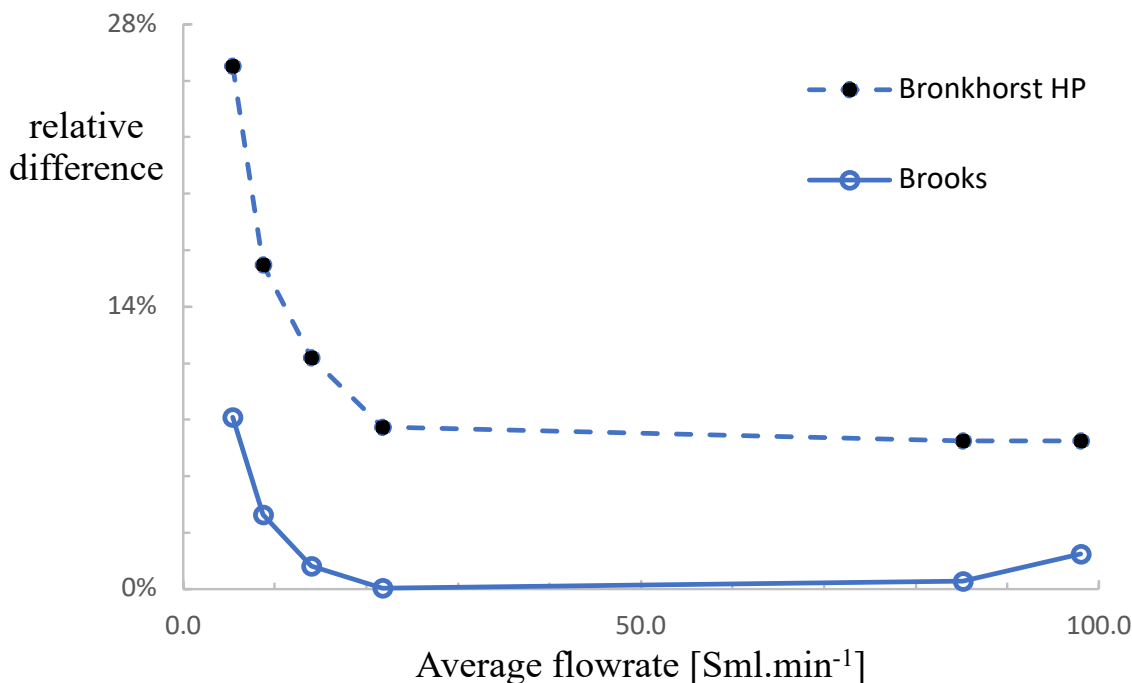


Figure 2.6: Comparison of measurements of flowrate with three different devices.

## 2.6 Temperature measurements

The measurement of accurate and representative temperature is a challenging task, as the temperature is affected by many factors. In a short time (minutes), the temperature is affected by the FID combustion and the vicinity of the body of the operator to the sensor. This short-term fluctuation is minimized by an insulation box prepared from polystyrene, which has a thermal conductivity of  $0.033 \text{ W}\cdot\text{m}^{-1}\cdot\text{K}^{-1}$ . However, there is still some degree Celsius variation in temperature of the test pipe, which is considered as uncertainty to our measurements.

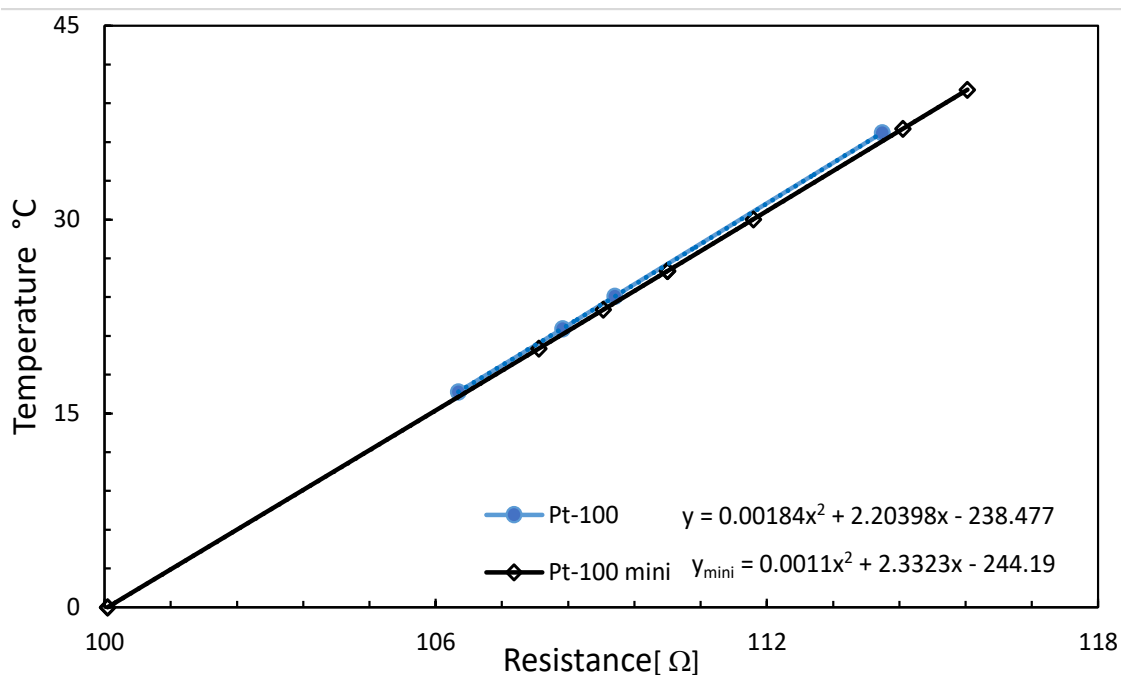


Figure 2.7: Temperature correlation model for Pt-100.

In medium time duration (hours), the temperature is affected by daily fluctuations, as reported in Figure 2.8. In long duration (days or months), the yearly fluctuations of temperature cause changes in making measurements at unique conditions. As the air and VOC coming from the cylinder are placed outside of the room at ambient temperature, the accurate measurements of representative temperature are important due to its effects on the flow rate. The gas expands at a higher temperature and thus changes the residence time inside the pipe.

For the measurement of temperature, two Pt-100 platinum resistance thermometers (Pt-100 and Pt-100 mini) are used, which have  $100 \text{ } \Omega$  resistivity at  $0^\circ\text{C}$ . The resistivities are measured, and the corresponding temperature is calculated using a correlation model. For PT100-mini, the data were measured in National Institute

of Metrological Research (INRiM) and certified, while for Pt-100, the measurements for correlation were performed in a different controlled temperature of the natural water using the hake 007 temperature controller in order to measure the same temperature by both the sensors. The temperature of the water is measured by Pt-100 mini and the same temperature is used for regression of model for Pt-100 sensor which are reported in Figure 2.7. The regression over measured data can be made in two ways; one is to consider the linear relationship and the other to consider the polynomial model. However, the error in the case of linear was higher than second degree polynomial model. Therefore, the second degree polynomial is the best model for correlation and temperature estimation.

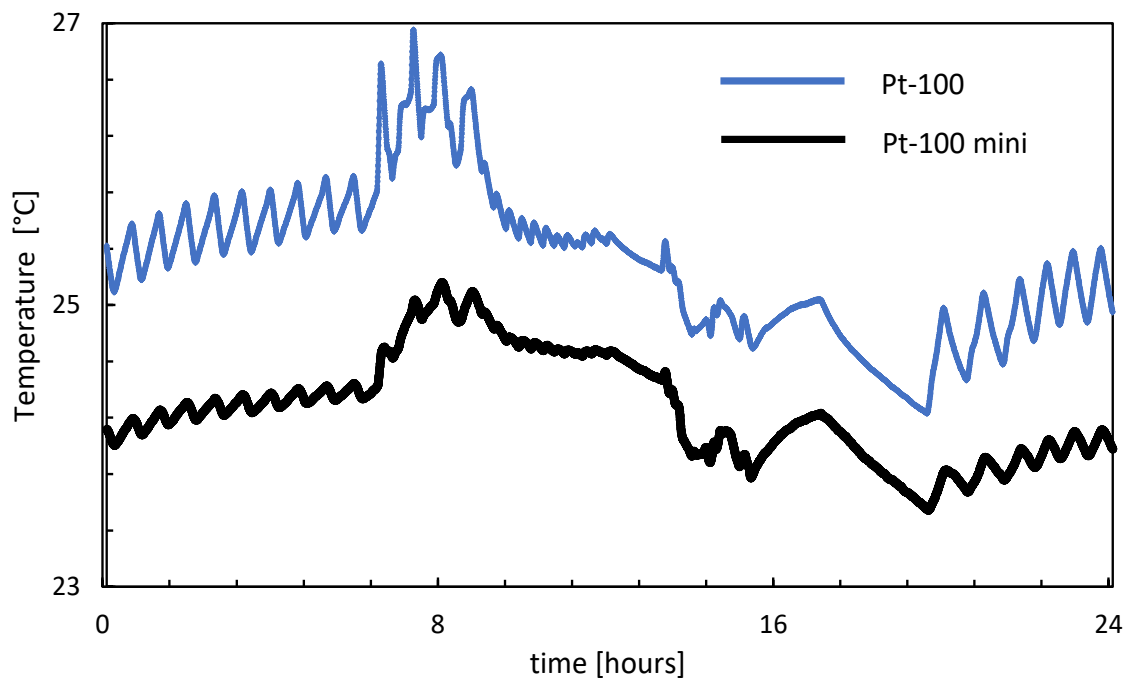


Figure 2.8: Daily temperature fluctuation measured by both sensors placed in the air.

## 2.7 Diameter measurements

Diameter is another important parameter that affects the uncertainty of our measurand in three different ways. First, it affects the volume and thus residence time; second, it changes the contact area of the pipe; third, it affects the Reynolds number and thus flows pattern. Usually, pipe diameter is declared by the manufacturer, but their degree of confidence is not guaranteed, some manufactures give 2% expanded uncertainty, but this 2% is very high as it is the most critical parameter for measurement. For this purpose, the measurement of diameter is performed by

measuring the volume inside the pipe. The measurement of volume can be done in two different ways, either by gas injection or by liquid injection. In gas injection, a known volume of air is injected into the pipe, and from the measurement of pressure change, the volume of the pipe is estimated, and thus the diameter of the pipe.

The liquid injection can be done in different ways, such as the pipe with both ends closed is placed inside a jar of water. The level is noticed, then water is allowed to enter the pipe by opening the ends, and the water level is read again. The difference of level will be the inner volume of the pipe. Another way is to weigh the pipe empty and then to fill it with water and weighing again. The differences of masses will be the mass of water inside the pipe, and then using a density of water, the volume of water inside the pipe is calculated, which is the volume of the pipe.

As the pressure measurement is affected by temperature and leakages, therefore the liquid injection was chosen for this study. The mass of the empty pipe and filled with water were measured repeatedly with the help of an electronic balance scale able to read until four digits. The diameter of the pipe was calculated for Sulfinert<sup>®</sup>, copper, and PFA tubing using the following equation 2.4 with uncertainty lower than 0.5%, while for Stainless steel the declared value of diameter by manufacturer were considered.

$$D = \sqrt{\frac{4(m_{fill} - m_{empty})}{\pi L \rho}} \tag{2.4}$$

where  $D$  is the measurand diameter of the pipe having length  $L$ ,  $m_{fill}$  is the mass of the pipe when filled with water and  $m_{empty}$  is the mass of pipe when clean from water,  $\rho$  is the density of water. Uncertainty budget is applied to equation 2.4, and the effect of influence quantities are approximated as shown in Table 2.2 for the estimation of diameter of PFA.

Table 2.2: Uncertainty budget of the diameter of PFA

<b>X</b>	<b>x</b>	<b>[X]</b>	<b>u(x)</b>	<b>u(x)/x</b>	<b>dM/dx=C<sub>i</sub></b>	<b>c<sup>2</sup>u(x<sub>i</sub>)<sup>2</sup></b>	<b>Is</b>
Density	0.997	g/ml	2E-04	0.02%	-1.96E-01	1.67E-09	<0.1%
mass filled	85.26	g	0.013	0.02%	2.51E-02	1.10E-07	20%
mass empty	77.47	g	0.03	0.04%	-2.51E-02	5.49E-07	100%
Length	65.2	cm	0.2	0.30%	-2.99E-03	3.58E-07	65%
Diameter	0.39	cm	0.001	0.26%		1.02E-06	

# Chapter 3

## Methodology

Gases, when they come into contact with solid surfaces, they interact through adsorption, desorption: permeation, diffusion, electrostatic forces, and gravitational settling [63]. The adsorption and desorption of over the surfaces are the sum of collective phenomena in series and/or parallel [62]. Volatile organic compounds will adsorb on contact surfaces, used for gas sample storage, gas standard preparation, transport, and analysis. These interactions are problematic for all VOCs. The measurement of oxygenated VOCs (OVOCs), like ethanol and methanol, is very challenging as these gases strongly interact with various metal surfaces, including stainless steel (usually used sampling lines or pressure regulators) and aluminum (used in gas cylinders). These interactions depend on thermodynamic properties and nature of the VOC, the properties of the wall, the VOC concentration, temperature, humidity, and air velocity [112].

Generally, molecules leave first the bulk of the fluid to reach the surface, then bind to the surface, move on the surface, and eventually move through the material pores. Desorption is the opposite pathway. Every single phenomenon takes place locally with an extension and a direction depending on the gradient of the free energy. When the gradient of free energy is null, phenomena are at equilibrium. Being or not at the equilibrium is time depending. Each phenomenon has its own relaxation time [80]. The observation leads to three different scenarios depending upon contact time and relaxation time.

$$(a). \frac{\text{Relaxation time}}{\text{contact time}} < 1$$

When the mixture of gases is leave for long time contact so that it has higher contact time than relaxation time of gas mixture and material. equilibrium establishes and the phenomenon become time independent.

$$(b). \frac{\text{Relaxation time}}{\text{contact time}} = 1$$

When the relaxation time has the same order of magnitude of relaxation time, the phenomenon can be described as a kinetic model. This model, too, depends on time.

$$(c). \frac{\text{Relaxation time}}{\text{contact time}} > 1$$

When the mixture of gases is leave for very short contact time so relaxation time of the phenomenon is much higher than contact time of gas mixture with material. The equilibrium is not established and the phenomenon is time dependent.

### Langmuir adsorption

The best-known model is the Langmuir adsorption isotherm developed by American chemist Irving Langmuir in 1916. Langmuir isotherm was developed for monolayer adsorption onto a surface containing a finite number of identical sites. The model assumes uniform adsorption energy onto the surface and no transportation of analyte in the plane of the surface. All assumptions are very well describing in a situation where a low concentration occurs in the gas and less amount of adsorption.

The fraction of the surface sites covered by a molecule of VOC ( $C_{A,VOC}$ ) is given by [37]:

$$C_{A,VOC} = \frac{K_{eq}^{VOC} p_{VOC}^*}{1 + K_{eq}^{VOC} p_{VOC}^*} = \frac{K_{eq}^{VOC} x_{VOC}^* P}{1 + K_{eq}^{VOC} x_{VOC}^* P} = \frac{K_{eq}^{VOC} C_{VOC}^* RT}{1 + K_{eq}^{VOC} C_{VOC}^* RT} \quad (3.1)$$

Using Dalton law, partial pressures can be substituted by molar fractions to directly accounting for the chemical potential of VOC. Applying Ideal gas law, which stated as:

$$PV = nRT \text{ so } x_{VOC} = \frac{C_{VOC}RT}{P} \text{ or } C_{VOC} = \frac{x_{VOC}P}{RT}$$

$C_{A,VOC}$  is the adsorbed amount of VOC per unit area of available solid surface;  $p_{VOC}^*$  is the partial pressure of VOC in the mixture at equilibrium with the surface;  $x_{VOC}^*$  is the molar fraction of VOC in the mixture at equilibrium with the surface.  $K_{eq}^{VOC}$  is the ratio of forwarding adsorption reaction and backward desorption reaction constants at equilibrium,  $K_{eq}^{VOC}$  is usually calculated by regression of experimental data of isothermal adsorption or from the properties of surface material and VOC molecules [37].

At very low concentration ppb-ppt level where  $\frac{p_A}{P} \cong 10^{-9}$  or  $K_{eq}^{VOC} p_{VOC} << 1$  so equation 3.1 is reduced to equation 3.2.

$$C_{A,VOC} = K_{eq}^{VOC} p_{VOC}^* = K_{eq}^{VOC} x_{VOC}^* P = K_{eq}^{VOC} C_{VOC}^* RT \quad (3.2)$$

In such situation the behavior between pressure and  $C_{A,VOC}$  is a linear and thus can be easy for calculations. this approach has been through experimentation by [59].



A simplified  $K_e = K_{eq}^{VOC} RT$  is considered can be written as ratio of the Actual concentration of the VOC and arial surface concentration equation 3.3

$$K_{eq} = \frac{x_{VOC}^* P}{C_{A,VOC} RT} = \frac{C_{VOC}^*}{C_{A,VOC}} \quad (3.3)$$

A model to predict the VOCs interacted with wall solid surfaces is developed to give a methodology for measurements of these interaction. The maximum amount interacted per unit surface area  $C_{A,VOC}$  during equilibrium or  $C_{A,e}$  is calculated from the mass balance over the pipe and hence equilibrium constant  $K_e$ . The irreversibly reacted mass ( $J$ ) and release mass due to memory ( $M$ ) are calculated over mass balance on saturated and clean pipe, respectively.

### 3.1 Definition of system

To have a clear understanding of these interactions we need to consider our system precisely for these interactions. Tubing proved to be far better option for the determination of gas-surface interaction owing to the minimal effect of variations in buoyancy and turbulence in the transport [52]. For the sake of simplicity, a cylindrical pipe is consider as shown in the Figure 3.1. The pipe surface is smooth thus the area of contact will be the geometrical area of pipe. Length and diameter of pipe must have a low uncertainty with significant Index (SI) < 1% as it contributes to our measurements.

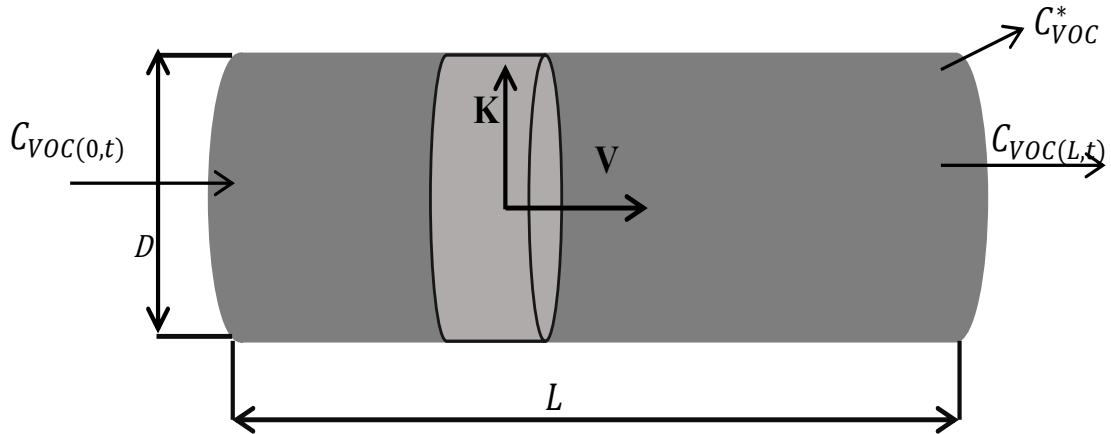


Figure 3.1: Scheme of mass balance over a test pipe.

### 3.2 Amount of VOC adsorbed and equilibrium constant

The measurand  $C_{A,e}$  is defined as “The amount of VOC adsorbed per unit area of wall at equilibrium” it can be calculated by mass balance using the information about the mixture entering and leaving the test pipe. The amount leaving the test pipe per unit time ( $q_{VOC,out}$  mol·min<sup>-1</sup>) is lowered from the amount entering the test pipe per unit time ( $q_{VOC,in}$ , mol·min<sup>-1</sup>) by the amount in moles adsorbed on the wall ( $dn_{VOC,wall}$ ) while the mixture is passing through the test pipe.

$$q_{VOC,in} = q_{VOC,out}(t) + \frac{dn_{VOC,wall}(t)}{dt} \quad \left[ \frac{\text{mol}}{\text{min}} \right] \quad (3.4)$$

The measurand ( $C_{A,e}$ ) can be calculated as the integral by parts on time of the difference between the amount entering ( $q_{VOC,0}$ ) and leaving ( $q_{VOC,L}$ ) the test pipe per unit time. The time interval is from clean pipe ( $t_0$ ) to saturated pipe ( $t_\infty$ ). The amount is referred to the unit surface area ( $A$ ) of the wall.

$$\begin{aligned} C_{A,e} &= \frac{n_\infty}{A} = \int_{t_0}^{t_\infty} \frac{q_{VOC,in} - q_{VOC,out}(t)}{A} dt \\ C_{A,e} &= \frac{q_{VOC,in}}{A} \int_{t_0}^{t_\infty} \left( 1 - \frac{q_{VOC,out}(t)}{q_{VOC,in}} \right) dt \end{aligned} \quad (3.5)$$

The areic amount of VOC at the equilibrium is thus the sum ( $n_\infty$ ) of all the aliquots of VOC adsorbed on the wall ( $n_{VOC,wall}$ ) moment by moment from the beginning of the exposure till the equilibrium, theoretically till infinitive time ( $t_\infty$ ).

The amount of VOC entering the test pipe ( $q_{nVOC,in}$ , mol·min<sup>-1</sup>) is independent of time, and it can be calculated as:

$$q_{VOC,in} = q_{v,g} C_{VOC,in} = q_{v,g}^o \chi_{VOC} \frac{P^o}{RT^o} \quad (3.6)$$

Where  $C_{VOC,in}$  (mol·ml<sup>-1</sup>) is the mole concentration, i.e., amount concentration, of VOC and  $q_{v,g,in}$  (ml·min<sup>-1</sup>) is the total volumetric gas flow rate feeding the test pipe;  $\chi_{VOC}$  (mol·mol<sup>-1</sup>) is the mole fraction, i.e., the amount fraction, of VOC in the mixture and  $q_{V0g}$  (Sml·min<sup>-1</sup>) is the total standard volumetric gas flow rate (0 °C, 1 bar), its value is practically uniform along the test pipe, i.e., the amount of VOC segregated at the wall is negligible with respect to the total amount flow rate;  $T^o$  (K) and  $P^o$  (kPa) are the temperature and pressure at standard conditions (0 °C, 1 bar) and  $R$  (L·atm · K<sup>-1</sup>·mol<sup>-1</sup>) is the gas constant. While the ratio between the amount flow rate of VOC entering and leaving the test pipe can be expressed as the dimensionless mole fraction of VOC ( $\zeta$ ) as long as the total mole flow rate accounted as standard volumetric flow rate ( $q_{V0g}$ ) is uniform along the test pipe (in other words as long as the amount of VOC adsorbed is negligible with

respect to the total amount of gas). A baseline signal of FID is related to several effects, and to account for all the possible effects, clean air has been flushed in the system [29]. FID signal shift from the baseline is proportional to the total amount of carbon burned in the flame in the unit time, and the response factor is proper of each substance mainly based on the molecular formula [29]. This quantity can be calculated from the signal as:

$$\zeta(t) = \frac{q(\text{Voc,out})}{q(\text{VOC,in})} = \frac{\chi(\text{Voc,out})}{\chi(\text{Voc,in})} = \frac{S_t - S_{\text{Air}}}{S_{\text{VOC}} - S_{\text{Air}}} \quad (3.7)$$

Where  $S$  (mV, in the case of FID) is the signal from the detector when flowing the Zero Air ( $S_{\text{Air}}$ ), the VOC Mixture from bypass ( $S_{\text{VOC}}$ ), the gas coming from the test pipe at time  $t$  ( $S(t)$ ), equation 3.8 is the final shape of the measurand equation, where  $\zeta$  is calculated from equation 3.7 and  $q_{\text{VOC,in}}$  is calculated from equation 3.6.

$$C_{A,e} = \frac{q_{v,g}^o \chi_{\text{VOC}} P^o}{A RT^o} \int_{t_0}^{t_\infty} \left( 1 - \frac{S_t - S_{\text{Air}}}{S_{\text{VOC}} - S_{\text{Air}}} \right) dt \quad \left[ \frac{\text{mol}}{\text{m}^2} \right] \quad (3.8)$$

The equilibrium constant  $K_e$  [m] can be calculated using equation 3.3 after calculating  $C_{A,e}$  or directly by re-shaping equations 3.3 and 3.8 considering the surface area of the pipe as the contact area of the test pipe.

$$K_e = \frac{q_{v,g}^o \cdot P^o \cdot T}{\pi D L T^o (P_{\text{atm}} + dP_{\text{wc}})} \int_{t_0}^{t_\infty} \left( 1 - \frac{S_t - S_{\text{Air}}}{S_{\text{VOC}} - S_{\text{Air}}} \right) dt \quad \left[ \frac{\text{mol}}{\text{m}^2} \right] \quad (3.9)$$

During the adsorption (from  $t_0$  to  $t_\infty$ ), the ideal plug flow ( $\zeta = 1$ ) is shifted to the actual dimensionless mole fraction ( $\zeta(t)$ ) because of adsorption, the integral of the difference ( $1 - \zeta(t)$ ) between the ideal dimensionless mole fraction. The actual one is the amount of adsorption effect in the test pipe.

### Procedure for equilibrium constant ( $K_e$ )

The procedure is aimed to realize the ideal conditions at which the measurand is realized. The pipe must be cleaned and then exposed to the VOC mixture at a time interval; after saturation, the pipe is cleaned again, and the second measurement of desorption is performed. For cleaning the pipe, scenario B is set till the signal is stabilized at  $S_{\text{ZeroAir}}$ .

After cleaning the test pipe, the pipe is maintained clean while the device is saturated with VOC (switch to scenario A first and then scenario C) till the signal is stabilized at  $S_{\text{VOC,mixture}}$  for the mixture. In these conditions, the pipe is exposed to a VOC mixture (switch to scenario D) till the signal is stabilized at  $S_{\text{VOC,mixture}}$  for mixture again.

Table 3.1: The sequence of configurations on measurement.

switch	Valve	$S_\infty$	Test Pipe		Gas	Operation and Effects
B		$S_{Air}$	In	Clean	Zero	Cleaning device and test pipe till Flat signal
B→A	$V_{s2}$	$S_{Air}$	Off	Clean	Zero	Spike ( $t_{s1}$ ) at switch
A→C	$V_{s1}$	$S_{Mix}$	Off	Clean	VOC	Spike ( $t_{s2}$ ) at switch, $t_{u0}$ , Saturating device
C→D	$V_{s2}$	$S_{Mix}$	In	Sat.	VOC	Spike ( $t_{s3}$ ) at switch Signal depletion ( $t_{d1}$ ) after a device residence time Spike ( $t_{s4}$ ) after test pipe residence times $t_{u1}$
D→C	$V_{s2}$	$S_{Mix}$	Off	Sat.	VOC	Spike ( $t_{s5}$ ) at the switch, Cleaning device
C→A	$V_{s1}$	$S_{Air}$	Off	Sat.	Zero	Spike ( $t_{s6}$ ) at switch $t_{d0}$ Spike ( $t_{s7}$ ) at the switch
A→B	$V_{s2}$	$S_{Air}$	In	Clean	Zero	Signal increase ( $t_{u2}$ ) after a device residence time Spike ( $t_{s8}$ ) after test pipe residence times, $t_{d2}$

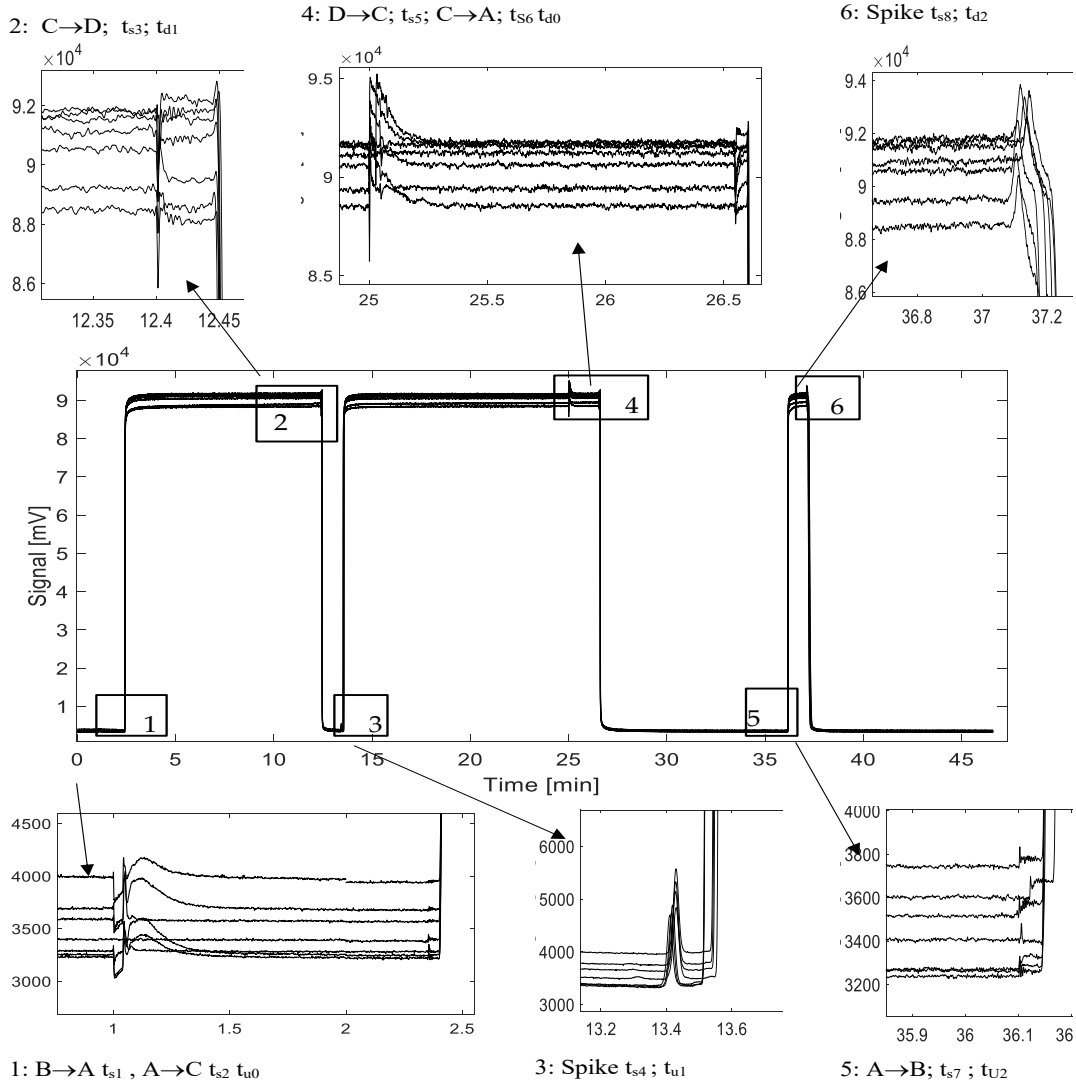


Figure 3.2: FID signal during measurement, spike times of events from Table 3.2 are reported at the boxes which zoom on the signal. Experimental raw data for the sample Sulfinert®A at 100 SmL/min, 6 repeated experiments

The procedure reported in Table 3.1 and shown in Figure 3.2 as the sequence of scenarios and switches performed during a single measurement the process is completed till desorption. The characteristic time corresponding to Figure 3.2 is reported in Table 3.2.

Table 3.2: Correspondence of signal times with residence/contact times, box refers to figure 3.2

Time	Box	Event	Characteristic Time
Spike $t_{s1}$	1	B→A switch	
Spike $t_{s2}$	1	A→C switch	
$t_{u0}$	1	VOC Mixture reaches FID	$t_{u0} - t_{s2}$ Residence time from $V_{s1}$ to detector no test pipe
Spike $t_{s3}$	2	C→D switch	
$t_{d1}$	2	Air entrapped reaches FID	$t_{d1} - t_{s3}$ Residence time from $V_{s2}$ to detector
Spike $t_{s4}$	3	VOC Mixture reaches FID without VOC (all adsorbed on the wall)	$\tau_r = t_{s4} - t_{d1}$ Residence time in test pipe
$t_{u1}$	3	VOC starts to overpass pipe	Delay of VOC appearance
Spike $t_{s5}$	4	D→C switch	
Spike $t_{s6}$	4	C→A switch	
$t_{d0}$	4	Zero Air reaches the FID	$t_{d0} - t_{s6}$ Residence time in the device without test pipe
Spike $t_{s7}$	5	A→B switch	
$t_{u2}$	5	VOC Mixture entrapped reaches FID	$t_{u2} - t_{s7}$ Residence time from $V_{s2}$ to the detector
Spike $t_{s8}$	6	Zero Air reaches FID	$\tau_r = t_{s8} - t_{u2}$ Residence time in test pipe
$t_{d2}$	6	VOC starts to overpass pipe	Delay of VOC disappearance

Experiments can be designed by allowing the gas mixture and air in different sequences for measurements and obtaining the data of our interest. FID of gas chromatograph GC-450 is used as a detector. FID is turning on for some time to get a stable response of FID. The experiment is arranged by different steps of switching valve  $V_{s1}$  and  $V_{s2}$ . The objective is to use less gas and perform the test in the least possible time with maximum stability.

### 3.3 Determination of irreversible losses

Gases when come into contact with metals they reacted sharply, and reach an equilibrium. In some materials like PFA, the losses due to permeation are a major concern for sampling. These losses were calculated based on the difference of the response signal in test pipe and bypass after the equilibrium. The signal in the

test pipe had a value lower than that of the signal in bypass; this is due to either irreversible reaction or permeation. The permeation can be explained by Fick's law of diffusion.

$$J = -D_j \frac{d\varphi}{dx} \quad (3.10)$$

Where  $J$  is the mass flux per unit area per unit time escapes from pipe due to permeation.  $D_j$  is the diffusivity coefficient,  $d\varphi$  is the concentration gradient over the thickness  $dx$  of the pipe. The mass escapes per unit time per unit area ( $J$ ) is measured by two different approaches.

In first approach, the difference of the signal is measured from the signal of a saturated pipe and bypass  $S_{VOC,in}$  and  $S_{VOC,out}$  as shown in the first part of Figure 3.3 as dimensionless concentration  $\zeta$ . The mass flux (mass per unit area per unit time) is calculated from the difference of  $[q_{VOC,in} - q_{VOC,out}(t)]$  as  $\text{mol} \cdot \text{min}^{-1}$ .

$$\frac{dn_{voc}}{dt} = q_{(Voc,in)} - q_{(VOC,out)} \quad (3.11)$$

$$J = \frac{dn_{voc}}{A \cdot dt} = \frac{C_{Voc} q_{vg}}{A} \left( 1 - \frac{q_{voc,out}}{q_{voc,in}} \right) = \frac{q_{v,g}^o \chi_{Voc}}{A} \frac{P^o}{RT^o} (1 - \xi(t)) \quad (3.12)$$

The second approach calculates the average losses using the integral of the curve. The mixture is stored in the test pipe, and the response in bypass is observed as maximum concentration. The stored mixture loses the concentration due to reaction, leading to a depletion of the stable curve, as shown in Figure 3.3. The approach helps in measuring the irreversible losses even for materials where these losses are very negligible. For example, the difference of signal in test pipe and bypass is very hard to measure with Sulfinert® pipe. But if we leave the test pipe for a time, a depletion in signal is observed that can be measured by the integral of the curve.

From the integral of curve starting from  $t_{b1}$  to  $t_{b2}$ , we calculate the mass escapes due to permeation or irreversibly reacted per unit area over a time  $\delta t = t_{s3} - t_{s1}$  as mass flux  $J$  using equation 3.13:

$$J = \chi_{voc} \frac{q_v^o \cdot P^o}{RT^o} \frac{\int_{t_{b1}}^{t_{sr2}} [1 - \xi(t)] dt + \int_{t_{sr2}}^{t_{b2}} [1 - \xi(t)] dt}{A(t_{s3} - t_{s1})} \quad (3.13)$$

$$J = \chi_{voc} \frac{q_v^o \cdot P^o}{RT^o} \frac{\int_{t_{sr2}}^{t_{b2}} [1 - \xi(t)] dt}{A(t_{sr3} - t_{s1})}$$

$\int_{t_{b1}}^{t_{s2}} [1 - \xi(t)] dt$  This part of the integral is  $[\xi - \xi = 0]$  over time as the signal of VOC in the bypass.

If the phenomenon is purely diffusion, the diffusivity constant  $D_j$  can be calculated using Fick's law.

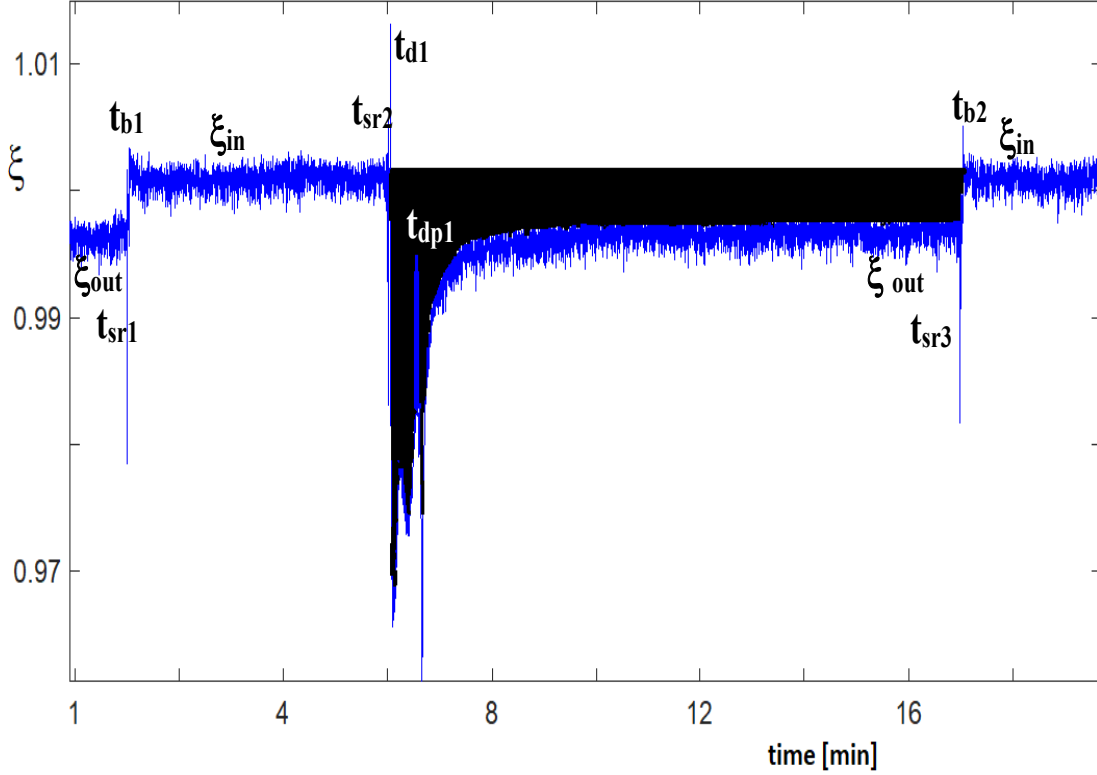


Figure 3.3: Model for irreversible losses in pipes, PFA  $100\text{Sml}\cdot\text{min}^{-1}$ .

$$D_j = -J \frac{dx}{d\varphi} = q_v \frac{\sum_{t_{s2}}^{b_2} [1 - \xi(t)] dt \cdot dx}{\pi DL (t_{sb2} - t_{sb1})} \quad (3.14)$$

Here  $d\varphi$  is the concentration gradient assuming outside concentration is null.  $d\varphi$  becomes  $C_{VOC}$ . The diffusivity constant  $D_j$  [ $\text{mol}\cdot\text{m}^{-1}\cdot\text{min}^{-1}$ ] can be compared between different materials.

### 3.3.1 Procedure for irreversible losses

From the analysis of VOC signal in bypass and in the test pipe, the irreversible losses can be calculated. For this purpose, the system is left for saturation in bypass and pipe to reach equilibrium. Once the equilibrium establishes in the phenomenon D, the switch from phenomenon D to C is made switch  $t_{sr1}$  (and  $t_{s4}$  in Figure 3.2 to analyze the signal in bypass. After a known storage time in which the irreversible interactions continue to occur, the switch from C to D is made to observe the depletion due to reaction/permeation. The sequence of scenarios while switching is reported in Table 3.3.



Table 3.3: Sequence of scenarios during irreversible losses estimation

Time	Event	Characteristic Time
Spike $t_{s1}$	D→C switch	
$t_{b1}$	VOC starts to overpass pipe	$t_{b1} - t_{s1}$ Residence time from $V_{s1}$ to detector no test pipe
Spike $t_{s2}$	C→D switch	
$t_{d1}$	VOCs entrapped reaches FID	$t_{d1} - t_{s2}$ Residence time from $V_{s1}$ to detector no test pipe
$t_{dp1}$	Fresh VOCs reaches FID	$\tau_R = t_{d1} - t_{dp1}$ Residence time of test pipe
Spike $t_{s3}$	D→C switch	
$t_{b2}$	VOC starts to overpass pipe	$t_{b2} - t_{s3}$ Residence time from $V_{s1}$ to detector no test pipe

The experiments are repeated many to at different storage times. The reproducibility over different residence times has been observed by repeating the measurements.

Another approach is the quantification of the difference of signal, which is proportional to the mass irreversibly interacted to the pipe either by reaction or permeation, diffusion. For this purpose, the signal in pipe phenomenon D is observed, and the signal of VOC at bypass phenomenon C is measured for a period to observe a stable signal.

### 3.4 Determination of mass release due to memory effect

Gases upon contact with surfaces reacted sharply, and reach a reversible and irreversible equilibrium. Upon flushing, with the clean air (B), the reversible masses are released instantly, while the irreversible losses are subject to many factors, including the type of materials. In some materials like PFA and Stainless steel, the memory effect is a major concern for sampling. These mass releases due to memory effect were calculated based on the difference of the response signal in pipe and bypass after the cleaning of the test pipe (B). Due to VOC release, the signal of air in the test pipe had a higher value than that of signal in bypass; this is due to either reversible mass not completely released or due to memory effect. The mass released due to memory can be calculated using two different approaches.

In first approach, the difference of the signal is measured from the signal of a cleaned pipe and bypass  $S_{AIR,in}$  and  $S_{AIR,out}$  as shown in Figure 3.4 as dimensionless concentration  $\xi$ . The mass flux is proportional to the  $[q_{in}(t) - q_{out}(t)]$ .

$$\frac{dn_{voc}}{dt} = q(Voc,out) - q(Voc,in) \quad (3.15)$$

$$M = \frac{dn_{voc}}{A \cdot dt} = \frac{C_{VOC} q_{vg}}{A} \left[ \frac{q_{voc,out}}{q_{voc,in}} - 1 \right] = \frac{q_{v,g}^o \chi_{Voc}}{A} \frac{P^o}{RT^o} [\xi(t) - 1]$$

The second approach calculates the average release using the integral of the curve. The air is stored in the cleaned pipe, and the response in bypass is observed as air concentration. This approach helps in estimating the release with materials having a small memory effect. The stored air capture, the mass of VOCs, is released due to the memory effect, which leads to a rise of stable curve upon arrival to FID, as shown in Figure 3.4.

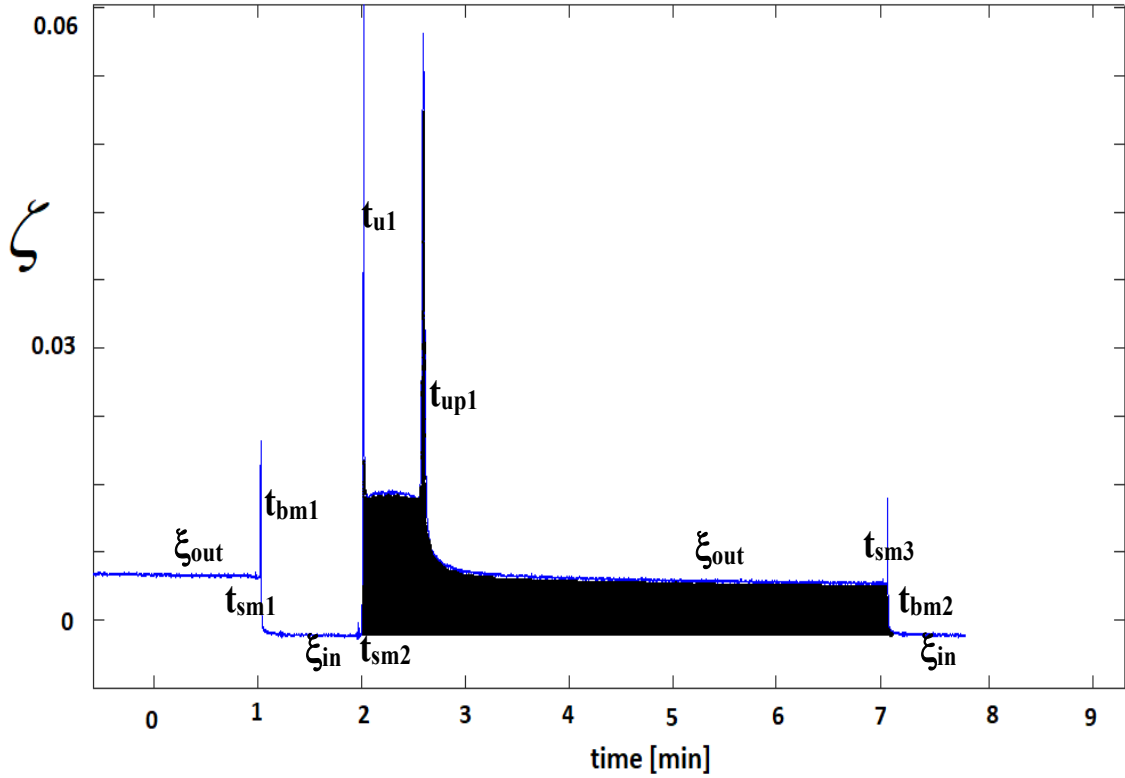


Figure 3.4: Model for memory effect in pipes, PFA 100Sml·min<sup>-1</sup>.

From the integral of this area, we calculate the mass releases due to permeation per unit area as mass flux  $M$  using equation 3.21.

$$M = C_{VOC} q_{vg} \frac{\sum_{t_{bm1}}^{t_{sm2}} [0 - \xi(t)] dt}{\pi DL \cdot (t_{bm2} - t_{bm1})} = \chi_{voc} \frac{q_{vg}^o \cdot P^o}{RT^o} \frac{\sum_{t_{bm1}}^{t_{sm2}} [0 - \xi(t)] dt}{\pi DL (t_{sb2} - t_{sb1})} \quad (3.16)$$

### 3.4.1 Procedure for memory release

From the analysis of air signal in bypass and in test pipe cleaned after the saturation, the mass releasing due to memory effect can be calculated. For this purpose, the system is left for cleaning in bypass and pipe to reach equilibrium. Once the equilibrium establishes in phenomenon B, the switch from phenomenon B to A is made to analyze the air signal in bypass. After a known storage time in which the irreversible interactions continue to occur, the switch from A to B is made to observe the release of VOCs due to the memory effect. The experiments are repeated many times to observe at different cleaning times. The sequence of scenarios while switching is reported in Table 3.4. The reproducibility over different residence times has been observed by repeating the measurements at different lengths for different materials.

Another approach is the quantification of the difference of signal, which is proportional to the mass release due to memory from the pipe. For this purpose, the signal in pipe phenomenon B is observed, and the signal of air at bypass phenomenon A is observing for a period to observe a stable signal.

Table 3.4: Sequence of scenarios during memory release flux ( $M$ ) estimation

Time	Event	Characteristic Time
Spike $t_{sm1}$	B→A switch	
$t_{bm1}$	AIR starts to overpass pipe	$t_{bm1} - t_{sm1}$ Residence time from $V_{s1}$ to detector no test pipe
Spike $t_{sm2}$	A→B switch	
$t_{u1}$	Air entrapped reaches FID	$t_{u1} - t_{sm2}$ Residence time from $V_{s1}$ to detector no test pipe
$t_{up1}$	Fresh VOCs reaches FID	$\tau_R = t_{u1} - t_{up1}$ Residence time of test pipe
Spike $t_{sm3}$	B→A switch	
$t_{bm2}$	AIR starts to overpass pipe	$t_{bm2} - t_{sm3}$ Residence time from $V_{s1}$ to detector no test pipe

## 3.5 Bias corrections

### 3.5.1 Bias correction for air inside the pipe

The main source of bias comes from the presence of a volume of zero air entrapped in the pipe at switch C→D. The first effect of zero air entrapped is to create a depletion in the signal, which modifies the integral ( $I$ ) of dimensionless mole fraction ( $\xi$ ) by a quantity that is theoretically equal to the residence time ( $I = (\xi_{Mix} - \xi_{Air}) \tau_R = (1-0)\tau_R = \tau_R$ ). The effect started when the air entrapped reaches the FID ( $t_{d1}$ ) and has a duration equal to the residence time ( $\tau_R = t_{s4} - t_{d1}$ ). The second effect is the desorption from the part of the device that connects the test pipe to the detector. This part is saturated by VOC at the  $V_{S2}$  switch time. The effect acts while the air entrapped in the pipe at the  $V_{S2}$  switch time ( $t_{s1}$ ) is crossing that part of the system. The second effect starts to act when the air entrapped reaches the FID ( $t_{d1}$ ), i.e., the  $V_{S2}$  switch time plus the residence time in the part, and has a duration equal to the residence time in the test pipe ( $\tau_R = t_{s4} - t_{d1}$ ). A third effect is the adsorption of the same part of the system that is saturated again while the signal raises up. The third effect starts to act when the gas mixture reaches the FID detector after the  $VS2$  switch ( $t_{s4}$ ) and is persisting till saturation of the part. The second and the third effects are equal and opposite. This results in a bias on the integral. This bias can be corrected by subtracting by two different approaches.

A: Subtracting the residence time:

In approach A, the residence time in the test pipe is subtracted from the total integral, which leads to equation 3.17 and as illustrated in Figure 3.5. This approach is working with all tested materials.

$$I = \int_{t_0}^{t_\infty} [1 - \zeta(t)] dt - \tau_r = \int_{t_0}^{t_\infty} [1 - \zeta(t)] dt - t_{res} = I_t - t_{res} \quad (3.17)$$

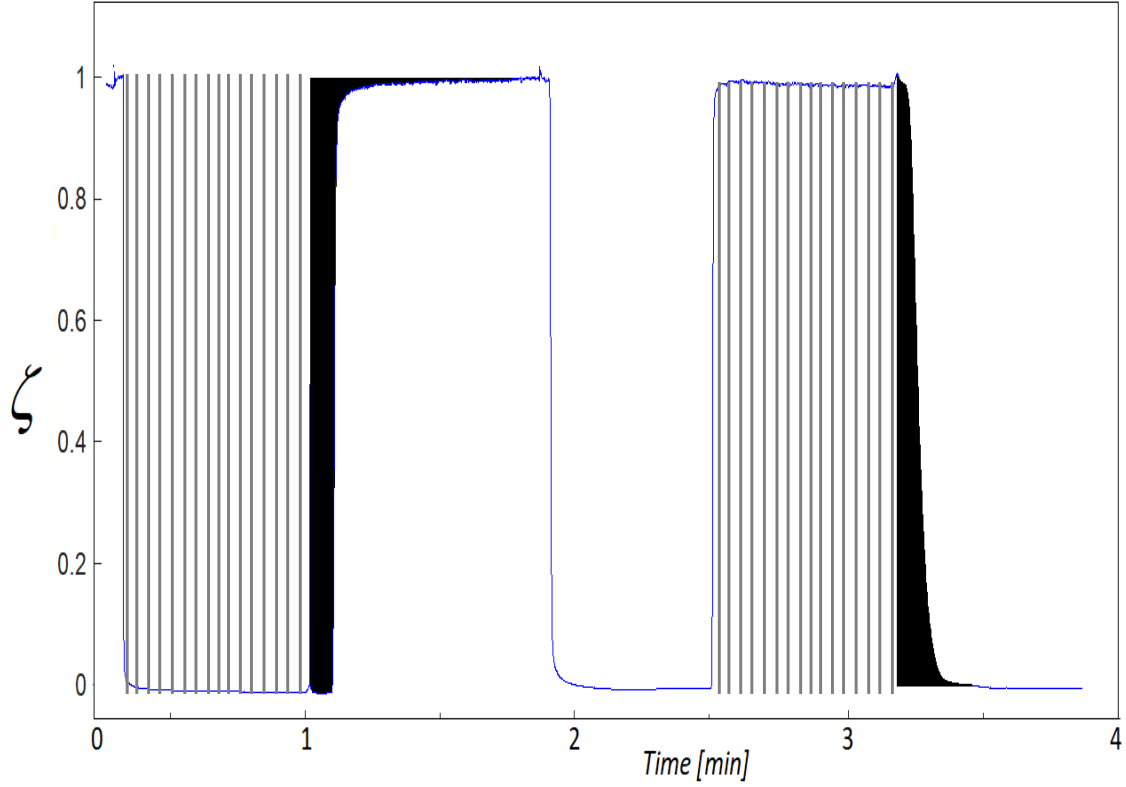


Figure 3.5: Approach A for bias correction: Lined area represents residence time, while black area represents net integral.

The residence time is the ratio of volume and flowrate while. The flow rate is measured as molar flow expressed in  $\text{Sml}\cdot\text{min}^{-1}$ . This leads to the final equation for  $C_{A,e}$  can be written as equation 3.18 explicitly for molar fraction using the equation for residence time.

$$C_{A,e} = \frac{\chi V_o C}{R} \left( \frac{q_{vg}^o P^o I_t}{\pi D L T^o} - \frac{D (P_{atm} + dP_{wc})}{4 T_{wc}} \right) \left[ \frac{\text{mol}}{\text{m}^2} \right] \quad (3.18)$$

The equilibrium constant  $K_e$  can be calculated directly using the  $C_{A,e}$  value or using the equation 3.18 for obtaining equation 3.19 for  $K_e$ :

$$K_e = \frac{q_{vg}^o P^o T_{wc} I_t}{\pi D L T^o (P_{atm} + dP_{wc})} - \frac{D}{4} \quad [m] \quad (3.19)$$

B: Splitting the integral:

In the other approach B, the bias can be corrected by splitting the integral in desorption in the interval for bypass and adsorption in the interval for the test pipe. The desorption mitigates the depletion of the signal from the part of the device that connects the test pipe to the detector, and the mitigation is restored

by adsorption when the signal raises up. This effect can be clearly visible in data obtained with all metallic pipes. The bias can be corrected by the summation of each separate integral for adsorption and desorption as shown in Figure 3.6 black and red, respectively, leading to equation 3.20

$$I = \int_{t_{D1}}^{t_{S4}} [0 - \zeta(t)] dt + \int_{t_{S4}}^{t_{\infty}} [1 - \zeta(t)] dt = I_{des} + I_{ads} \quad [\text{min}] \quad (3.20)$$

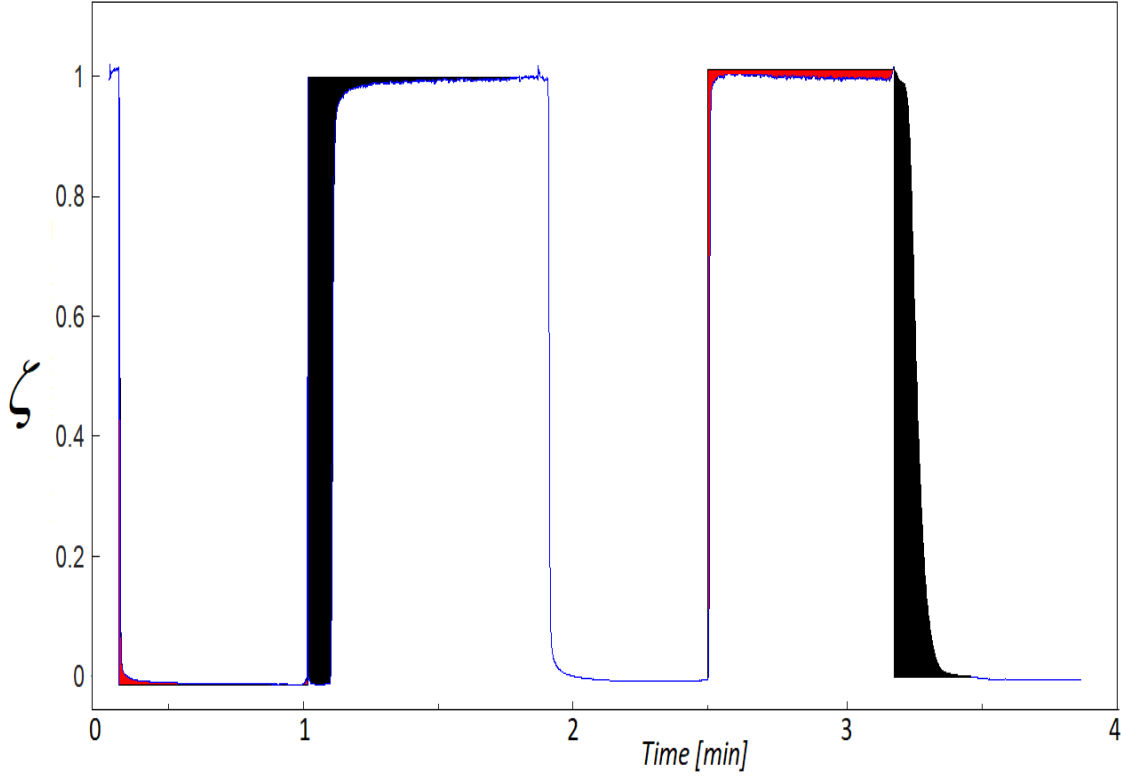


Figure 3.6: Method B for calculating the integral: Red area represents the desorption of bypass, and black represents the adsorption over the test pipe.

The second approach was much more reproducible and was used in this work. The measurand equation with approach B bias correction can be written for molar fraction explicitly and signal as equation 3.21:

$$C_{A,e} = \frac{\chi_{VOC}}{R} \frac{q_{vg}^o \cdot P^o}{\pi DL T^o} (I_{des} + I_{ads}) \quad \left[ \frac{\text{mol}}{\text{m}^2} \right] \quad (3.21)$$

$$C_{A,e} = \frac{\chi_{VOC}}{R} \frac{q_{vg}^o \cdot P^o}{\pi DL T^o} \left( \int_{t_{d1}}^{t_{S4}} \left( \frac{S_{Air} - S_t}{S_{VOC} - S_{Air}} \right) dt + \int_{t_{S4}}^{t_{\infty}} \left( \frac{S_{VOC} - S_t}{S_{VOC} - S_{Air}} \right) dt \right)$$

while the measurand equation for direct estimation of  $K_e$  can be written as:

$$K_e = \frac{q_{vg}^o \cdot P^o \cdot T}{\pi DLT^o (P_{atm} + dP_{wc})} (I_{des} + I_{ads}) \quad [m] \quad (3.22)$$

$$K_e = \frac{q_{vg}^o \cdot P^o \cdot T}{\pi DLT^o (P_{atm} + dP_{wc})} \left( \int_{t_{d1}}^{t_{S4}} \left( \frac{S_{Air} - S_t}{S_{VOC} - S_{Air}} \right) dt + \int_{t_{S4}}^{t_{\infty}} \left( \frac{S_{VOC} - S_t}{S_{VOC} - S_{Air}} \right) dt \right)$$

The same reasoning can be applied to the desorption section of the experiment to calculate the areic desorbed amount corrected for the bias that comes from the VOC mixture entrapped in the pipe at switch A→B to calculate the measurand. During the adsorption interval (from  $t_{u2}$  to  $t_{s8}$ ), the gas entrapped in the pipe at  $t_{s5}$  adsorbs the VOC to the connection between the test pipe and the detector and modifies the dimensionless mole fraction from the ideal VOC mixture ( $\xi = 1$ ) entrapped to the actual dimensionless mole fraction ( $\xi$ ), the integral of the difference ( $1 - \xi$ ) between the ideal dimensionless mole fraction, and the actual one is the amount of adsorption effect in the connection between the test pipe and the detector. While in the desorption interval (from  $t_{s8}$  to  $t_{\infty}$ ), the ideal zero air plug flow ( $\xi = 0$ ) is shifted to the actual dimensionless mole fraction ( $\xi$ ) because of the desorption, the integral of the difference ( $0 - \xi$ ) between the ideal dimensionless mole fraction, and the actual one is the amount of desorption effect in the test pipe and in the connection between the test pipe and the detector. The sum of the two integrals is the desorption effect in the test pipe only.

$$I = \int_{t_{u2}}^{t_{s8}} [1 - \zeta(t)] dt + \int_{t_{s8}}^{t_{\infty}} [0 - \zeta(t)] dt = I_{des} + I_{ads} \quad [\text{min}] \quad (3.23)$$

the mass desorbed from the unit surface area, and the equilibrium constant can be calculated using equation 3.24.

$$C_{A,e} = \frac{\chi_{VOC}}{R} \frac{q_{vg}^o \cdot P^o}{\pi DL \cdot T^o} \left( \int_{t_{u2}}^{t_{s8}} \left( \frac{S_{Air} - S_t}{S_{VOC} - S_{Air}} \right) dt + \int_{t_{s8}}^{t_{\infty}} \left( \frac{S_t - S_{Air}}{S_{VOC} - S_{Air}} \right) dt \right) \quad (3.24)$$

$$K_e = \frac{q_{vg}^o \cdot P^o \cdot T}{\pi DLT^o (P_{atm} + dP_{wc})} \left( \int_{t_{u2}}^{t_{s8}} \left( 1 - \frac{S_{Air} - S_t}{S_{VOC} - S_{Air}} \right) dt + \int_{t_{s8}}^{t_{\infty}} \left( \frac{S_t - S_{Air}}{S_{VOC} - S_{Air}} \right) dt \right)$$

## 3.6 Experimental biases

Actual measurements are often quite different from than above discussed ideal methodology. There are many factors affecting our measurements. Other possible sources of bias are the interactions with different parts of the system. Valves and pressure reducers are the main sources of uncertainty. Valves have internal surfaces uncoated that can react with Acetone, reducing the accuracy of the method. Pressure reducers have membranes that can release substances that interfere with the detector signal. A detailed analysis of all experimental biases is discussed in the sub sequent section.

### 3.6.1 Instability of FID and system saturation

The electronics of the gas chromatograph need a certain time to stabilize the signal of FID. This affects the signal of air and VOCs and thus affects our final calculations of the equations 3.21, 3.22, and 3.23. In some cases, especially at the lower flow rate, this effect is evident. The signal of FID rises over time, and this may take hours for the detector to completely stabilize. The same effect can occur due to the saturation of the system. Initially, when the system is not saturated, some VOCs are going to interact over the parts of the system and detector. After the saturation, the signal becomes stable and flat. For the zero gas, the effect of instability of FID is relatively lower. However, the cleaning of bypass affects the signal contrary to the saturation in the case of VOC mixture the signal will drop continuously with time.

The stability of the signal of zero air and VOC mixture depends on the time of operations and the stability of electronics and the joints and fittings in the line that can be seen in Figure 3.7. The stability of air signal (zero lines) depends on the purity of zero air and working conditions [30]. The signal with the mixture is rising with time with some fluctuation after initial stabilization, as seen in box 2 of Figure 3.7. The difference of signal in bypass and test pipe is reducing over time indicates the saturation and establishment of equilibrium. After the complete establishment of equilibrium, the difference is due to the irreversible reaction or permeation that can be calculated after the complete establishment of equilibrium.

The rise of the curve over time in the pipe, as shown in Figure 3.7, is combined with the effect of saturation of the test pipe. The device's saturation and stability can be estimated by observing the signal in the bypass at different times from the start of the experiment. Figure 3.8 shows the signal in bypass with two different flow rates at three different groups of time from the start. The signal was quite reproducible for all the flow rates with a variation due to flow rate. The signal variation due to flowrate fluctuation was higher for the high flow rate, but a signal of FID was stable and reproducible and vice versa for the lower flow rate.



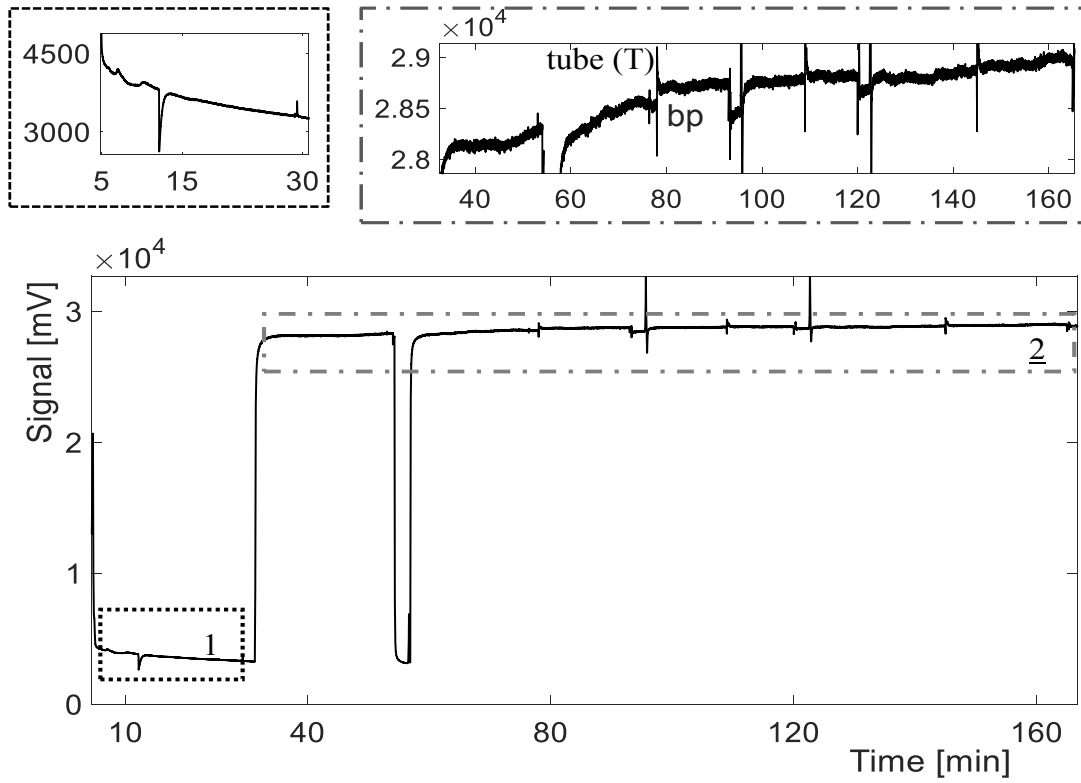


Figure 3.7: Stability analysis of signal with zero air and VOC mixture during an experiment on sulfiner® at  $32\text{Sml}\cdot\text{min}^{-1}$  flowrate.

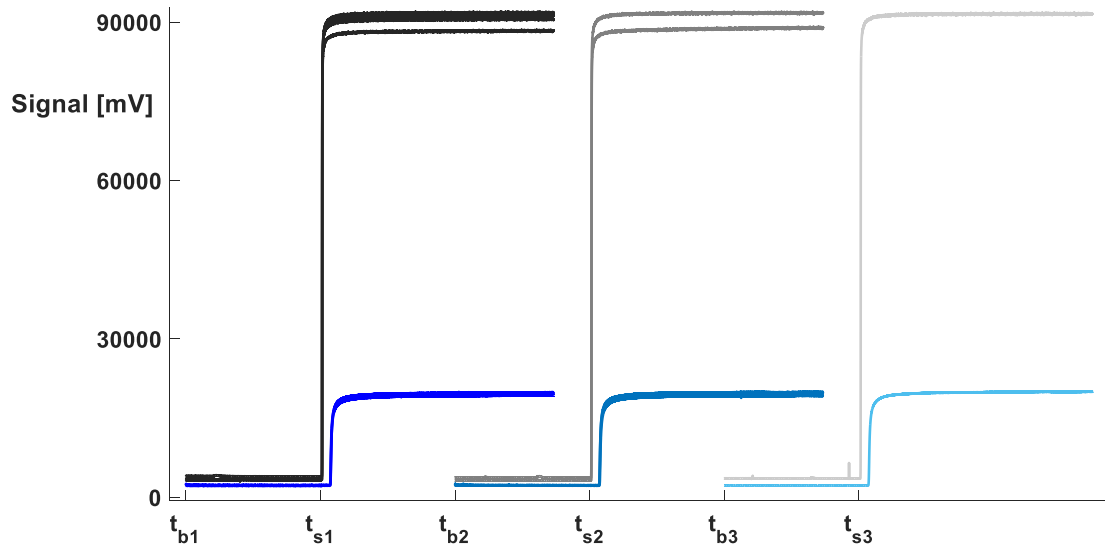


Figure 3.8: Signal for zero air and VOC mixture in bypass during  $100\text{Sml}\cdot\text{min}^{-1}$  flowrate (shown in black) and  $9\text{ Sml}\cdot\text{min}^{-1}$  shown in (blue). The intensity represents the distance from the saturation point.

The mean value of a stable signal over two minutes is considered for zero air and for VOC mixture as representative signal values, respectively. The signal is considered stable if the  $dS/dt \leq 100 mV \cdot min^{-1}$ . Where  $dS$  is the difference of averages of signal over  $ds = 2$  minutes. A comparison of the two criteria for VOC signal stability with  $dS = 0.5$  min and 2 mins for ten experiments with Sulfinert® 26 m pipe is shown in Figure 3.9. The slope calculated as the difference of averages over  $dt$  time reduces with time. For the criterion with  $dt = 2$  min, all the experiments were fully stable after 7 min of the switch, with a slope value less than  $100 mV \cdot min^{-1}$  while  $dt = 0.5$  min some experiments were not stable even after 12 mins. With the criteria 0.5 min after complete stabilization, the variance of the signal increases. This effect is more evident with smaller flowrate and higher residence times and can be confused with the stability of flowrate.

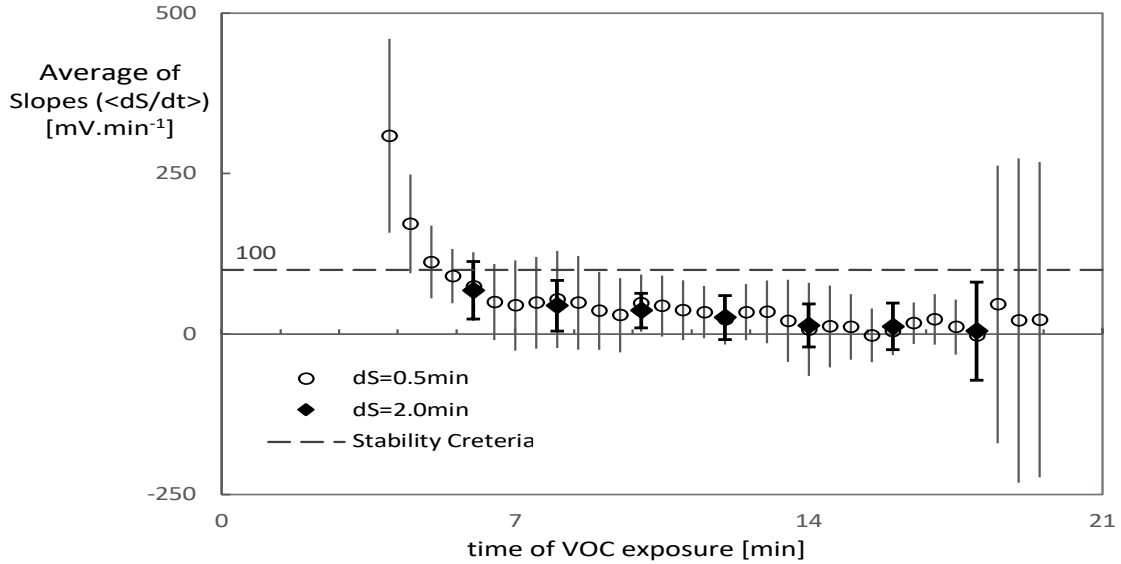


Figure 3.9: Stability of signal for VOC mixture for ten experiments at flowrate  $35 \text{ Sml} \cdot \text{min}^{-1}$ .

While the signal of air is falling with operation time having reduction of the slope with time as shown in box 1 of Figure 3.7. This effect is due to either stability of the electronics or the memory and cleaning effect of the bypass. The signal of VOC and air is analyzed in detail, and the effect of the stability of electronics is reduced by considering a correction to the signal based on a slope of the corresponding signal while using equation 3.12. A positive slope  $m_{VOC}$  was observed for VOC signal over time (before and after the experiment), and a negative slope ( $m_{AIR}$ ) was observed for air signal.

Both the signals are corrected using their slope as:

$$\begin{aligned}
S_{VOC} &= S'_{VOC} + m_{VOC}dt \\
S_{AIR} &= S'_{AIR} + m_{AIR}dt \\
\zeta(t) &= \frac{\chi(VOC, out)}{\chi(VOC, in)} = \frac{S_t - (S'_{AIR} + m_{AIR}dt)}{(S'_{VOC} + m_{VOC}dt) - (S'_{AIR} + m_{AIR}dt)} \quad (3.25)
\end{aligned}$$

### 3.6.2 Instability of flowrate

A fixed number of VOCs with less variation will produce a stable signal, and thus, a stable and constant flow rate is necessary to have stable amount of VOCs. The flow rate of both mixture and air steams is controlled by the sonic nozzle. However, the temperature of the sonic nozzle is poorly controlled, and thus, the flow rate varies due to the variation of temperature and density of flowing gas from the sonic nozzle. This effect becomes more dominant at a lower flow rate where the relative variance is higher. Besides the direct effect on the signal of VOC, the flow rate also vary the residence time of the test pipe and thus the integral of the curve.

The signal of VOCs behaves linearly with the flow rate of the VOC mixture that can be seen in Figure 3.10. The signal of VOCs is a function of the amount of carbon inside the gas; the higher the flowrate will, send a high amount of carbon to FID and thus leads to a higher signal. Ideally, for clean, dry air containing no hydrocarbon, the signal of air should not affect the flow rate. However, it was observed that changing flowrate of air through manual pressure reducer for column line; the signal rises with rising of flowrate to a maximum 4000 mV for a flowrate of 25 Sml·min<sup>-1</sup> and then decrease with the rise of flowrate as depicted in black (Figure 3.10). This may be because of some release from the membrane, which increases to a high level at 25Sml·min<sup>-1</sup> and then falls due to cleaning at a high flow rate. As expected, the change in airflow rate internally through electronic flow controller (EFC) in GC the change in response due to air flow change were negligible. The variation is reduced by applying proper control to the temperature of the sonic nozzle. Still, there is a significant amount that contributes as a source of uncertainty.

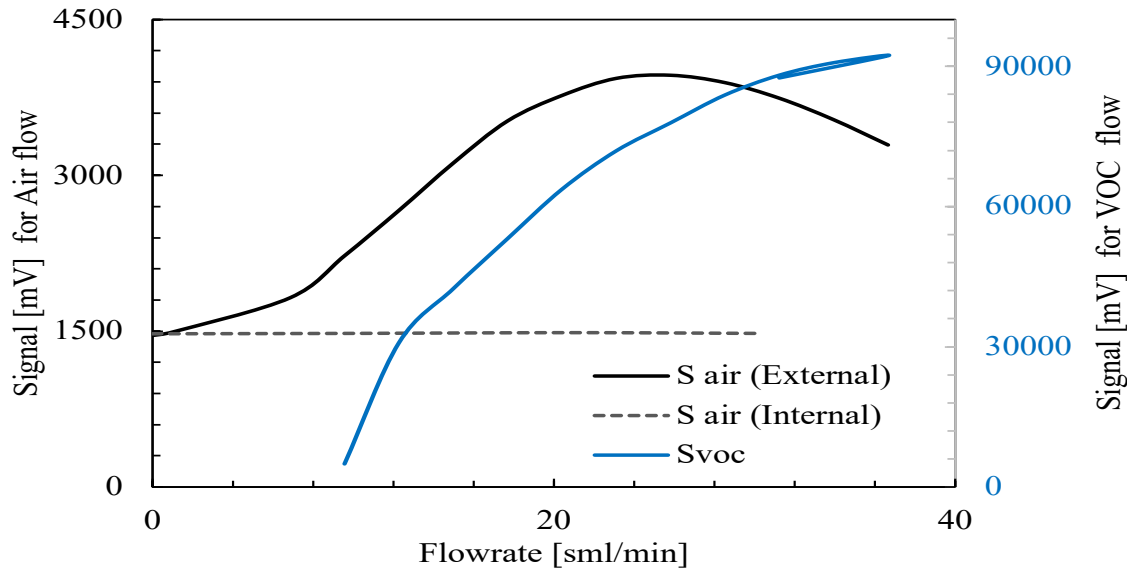


Figure 3.10: FID response signal against different flowrate for air flowing internally in the GC and externally (left) and VOC mixture (right).

### 3.6.3 Interactions in system

The interaction in the bypass leads to some losses and thus affects the shape of the input signal. While switching from Zero gas to mixture, the rise must be an instant and sharp jump to VOCs. However, due to losses in bypass, the signal takes time to stabilize the VOC signal. This effect is corrected by measuring the number of VOCs interacted in the bypass and subtracted from the total VOCs in the pipe as explained in section 3.5.1.

The mass balance over the pipe and bypass is shown in Figure 3.11. An amount of  $VOC_0$  enters the test pipe, and an amount of  $Air_0$  enters the bypass after the switching  $t_{s3}$  of Figure 2.4.

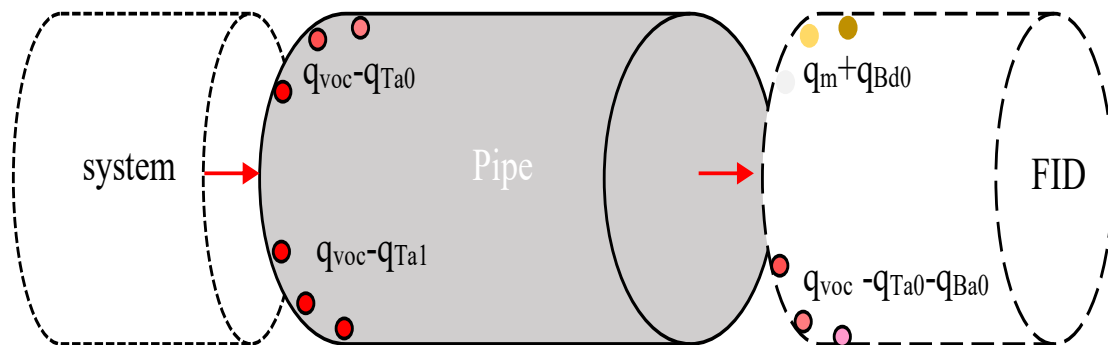


Figure 3.11: Scheme of sequences for mass balance over a test pipe and bypass.

**Air<sub>0</sub>**: This air is subject to clean the bypass, and the amount of VOCs adsorbed over the bypass surface is desorbed (amount  $q_{Bd0}$ ) by this molecule. This leads to VOC-rich air to FID. The following molecule will do the same but lesser rich as the bypass is relatively cleaned.

**VOC<sub>0</sub>**: This VOC is subject to subject to face a clean test pipe, and there the adsorption occurs with full potential. The mixture inside the pipe becomes lean of VOC with less amount of VOC (amount  $q_{TA0}$ ) when exposed to FID. The following molecules will do the same with lesser interactions and thus richer of VOC.

Table 3.5: Sequences of mass balance over a test pipe and bypass

time [ $t_R$ ]	Test Pipe in	Test Pipe out	FID
0+	$q_{voc}$	$q_m$	$q_{VOC}$
0+ $t_{Rcon}$	$q_{voc}$	$q_m$	$q_{VOC} \rightarrow q_m + q_{Bd0}$
0+ $t_{Rp}$	$q_{voc}$	$q_m \rightarrow q_{voc} - q_{Ta0}$	$q_m + q_{Bd0}$
0+ $t_{Rp}+t_{Rcon}$	$q_{voc}$	$q_{voc} - q_{Ta1}$	$q_{voc} - q_{Ta0} - q_{Ba1}$
0+ $2t_{Rp}+t_{Rcon}$	$q_{voc}$	$q_{voc} - q_{Ta3}$	$q - q_{Ta2} - q_{Ba3}$
$n \rightarrow (n+1)t_{Rp}$	$q_{voc}$	$q_{voc} - q_{Tan}$	$q - q_{Tan-1} - q_{Ban}$

Where 0+ is the initial time just after switching from C to D configuration and subscript 0 refers to phenomenon between 0 $\rightarrow$  $t_{Rcon}$  connection residence time.  $q_{Ta}$  is the amount of VOCs adsorbed over the test pipe at any time (0 $\rightarrow$ n). This is the required measurand mass adsorbed over the pipe at the time 0 $\rightarrow$ 1, the potential from the transfer is high, and it has a high speed. After a residence time, the saturation is expected to occur, and the potential for transfer decreases till it reaches equilibrium.

$q_m$  is the amount of VOCs released from the wall either due to memory effect or due to improper cleaning of the pipe. For a complete clean pipe,  $q_m$  is the amount due to memory of the test pipe.

$q_{Bd0}$  is the amount of VOCs desorbed by the clean air (stored inside the pipe) from the bypass (saturated before the switch from C to D). This phenomenon continues for a single residence time until the finishing of air in the test pipe and the VOCs arrived at the bypass. The potential for  $q_{Bd0}$  is the amount of VOCs adsorbed on the surface of bypass and the VOCs in the stored air. The amount of VOCs adsorbed on the surface depends on the saturation time of the device before the switch. In many cases, the bypass is saturated for time enough to reach equilibrium and is considered completely saturated. The amount of VOCs in the stored air ( $q_m$ ) varies from experiment to experiment. For the first experiment, when the air is stored in the pipe over a night for cleaning purposes, lesser VOCs are expected to be desorbed into the stored air from the cleaner pipe ( $q_m \cong 0$ ). and thus, decreases the potential of transfer for  $q_{Bd0}$ . While for the consecutive

experiments, the stored air becomes richer of VOCs ( $q_m > 0$ ) (due to not fully cleaned pipe or memory effect) and the potential for  $q_{Bd0}$  is decreases.

This phenomenon is clearer for Copper and PFA due to the memory effect of the test pipe and the long time required for cleaning the pipe ( $q_m \cong 0$ ). For the next experiment, the stored air is VOC richer (compare to the first ever experiment( $q_m > 0$ )) and has lesser potential for  $q_{Bd0}$ . A correction is needed for equation 3.23, subtracting the amount  $q_m$  by considering the signal of air in the pipe and not in bypass. This correction is important for polymeric materials with more expected memory and cleaning effect.

$$\zeta(t) = \frac{q(\text{Voc,out})}{q(\text{Voc,in})} = \frac{\chi(\text{Voc,out})}{\chi(\text{Voc,in})} = \frac{S_t - S_{\text{Air,pipe}}}{S_{\text{VOC}} - S_{\text{Air,pipe}}}$$

### 3.6.4 Pressure fluctuation during experiment

The signal of the detector is greatly affected pressure. A stable pressure are required in order to observe the difference of signal for test pipe and bypass due to its different materials, not due to the difference of pressure and fluid dynamics. The pressure difference across the switch is reduced by using a proper length of the capillary tube. However, still, there is atmospheric pressure variation due to daily seasonal variation and the difference of pressure drop in test pipe and bypass. The atmospheric pressure variation effects the same way our measurements and the different of the pressure at start and end of experiment is consider as uncertainty to the pressure. A sensitivity of pressure fluctuation was performed with high pressure and low pressure in order to see the effect of reducing the relative pressure difference. In a system with nearly 5 kPa, an absolute difference of 520 Pa, and a relative difference of 10.3%, a fluctuation of signal up to 8% was observed. The relative difference was reduced by increasing the total pressure to 14.7 kPa for Sample A and 13.8kPa for Sample B, the absolute differences 520 Pa and 320 Pa, respectively. However, the relative difference was reduced by 3.5% for Sample A and 2.7% for Sample B. This reduces the fluctuation of the signal to <1%, a very negligible change. A higher fluctuation of signal 16% was observed for an experiment performed with a total pressure of 14 kPa and an absolute difference of 1470 Pa, and a relative difference of 10.5% (almost the same relative as the first case). This depicts that for the same relative difference of pressure, the signal fluctuation is affected greatly for higher pressure than for lower pressure.

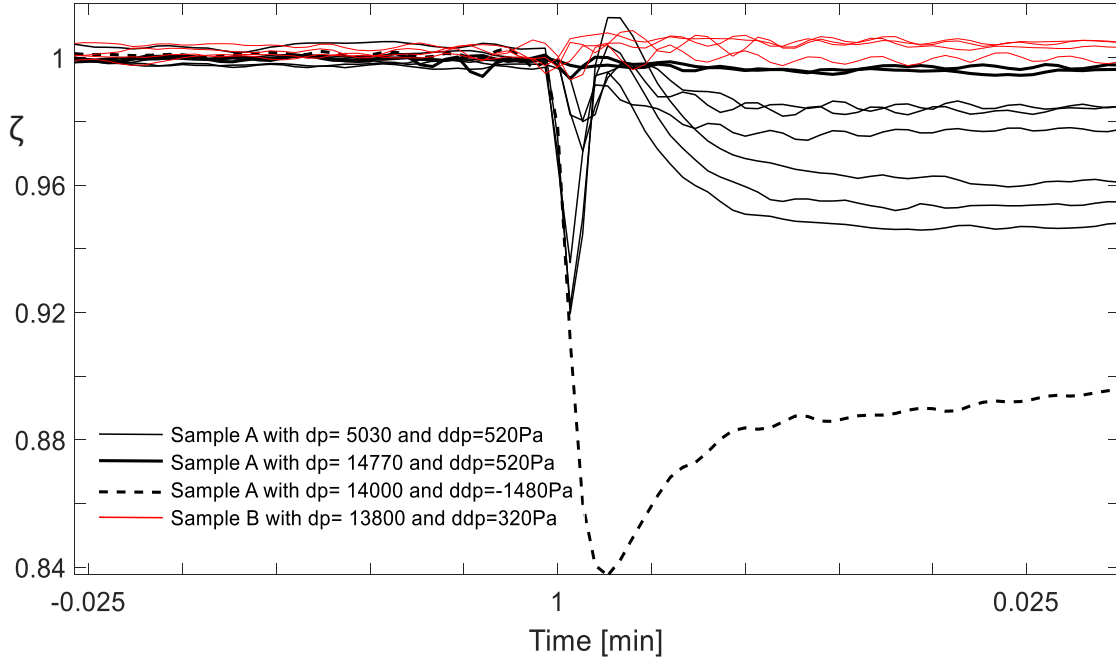


Figure 3.12: Effect on signal with different pressure drops for flowrate  $35\text{Sml}\cdot\text{min}^{-1}$ .

### 3.6.5 Irreversible losses in equilibrium

The irreversible losses during the establishment of equilibrium play an important role for some materials where the irreversible losses are significant, for example, PFA or electropolished stainless steel. The time required for establishing complete equilibrium can be up to a few hours through this period. The losses due to irreversible reactions or permeation are accounted as reversible losses. These losses must be removed from equation 3.16 after proper measurements. For Sulfinert® and Copper, these losses were very negligible but for PFA and Stainless steel; these losses are an important part of the total amount of losses. The total losses over a period can be calculated as:

$$q_j = J \cdot \Delta t_I$$

Where  $J$  is the mass flux per unit area calculated using the equation 3.13 and  $\delta t_I$  is the time of integral from switch till assumed equilibrium establishes.

### 3.6.6 Equilibrium not established

The irreversible losses are overestimated due to account of reversible losses in the case of premature equilibrium. In such cases, the losses during equilibrium are not yet finished as the test pipe is not completely saturated. This part of the

integral is assumed based on the trend line of the equilibrium curves till the  $S_{VOC,out}$  reaches its maximum value and an amount of VOCs  $q_b$  is calculated and added to equation 3.16. The maximum value of  $S_{VOC,out}$  can reach  $S_{VOC,in}$  in the case of no irreversible losses.

The estimation of this part is more as it is a source of uncertainty or bias for the irreversible losses' estimation. An amount  $q_b$  is removed from the  $q_j$  in the case of estimation of irreversible losses in a premature equilibrium condition.

### 3.6.7 Temperature variation during measurement

The temperature and pressure of the system are not under control as the temperature is subjected to daily and seasonal variation. Similarly, the atmospheric pressure follows a nonlinear trend and can be varies depending upon whether conditions. This variation affects the measurand directly by affecting the position of equilibrium and indirectly by affecting the parameters such as flow rate.

The flowrate flowing through the sonic nozzle is controlled by its density as

$$q_{v,g}^o = \rho_g \cdot v_{\text{sound}} \cdot A_{SN}$$

while the density of the flowing gas changes with temperature as

$$q_{v,g}^o = \frac{P_{sup} T_{sc}}{P_{sc} T_{wc}} \cdot [v_{\text{sound}} \cdot A_{SN}]$$

and the sensitivity of flowrate to temperature can be calculated in  $\text{Sml} \cdot \text{K}^{-1}$  as:

$$\frac{d(q_{v,g}^o)}{d(T_{wc})} = \frac{P_{\text{supp}} T_{sc}}{P_{sc}} \cdot [v_{\text{sound}} \cdot A_{SN}] \cdot \frac{-1}{T_{wc}^2}$$

where  $P_{sup}$  is the supply pressure to sonic nozzle and  $v_{\text{sound}}$  is the velocity of sound,  $A_{SN}$  is the cross-section area of the sonic nozzle. Depending upon the area of the sonic nozzle or the nominal flow rate of the sonic nozzle, the temperature has an impact on the performance of sonic outflow. A sensitivity of flowrate on temperature was performed to diagnoses the impact on our measurand as shown in Figure 3.13. For the flowrate,  $55 \text{ Sml} \cdot \text{min}^{-1}$  and  $9 \text{ Sml} \cdot \text{min}^{-1}$  up to 1% variation was observed against a temperature change of  $1.5^\circ\text{C}$  and  $3^\circ\text{C}$ , respectively. This change is quite significant for lower flow rate and causes changes in the residence time of the gas in the test pipe and thus the total integral of the curve.



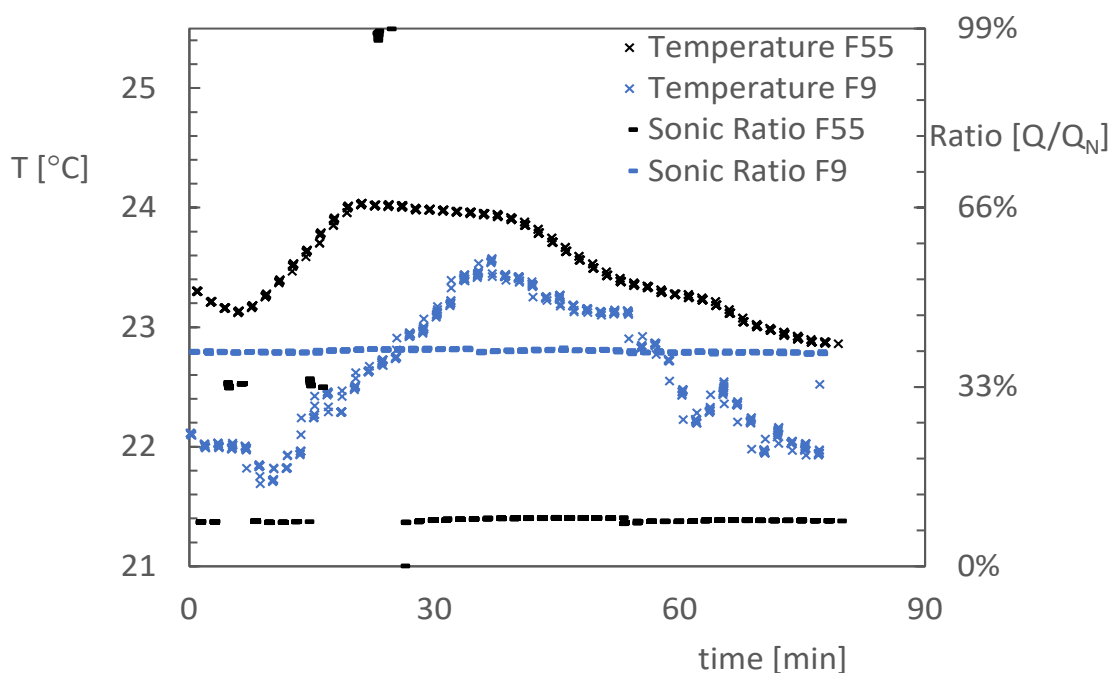


Figure 3.13: Temperature and flowrate profile over time.

Besides the indirect impact, temperature has a direct impact on the kinetics of the reaction and leads to uncertainty of the measurand.

### 3.6.8 Artifacts during measurement

Human artifact is always a contributing factor for the biases and uncertainty estimation. The flow rate is manually controlled, and the position of the valve determines the signal of VOC and integral. Thus estimation of mass adsorbed. Similarly, the temperature in the lab changes with every activity in the lab and leads to direct and indirect biases on measurements. The effect of temperature is more relevant while estimating the leakages where the syringe is in direct contact with the human body and leads to volume and pressure changes. The estimation of diameter is another critical step where human precision is greatly affecting the average diameter of the pipes. In short, in every activity and for any measurements, there is a source of uncertainty coming from human artifacts.

## 3.7 Measurement uncertainty

Accurate measurement has importance in any scientific and engineering activity. The accuracy in quantification depends on the instrument, its capacity to identify changes in the system. The uncertainty of the measured value depends on the

accuracy and the reproducibility of the measurement. However, if the property or value is a function of other measurements, then the uncertainty estimation will be dependent on the uncertainty of its influence quantities [13]. The combined uncertainty of the measurand  $K_e$  is computed from the uncertainty of the input quantities that have been determined from the information available or the performed measurements [13]. An uncertainty budget is calculated using the Guide to the expression of Uncertainty in Measurement (GUM) for equation 3.21 and 3.22. The influence quantities ( $X_i$ ) are listed in rows, and columns represent: symbol  $X_i$  and units  $[X_i]$ ; value  $x_i$ ; uncertainty  $u_i = u(x_i)$ ; relative uncertainty  $u_i/x_i$ ; sensitivity coefficients  $c_i = c(x_i) = \partial y / \partial x_i$ ; significance index [86].  $SI = [u_i c_i / \max(u_i c_i)]^2$ .  $SI$  identifies the largest source of uncertainty of the model ( $SI = 100\%$ ). The relevant contributors ( $SI > 10\%$ ) and negligible contributors ( $< 1\%$ ) The last row identify the measurand  $Y = K_e$ . The template of budget is reported in Table 3.6.

Table 3.6: Template for uncertainty budget using GUM procedure

$X_i$	$[X_i]$	$u(X_i)$	$C(X_i)$	$[C(X_i) \cdot u(X_i)]^2$	$SI$ [%]
Input Quantity $X_i$	Units $X_i$	$u(X_i)$	$\frac{dF}{d(X_i)}$	$\left[\frac{dF}{d(X_i)}\right]^2 \cdot [u(X_i)]^2$	$\frac{[C(X_i) \cdot u(X_i)]^2}{\max[C(X_i) \cdot u(X_i)]^2}$
		Combined Uncertainty	$u(Y)^2 = \sum_{i=1}^N \left[\frac{dF}{d(X_i)}\right]^2 \cdot [u(X_i)]^2$		

Pipe length  $L$ , internal diameter  $D$  measured for each pipe to keep their contribution to total uncertainty negligible.  $q_{v,g}^o$  was measured by a mass flow meter, its uncertainty comes from information and characterization of the instrument [87].  $C_{VOC,0}$  is determined from the certification of the mixture (SIAD, 1945-246276/41).

$S_{ZeroAir}$  was determined as  $S_\infty$  in scenario B, while  $S_{VOC}$  mixture was determined, taking into account  $S_\infty$  in scenarios C and D to correct for the derive of the signal along with the measurement. The values of  $I_{des}$  and  $I_{ads}$  were analyzed for repeatability over a number of experiments. The accuracy of  $I_{ads}$  and  $I_{des}$  is considered as the duration of the peak in time and uncertainty of the falling point of the response curve, respectively.

# Chapter 4

## Losses during equilibrium

The data obtained from experiments for maximum mass interacted during duration equilibrium is analyzed, and the response of every single step carried out during experiments is verified. The response of the detector to the change in physical quantities and conditions is analyzed to better understand the reproducibility of the method. The different approaches for the calculation of integrals are compared, and the applicable methods are applied to 4 different materials at different conditions.

### 4.1 Comparison of two different approaches

The net mass interaction can be calculated by two different approaches, which were discussed in the methodology chapter. The most important is to define the zero line obtained during zero air flow to the detector and the maximum line (1-line) obtained for the VOC mixture. Zero lines tend to decrease over time due to cleaning of the pipe, and one-line tends to increase over time due to saturation of FID. Another challenge is from where to start integration and where the end, as the switch is manually performed and thus included a human error. The start and end of integral causes change in total integral as curves follow trends increasing for one-line ( $S_{VOC}-S_{AIR}$ ) and decreasing for zero lines. For that purpose, the curves are integrating with respect to inclined lines following a slope for 1-line; in this way, the effect of starting and ending of curves are reduced.

The other challenging task is to know the actual residence time with the minimum possible uncertainty and maximum reproducibility. For both methods, the residence time is estimated in two different approaches as discussed in section 3.5.1.

The mass adsorbed per unit area ( $C_{A,e}$ ) measured with both approaches using the equation 3.19 and 3.21 is compared for the number of experiments at different residence times. The results with two different approaches are reported in Figure 4.1.

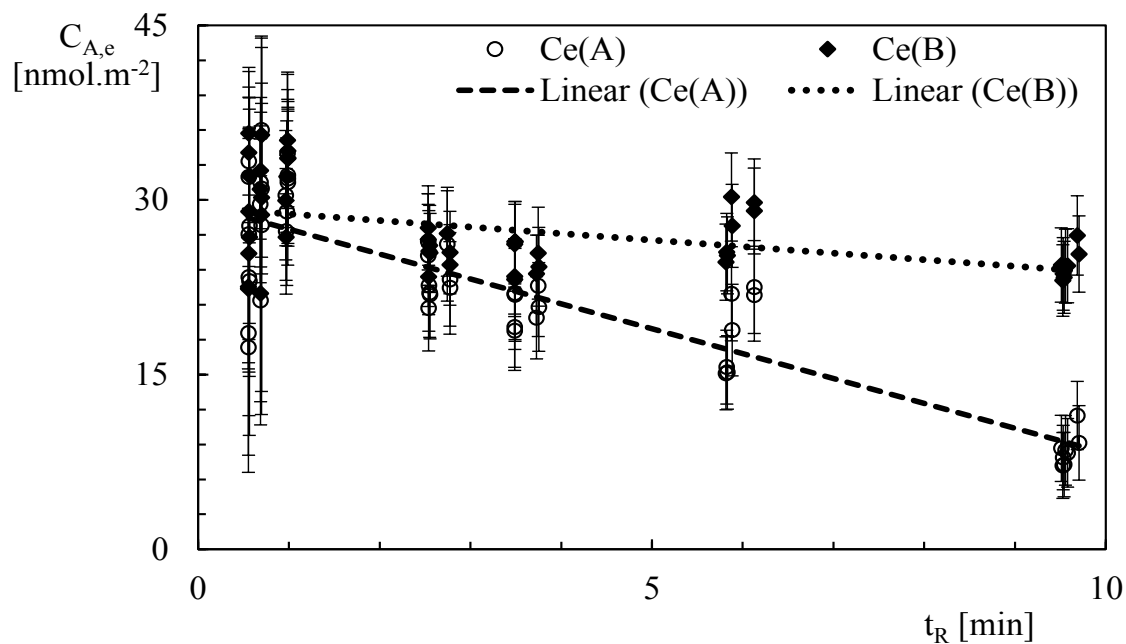


Figure 4.1: Comparing the results of  $C_{A,e}$  plotted against residence time  $t_R$  for Sulfinert® with two different approaches.

Method A was residence time dependant, and at higher residence time, the results were quite far from the result with method B and out of the trend followed at lower residence time. It is because, with higher residence time, the uncertainty of residence time is not well approximated. While method B was more reproducible; and that is why it is used as a representative approach for all metallic pipes.

## 4.2 Adsorption and desorption with Sulfinert® treated stainless steel pipe

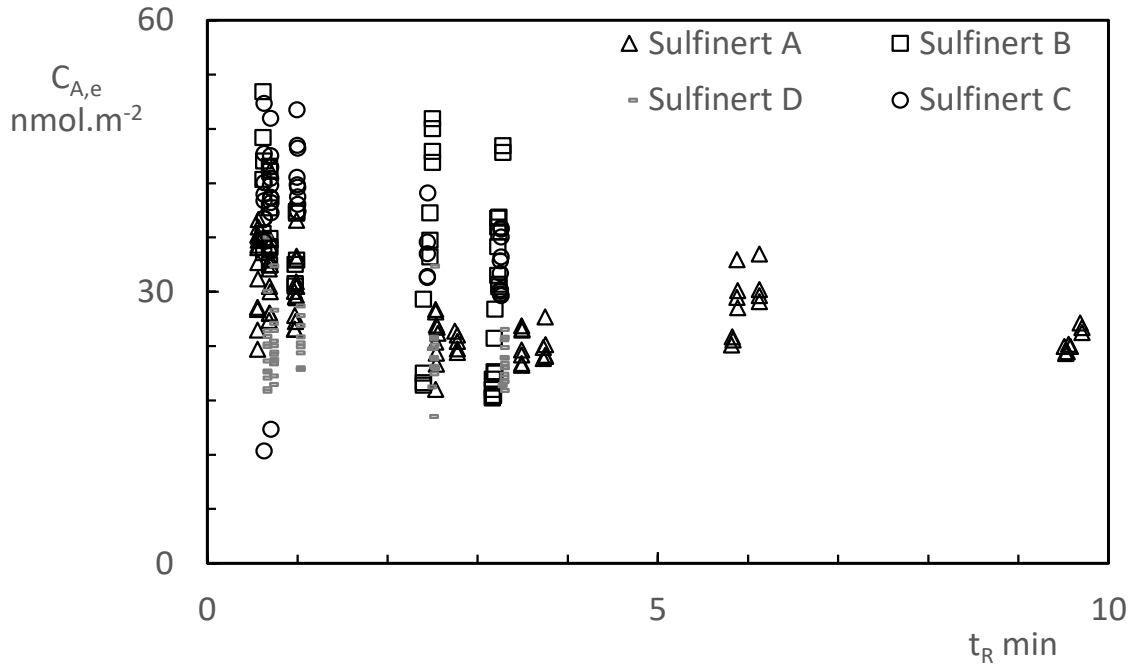
Four different Sulfinert® pipes with two different lengths have been tested at different conditions. A sample of Sulfinert® pipe (Sample A) as a whole is cut into three subsamples of the same lengths (Sample B, C, D) to verify the effects of operating conditions and to verify the reproducibility on the sample. Tests were performed at different residence times, flow rates, Reynolds numbers, and temperatures at atmospheric pressure (plus pressure drop). The ranges of test conditions are reported in Table 4.1. Tests were repeated on each sample over different conditions, and the effect of different parameters are discussed.

The mass interaction of VOC per unit surface area of the pipe is computed using equation 3.21. The mass interacted during the adsorption at a different  $t_R$  is shown in Figure 4.2, which depicts that the  $C_{A,e}$  is reproducible for all the flow rates

Table 4.1: Number of experiments on Sulfinert®, pipe length, and test condition ranges (residence time, temperature, pressure, and Reynolds number)

Sample	N (Ads.)	N (Des.)	L m	$t_R$ min	T °C	P kPa	Re –
Sample A	53	33	26	0.5 – 9.5	22 – 27	100 – 130	5 – 150
Sample B	26	20	8.5	0.6 – 3.2	17 – 30	100 – 120	5 – 40
Sample C	23	18	8.5	0.6 – 3.2	20 – 22	100 – 120	5 – 40
Sample D	28	28	8.5	0.6 – 3.2	20 – 22	100 – 120	5 – 40
All	109	99	8.5 – 26	0.5 – 9.5	17 – 30	100 – 130	5 – 150

within a range of reproducibility at different residence times. The adsorbed amount was the same as that of the desorbed amount, and the data were considered unique for both desorption and adsorption. All four samples are considered as a unique population with respect to temperature and pressure dependency of interaction phenomena. Welch statistical t-tests cannot reject the hypothesis that all data for adsorption and desorption and for different samples belong to a unique population with a confidence of 95%. However, there was a significant difference observed for sample D, which allowed the possibility to measure the difference between the different samples discussed later.

Figure 4.2: Comparative analysis of reproducibility of Raw- $C_{A,e}$  over two different lengths– Sulfinert® Sample A (26m) and Sample B, C, D (8.5m).

Sample D has the value of  $C_{A,e}$  quite lower than the other samples. It may be because this is the central part of the total pipe, and the treatment is completely preserved, which causes lower interactions. Detailed analysis on the effect of temperature pressure and sensitivity with respect to residence time and Reynolds number is presented in the subsequent section to verify the effect of fluid dynamics and physical conditions.

### 4.2.1 Sensitivity with temperature and correction

The gas-wall interactions are higher at high pressure and low temperature, while at low pressure and high temperature, these are lower [20, 114, 44]. The temperature was calculated as the mean of temperature measured on the external surface of the test pipe along the run time in a different position along the test pipe.

The temperature has been the most varying parameter, which affects the reproducibility of measurements. to investigate the effect of the temperature on adsorption, the temperature is adjusted by room chiller in a range from 17 °C to 30 °C. A sensitivity coefficient of  $1.6 \pm 0.12 \text{ nmol}\cdot\text{m}^{-2}\cdot\text{K}^{-1}$  was calculated for the temperature Figure 4.3 as the slope of the linear regression curve on the whole dataset from the four samples, i.e., Samples A, B, C, and D. A different slope was observed for each sample. This is mainly because of the different range of temperature, and it is particularly evident in the sample C and D datasets with a range of temperature of 2-3 °C against 5 °C for Sample A and 13 °C for Sample B.

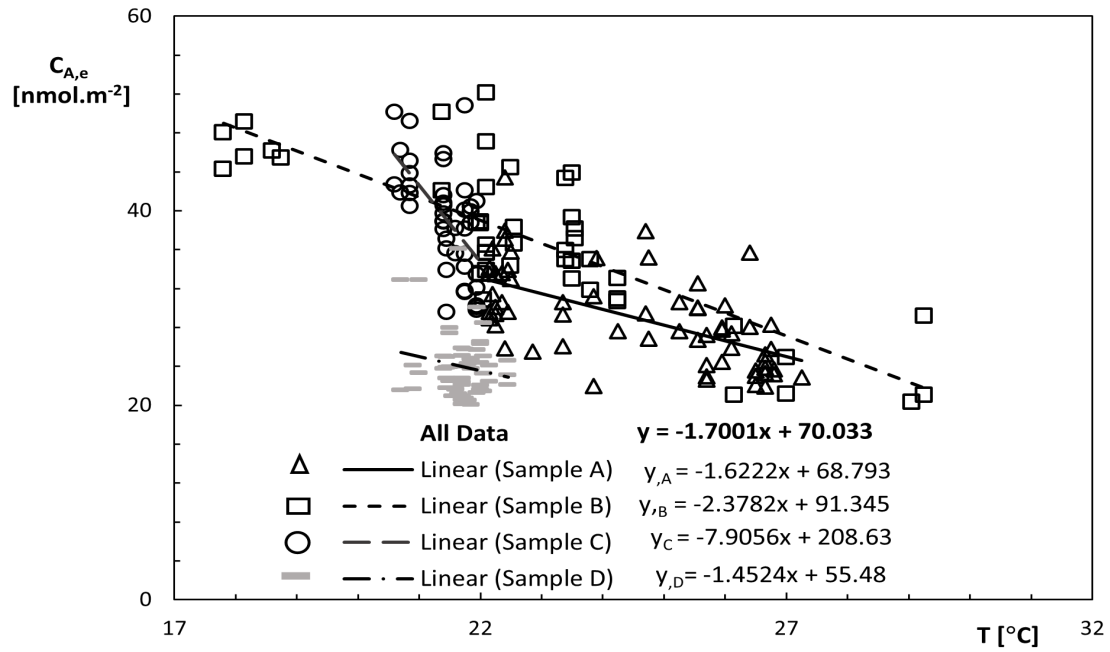


Figure 4.3: Sensitivity of adsorbed amount per unit area of Sulfinert<sup>®</sup>, on temperature.

To investigate the effect of temperature on the equilibrium constant  $K_e$ , the values of  $K_e$  are plotted against temperature, as seen in Figure 4.4. A sensitivity coefficient of  $3.43 \pm 0.12 \mu m \cdot K^{-1}$  was calculated for the temperature of  $K_e$  as the slope of the linear regression curve on the whole dataset, including adsorption and desorption from the four samples, i.e., Samples A, B, C, and D. Different slopes were observed for each sample like that of  $C_{A,e}$ .

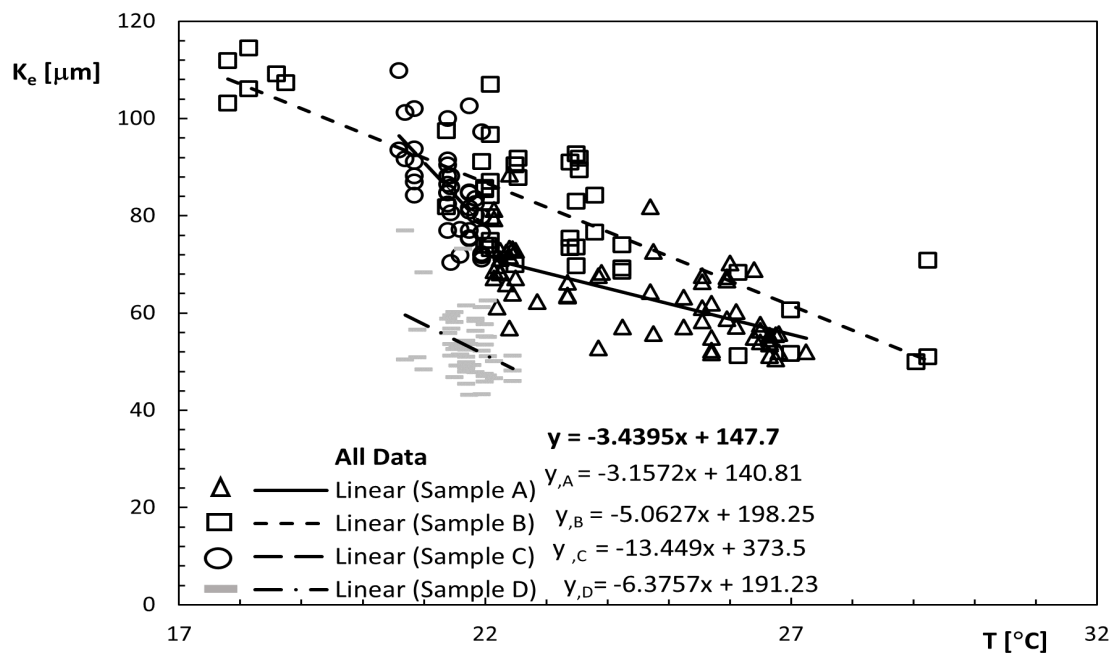


Figure 4.4: Sensitivity of equilibrium constant  $K_e$  [ $\mu\text{m}$ ] on temperature.

Data for  $C_{A,e}$  and  $K_e$  were corrected for the temperature bias at 20  $^{\circ}\text{C}$  in both the way considering all the datasets as unique and separately considering each sample differently. The datasets corrected for temperature are reported in Table 4.3.

#### 4.2.2 Sensitivity with pressure

The variability of pressure is important due to its direct effect on the adsorption phenomenon and indirectly the change of flow and residence time. Atmospheric pressure varies over time and cannot be controlled. The pressure was calculated as the mean of maximum and minimum ambient pressure observed during the run added to the mean of pressure drop with and without the test pipe, i.e., an estimation of the average pressure along the test pipe. The pressure drop of the system was controlled by controlling the length of the capillary tube. Experiments were repeated over the same conditions for the same sample for different pressure drop. However, the effect of the pressure was minimal on the response signal and adsorption/desorption phenomenon. A sensitivity coefficient for  $C_{A,e}$  is  $258 \pm 31 \text{ nmol}\cdot\text{m}^{-2}\cdot\text{MPa}^{-1}$  for the pressure calculated as the slope of the linear regression curve on the whole dataset from the four samples of Sulfinert  $\text{\textcircled{R}}$ , for data corrected for temperature bias. The data are plotted against pressure, as shown in Figure 4.5 is used for the linear regression. For every sample, a different slope was observed. This is mainly due to the different range of pressure drop for different samples. For



Sample A with a longer pipe, the pressure drop was higher, while for Sample B, C, and D, different capillary lengths were used in order to observe the sensitivity on different pressure.

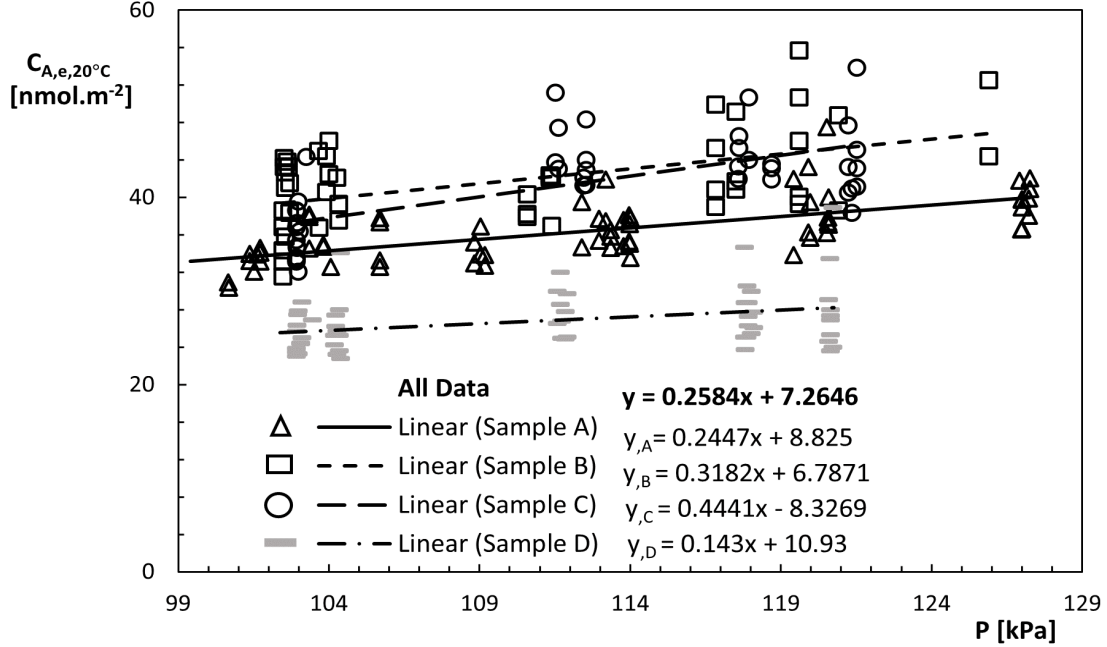


Figure 4.5: Sensitivity of adsorbed amount per unit area  $C_{A,e}$  of sulfinert® on pressure. The data set was corrected for temperature bias at 20 °C.

The dependency of  $K_e$  on pressure was analyzed by plotting all the  $K_e$  values for all four samples against pressure, as shown in Figure 4.5. A sensitivity coefficient is  $7.1 \pm 31 \mu\text{m} \cdot \text{MPa}^{-1}$  for the pressure as the slope of the linear regression curve on the whole dataset from the four samples of Sulfinert®, for data corrected for temperature bias. For every sample, a different slope was observed as that for  $C_{A,e}$ .

Using the sensitivity coefficients, the data for  $C_{A,e}$  and  $K_e$  were corrected for the pressure bias at 1 bar that is reported in Table 4.2 and Table 4.3, respectively.

Table 4.2 reports the standard deviation ( $\sigma$ ) of the datasets, including adsorption and desorption values. The horizontal lines account for different datasets: single datasets considering samples A, B, C, and D separately as single data, all the data in one set considering a unique population. The variability of data is evidently reduced by the correction of biases depending on the wideness of the temperature and pressure ranges in the specific datasets. The variability of Sample A is reduced from 16% to 7%, B from 21% to 12%, C from 14% to 11% and D from 13% to 12% using the significant index of the whole data set. While the variability of the whole data set is reduced from 25% to 20% and the variability of the means is reduced from 15% to 4.4% as reported in Table 4.2.

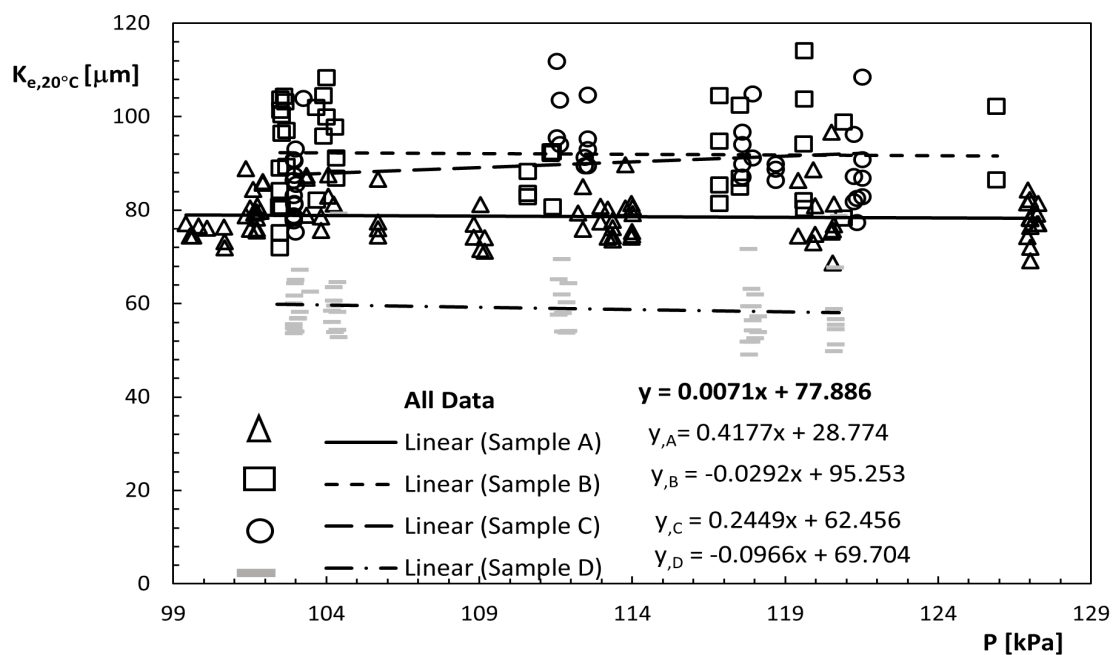


Figure 4.6: Sensitivity of equilibrium constant  $K_e$  area on pressure. The data set was corrected for temperature bias at 20 °C.

The standard deviation ( $\sigma$ ) of the equilibrium constant datasets, including adsorption and desorption as unique data sets, are reported in Table 4.3. The variability of Sample A is reduced from 12% to 6%, B from 20% to 11%, C from 11% to 9%, and D from 13% to 11% using the significant index of the whole data set. While the variability of the whole data set is reduced from 23.5% to 18%, and the variability of the means is reduced from 19% to 17%.

Table 4.2: Areic amount adsorbed per unit area of Sulfinert® ( $C_{A,e}$ ), Raw data and data corrected at 20 °C 1 bar with experimental standard deviations for a single sample and all data aggregated considering adsorption and desorption as a unique population.

Sample	$C_{A,e}$ (nmol·m <sup>-2</sup> )	$\sigma$ (nmol·m <sup>-2</sup> )	$\sigma\%$ $\sigma/C_{A,e}$	$C_{A,e,20^\circ C,1bar}$ (nmol·m <sup>-2</sup> )	$\sigma_{20^\circ C,1bar}$ (nmol·m <sup>-2</sup> )	$\sigma\%_{20^\circ C,1bar}$ $\sigma/C_{A,e}$
Sulfinert A	28.4	4.7	16%	36.3	33.4	7%
Sulfinert B	36.8	7.8	21%	41.8	38.9	12%
Sulfinert C	39.1	5.4	14%	41.6	38.4	11%
Sulfinert D	24	3.2	13%	26.9	24.1	12%
All data	30.9	7.9	25%	36	33.2	20%
Mean ABCD	32.1	6.2	19%	36.6	33.7	18%

Table 4.3: Equilibrium constant  $K_e$  with Sulfinert®; Raw data and data corrected at 20 °C 1 bar with experimental standard deviations for a single sample and all data aggregated considering adsorption and desorption as a unique population

Sample	$K_e$ ( $\mu\text{m}$ )	$\sigma$ ( $\mu\text{m}$ )	$\sigma\%$ $\sigma/K_e$	$K_{e,20^\circ C}$ ( $\mu\text{m}$ )	$K_{e20^\circ C,1bar}$ ( $\mu\text{m}$ )	$\sigma\%_{20^\circ C,1bar}$ $\sigma K_e / K_e$
Sulfinert A	62.9	7.8	12.30%	78.6	78.5	6%
Sulfinert B	82.2	16.1	19.60%	92	92	11%
Sulfinert C	85.1	9.3	11.00%	90	90.7	9%
Sulfinert D	53.3	6.7	12.60%	59	58.9	11%
All data	68.6	16.1	23.50%	78.7	78.7	18%
Mean ABCD	70.9	13.3	18.70%	79.9	80	17%

In the second approach, each sample is considered as a separate pipe, and the adsorption and desorption datasets were considered as separate datasets in order to measure the difference. Table 4.4 reports the data for  $C_{A,e}$  with percentage standard variation and corrected for 20 °C temperature and 1 bar pressure with variation for adsorption followed by desorption separately. All the datasets were corrected based on the coefficient calculated as the slope from the corresponding data set. The sensitivity coefficient for temperature was following the same trend for both

adsorption and desorption. However, a lower slope was observed for desorption than adsorption. This is due to the gradient of the phenomenon. In adsorption, higher pressure enhance the gradient of concentration and thus the adsorption process, while in desorption, the pressure of the air is increased, and the concentration gradient for desorption remains unchanged. The correction to the temperature and pressure allows the reduction of variation for each data set to more significant however the variation over the whole data set was reduced in the same order. The variability over whole data for adsorption was reduced from 27% to 19% and for the whole desorption data set from 26% to 22%.

Table 4.4: Areic amount adsorbed per unit area of Sulfinert® ( $C_{A,e}$ ), Raw data and data corrected at 20 °C 1 bar with experimental standard deviations for a single sample considering adsorption and desorption as separate population.

	<b>Sample</b>	$C_{A,e}$ ( $\text{nmol}\cdot\text{m}^{-2}$ )	$\sigma\%$ $\sigma/C_{A,e}$	$C_{A,e,20^\circ\text{C},1\text{bar}}$ ( $\text{nmol}\cdot\text{m}^{-2}$ )	$\sigma_{20^\circ\text{C},1\text{bar}}$ ( $\text{nmol}\cdot\text{m}^{-2}$ )	$\sigma\%_{20^\circ\text{C},1\text{bar}}$ $\sigma/C_{A,e}$
<i>Ads.</i>	Sulfinert A	28.5	16%	39.6	37.9	7%
	Sulfinert B	36.3	27%	45.9	41.9	8%
	Sulfinert C	39.4	16%	53.2	48.5	8%
	Sulfinert D	24.5	17%	29.7	29	11%
	All data	31.2	27%	38.5	36.8	19%
	Mean ABCD	32.2	19%	42.1	39.3	18%
<i>Des.</i>	Sulfinert A	28	17%	36.3	32.6	7%
	Sulfinert B	32.8	23%	40.6	40.2	9%
	Sulfinert C	38.7	9%	47.6	44.4	3%
	Sulfinert D	22.4	11%	21.9	21.9	11%
	All data	29.1	26%	34.5	31.2	22%
	Mean ABCD	30.5	20%	36.6	34.8	25%

In the second approach, the adsorption and desorption data set for  $K_e$  were considered as separate data sets. To avoid repeated images, the plot of data and effect on temperature, pressure is not shown here. However, the data for  $K_e$  with percentage standard variation, data corrected for 20 °C temperature and 1 bar pressure with percentage variation are reported in Table 4.5 separately for adsorption and desorption dataset. The variability over whole data for adsorption was reduced from 24% to 19% and increased for the desorption over the whole dataset from 19% to 20%.

Acetone that disappeared in the first part of the run and appeared in the second part of the run was calculated to be  $1.7 \text{ nmol}\cdot\text{m}^{-2}$  as the difference of the mean values corrected for the temperature and pressure biases and  $2.0 \text{ nmol}\cdot\text{m}^{-2}$  as the mean of the differences measured in each run. The difference of the values of the equilibrium constant indicates the difference of phenomenon. A difference of  $2.6 \mu\text{m}$  was calculated as a difference between the average values of  $K_e$  corrected for

Table 4.5: Equilibrium constant ( $K_e$ ) with Sulfinert®; Raw data and data corrected at 20 °C 1 bar with experimental standard deviations for a single sample considering adsorption and desorption as separate population

	Sample	$K_e$ ( $\mu\text{m}$ )	$\sigma\%$ $\sigma/K_e$	$K_{e,20^\circ\text{C}}$ ( $\mu\text{m}$ )	$K_{e,20^\circ\text{C},1\text{bar}}$ ( $\mu\text{m}$ )	$\sigma\%$ $_{20^\circ\text{C},1\text{bar}}$ $\sigma K_e/K_e$
<i>Ads.</i>	Sulfinert A	63.6	10%	77.9	76.6	6%
	Sulfinert B	81.1	24%	101.2	99.5	7%
	Sulfinert C	86.2	13%	109.7	107.1	8%
	Sulfinert D	54.1	15%	71.8	71.3	10%
	All data	69.2	24%	78.7	77.3	19%
	Mean ABCD	71.3	18%	90.2	88.6	17%
<i>Des.</i>	Sulfinert A	61.1	16%	81.6	84.3	5%
	Sulfinert B	73.5	22%	88.8	93.7	9%
	Sulfinert C	83.8	7%	100.4	101.2	3%
	Sulfinert D	49.8	13%	53	57.7	10%
	All data	64	25%	77.5	79.8	19%
	Mean ABCD	67.1	19%	81	84.2	20%

the temperature and pressure for all four samples. These small difference lies inside the experimental variability and thus allows us to consider the whole population for adsorption and desorption as a unique population.

The dependency of the adsorbed amount and equilibrium constant  $K_e$  on the dynamic fluid effects inside the pipe is checked by the sensitivity of adsorbed amount and equilibrium constant  $K_e$  at different Reynolds Numbers ( $Re$ ). The average values of the four samples grouped at 6 different Reynolds number ( $Re$ ) are plotted in Figure 4.4 for  $C_{A,e}$  and Figure 4.8 for  $K_e$ , respectively.  $Re$  was always lower than 200, so a laminar regime always occurred in the test pipes. A slope of  $-0.00037 \text{ nmol}\cdot\text{m}^{-2}$  for  $C_{A,e}$  was calculated by linear regression on all the data and  $-0.0003 \text{ nmol}\cdot\text{m}^{-2}$  by linear regression on the mean values. While for the  $K_e$ , a slope of  $-0.0003 \mu\text{m}$  was calculated by linear regression on all the data and  $-0.0064 \mu\text{m}$  by linear regression on the mean values. The resulted curves are plotted in Figure 4.7 and Figure 4.8, but they are not evidently different from the line of the mean value.

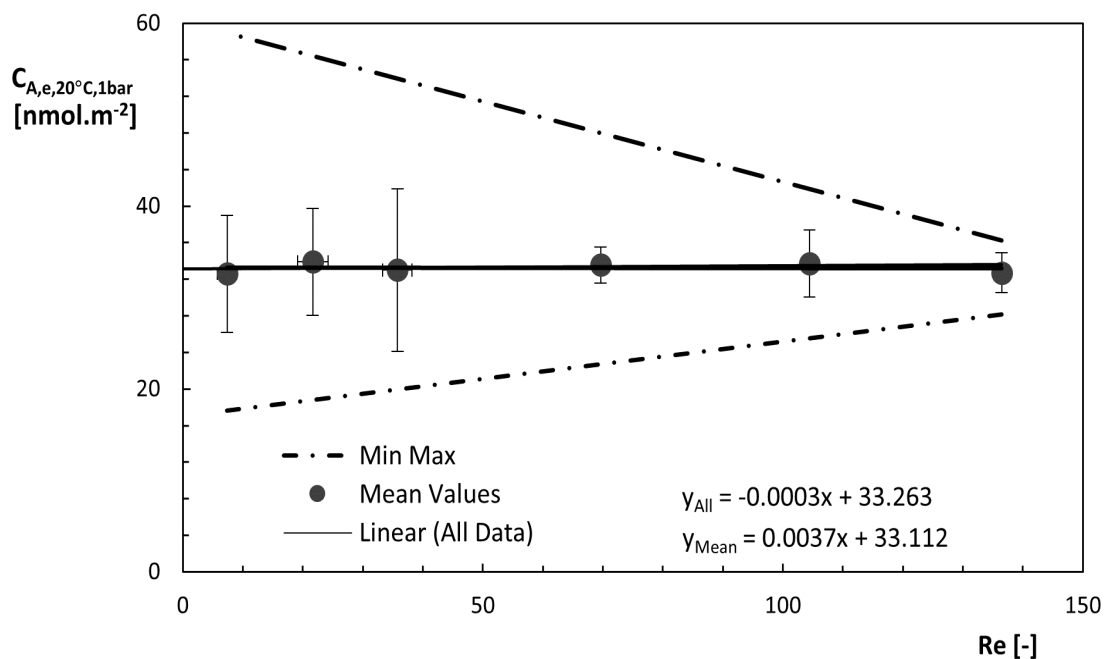


Figure 4.7: Sensitivity of adsorbed amount per unit area  $C_{A,e}$  on Reynolds number. Values corrected at 20 °C, 1bar, and grouped on  $Re$ .

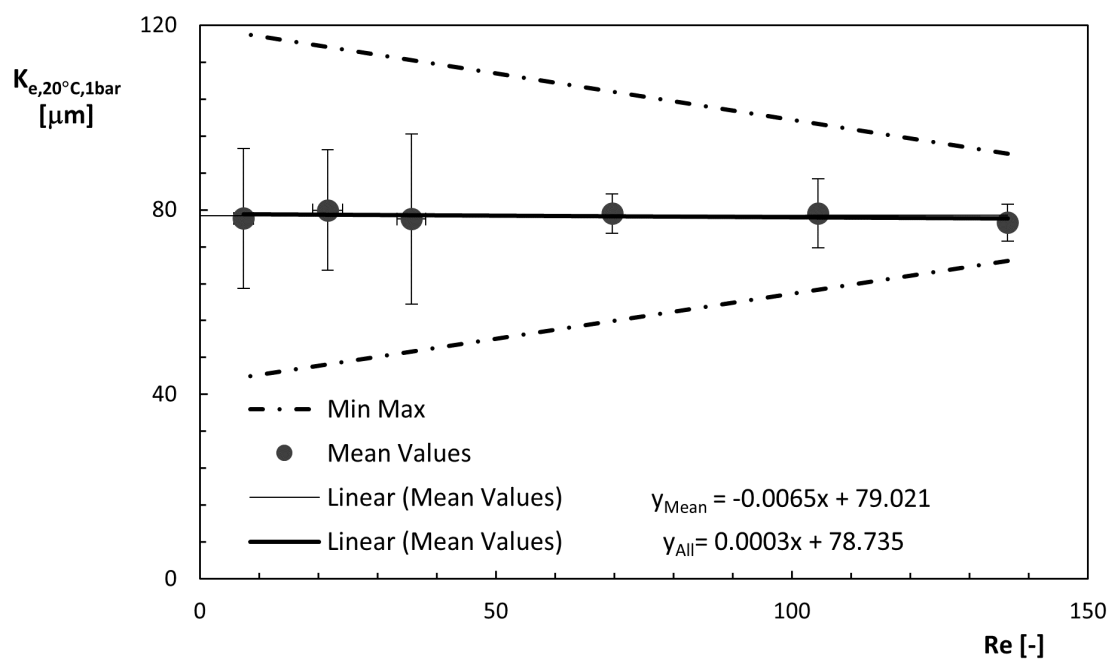


Figure 4.8: Sensitivity of equilibrium constant on Reynolds number. Values corrected at 20 °C, 1bar, and grouped on  $Re$ .

The deviation from the mean value was lower than variability on the whole range of  $Re$ , and the effect of the slope on the whole range was observed to be lower than the variability of each data subset. Upper and lower lines are the envelopes of all data; maximum and minimum values have an opposite trend against  $Re$ . In conclusion, as expected,  $Re$  does not affect the amount of Acetone adsorbed per unit area  $C_{A,e}$  and on  $K_e$  of the pipe wall.

Figure 4.9 and Figure 4.10 show the plots of average values of the four samples grouped at 5 different residence times in order to check a dependency of the adsorbed amount and equilibrium constant on the contact time. Contact time ranged between 0.5 and 9 min for all the samples. A slope of  $-0.162 \text{ nmol}\cdot\text{m}^{-2}\cdot\text{min}^{-1}$  was calculated by linear regression on all the data and  $-0.159 \text{ nmol}\cdot\text{m}^{-2}\cdot\text{min}^{-1}$  by linear regression on the mean values.

The variability of the mean values seems lower for residence time lower than 4 min. The upper and lower lines in Figure 4.9 and Figure 4.9 are the envelope of all data; minimum values have a flat trend against the residence time. The effect of residence time on the adsorbed amount per unit area is not completely clear but, in any case, very limited. A slope of  $-0.323 \text{ }\mu\text{m}\cdot\text{min}^{-1}$  was calculated by linear regression on all the data and  $-0.41 \text{ }\mu\text{m}\cdot\text{min}^{-1}$  by linear regression on the mean values. The longer sample, Sample A, was the only one working at a high Reynolds number (more than 50) and at a high residence time (more than 4 min). All the Figures 4.7,4.8,4.9, and Figure 4.10 depict that the effect of adsorption on fluid dynamics and contact time is very limited.

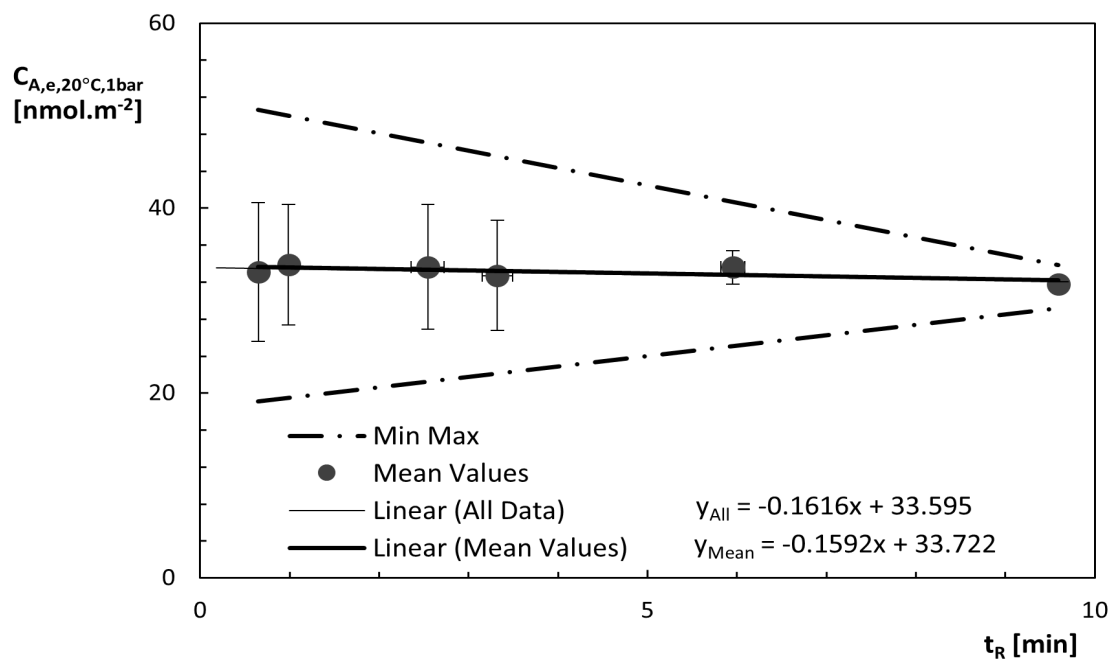


Figure 4.9: Sensitivity of adsorbed amount per unit area on residence time. Values corrected at 20 °C, 1bar and grouped on  $\tau_R$ .

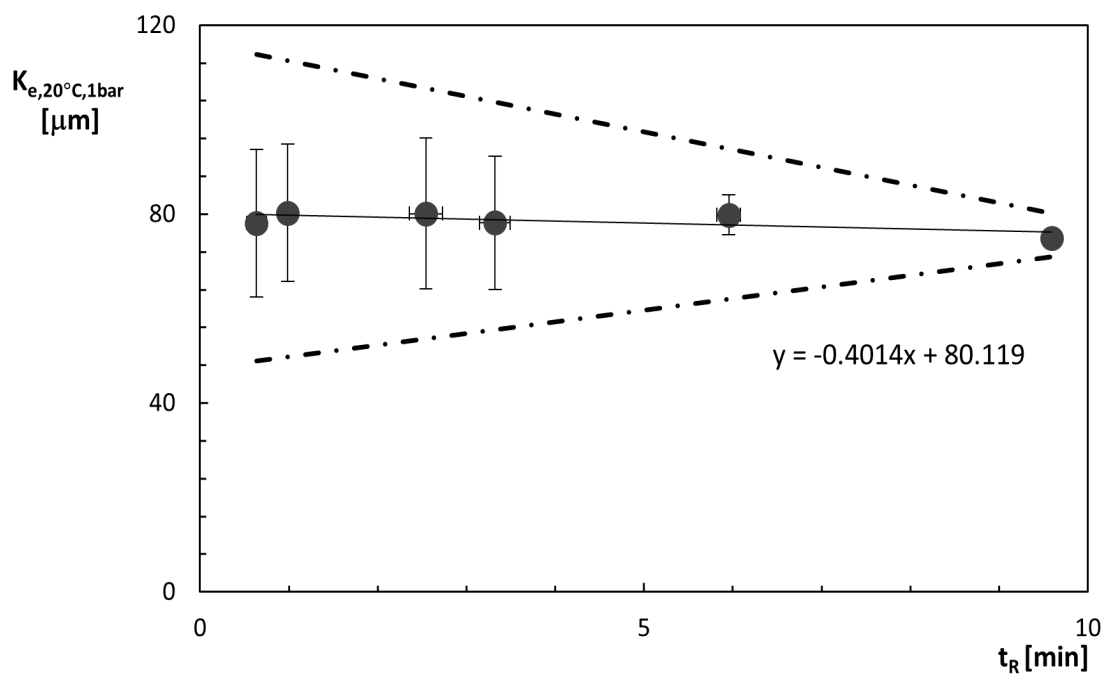


Figure 4.10: Sensitivity of equilibrium constant  $K_e$  on residence time. Values corrected at 20 °C, 1bar and grouped on  $\tau_R$ .



### 4.2.3 Reproducibility and accuracy for Sulfinert®

The uncertainty budget formulation is shown in section. 3.7 is applied to equation 3.21 and 3.22. For  $q_{vg}^o$ ,  $L$ , and  $D$ , the measurement accuracy with  $k = 2$  is considered uncertainty. The uncertainty of  $\chi_{VOC}$  is the certified value of the gas cylinder. The uncertainty of  $I_{ads}$  and  $I_{des}$  is considered as the length of the peak and unpredictability of the falling position of the response curve, respectively.

The combined uncertainty of the measurand  $C_{A,e}$  is computed from the uncertainty of the input quantities that have been determined from the information available or the performed measurements [13]. An uncertainty budget is calculated for  $C_{A,e}$  Equation 3.21 and  $K_e$  Equation 3.22 for every single experiment. The budget for the most conservative experiment having higher uncertainty is reported in Table 4.6 for  $C_{A,e}$  and Table 4.7 for  $K_e$ . In both of the cases, the accuracy of measurand was less than 41% for  $C_{A,e}$  and 50% for  $K_e$ .

Table 4.6: Uncertainty budget for  $C_{A,e}$  for most conservative experiment on Sulfinert® Sample D

$\mathbf{X}$	$\mathbf{x}$	$[\mathbf{X}]$	$\mathbf{u} = \mathbf{u}(\mathbf{x})$	$\mathbf{u}/\mathbf{x}$	$\mathbf{c} = \partial\mathbf{K}_e/\partial\mathbf{x}_i$	$S I$
$\chi_{Voc}$	10	$\mu\text{mol} \cdot \text{mol}^{-1}$	1	10.00%	2.34	8.1%
$q_{v,g}^o$	35	$\text{Sml} \cdot \text{min}^{-1}$	1.00	5.00%	.670	0.66%
$I_{ads}$	0.116	min	0.030	26.90%	271	100.0%
$I_{des}$	0.029	min	0.015	50.00%	-271	22.7%
$L$	8.5	m	0.05	0.50%	-2.76	0.03%
$D$	2.159	mm	0.011	0.50%	-10.9	0.02%
$C_{A,e}$	23.44	$\text{nmol} \cdot \text{m}^{-2}$	9.46	40.4%		

Table 4.7: Uncertainty budget for  $K_e$  for the most conservative experiment of Sulfinert® Sample D

$\mathbf{X}$	$\mathbf{x}$	$[\mathbf{X}]$	$\mathbf{u} = \mathbf{u}(\mathbf{x})$	$\mathbf{u}/\mathbf{x}$	$\mathbf{c} = \partial\mathbf{K}_e/\partial\mathbf{x}_i$	$S I$
$q_{v,g}^o$	35	$\text{Sml} \cdot \text{min}^{-1}$	1	10.00%	1.62	0.66%
$I_{ads}$	0.116	min	0.030	5.00%	654.85	100.0%
$I_{des}$	0.029	min	0.015	26.90%	-654.85	22.66%
$L$	8.5	m	0.05	50.00%	-6.67	0.03%
$D$	2.159	mm	0.0108	0.50%	-26.25	0.02%
$T$	22	$^{\circ}\text{C}$	2	0.50%	0.19	0.04%
$P_{atm}$	99.5	kPa	0.1	0.50%	-56.58	8.04%
$dP_{wc}$	2	kPa	0.285	0.50%	-56.58	65.28%
$K_e$	56.68	$\mu\text{m}$	27.99	49.4%		

Reproducibility was calculated as the standard deviation of the mean. The standard deviation of the mean of the dataset with data corrected for temperature and pressure is considered as the total uncertainty of the measurement [63]. The value is around 20% for  $C_{A,e}$  and 18% for  $K_e$ , considering adsorption and desorption of all the samples as unique population, 17% for  $C_{A,e}$ , and 18% for  $K_e$  as variance over the mean values of different samples. In any case, the reproducibility is limited, and this could mainly be due to the characteristic of Sulfinert® coating on stainless steel that assures very low irreversible interferences and no permeation into the pipe wall, limiting the instability of measurand. A poorer reproducibility is expected with polymeric materials or uncoated metals, which is discussed in subsequent sections.

### 4.3 Adsorption and desorption with Copper pipe

The methodology for the quantification of aeric amount adsorbed was extended on the Copper surface. Experiments were performed with 1/8" Copper pipe. Tests were performed at different physical conditions such as residence times, flow rates, Reynolds numbers, and temperatures at atmospheric pressure (plus pressure drop). The ranges of test conditions are reported in Table 4.8. Tests were repeated on the same conditions with the same sample.

Table 4.8: Number of experiments on Copper pipe, pipe length and test condition ranges (residence time, temperature, pressure, and Reynolds number).

Sample	N Ads.	N Des.	L m	$t_R$ min	T °C	P kPa	Re –
Copper	18	18	11.1	0.45 – 1.0	21 – 25	100 – 116	20 – 50

The adsorbed amount was quite different than that of the desorbed amount, and the data cannot be considered unique for both desorption and adsorption. The number of VOCs adsorbed over the surface was always a notice 2-3 times than the number of desorbed VOCs. There was a significant difference between the adsorbed and desorbed amount of VOCs. All the data for adsorption and desorption were considered as a separately unique population with respect to temperature and pressure dependency of interaction phenomena. Welch statistical t-tests reject the hypothesis that all data for adsorption and desorption belong to a unique population with a confidence of 100%.

#### 4.3.1 Sensitivity with temperature

A sensitivity coefficient of  $4.736 \text{ nmol}\cdot\text{m}^{-2}\cdot\text{K}^{-1}$  was calculated for the temperature Figure 4.11 as the slope of the linear regression curve on the adsorption data set

and  $1.513 \text{ nmol}\cdot\text{m}^{-2}\cdot\text{K}^{-1}$  on the desorption data set. The dependency of adsorbed amount on temperature was higher than that of desorption due to the fact that the gradient (driving force) for adsorption decreases with the increases in temperature, while for desorption, the gradient increases with temperature. The slope is greatly affected by different ranges of temperature, and it is particularly evident in the Copper with a range of temperature of  $4 \text{ }^\circ\text{C}$  against  $13 \text{ }^\circ\text{C}$  for Sulfinert<sup>®</sup>. With this small range of temperature, there was a negligible change after temperature correction; however, the variability of the experimental data was reduced from 23% to 18% for adsorption and from 12% to 11% for the desorption data set. The data set was corrected to the temperature of  $23 \text{ }^\circ\text{C}$  as reported in Table 4.9.

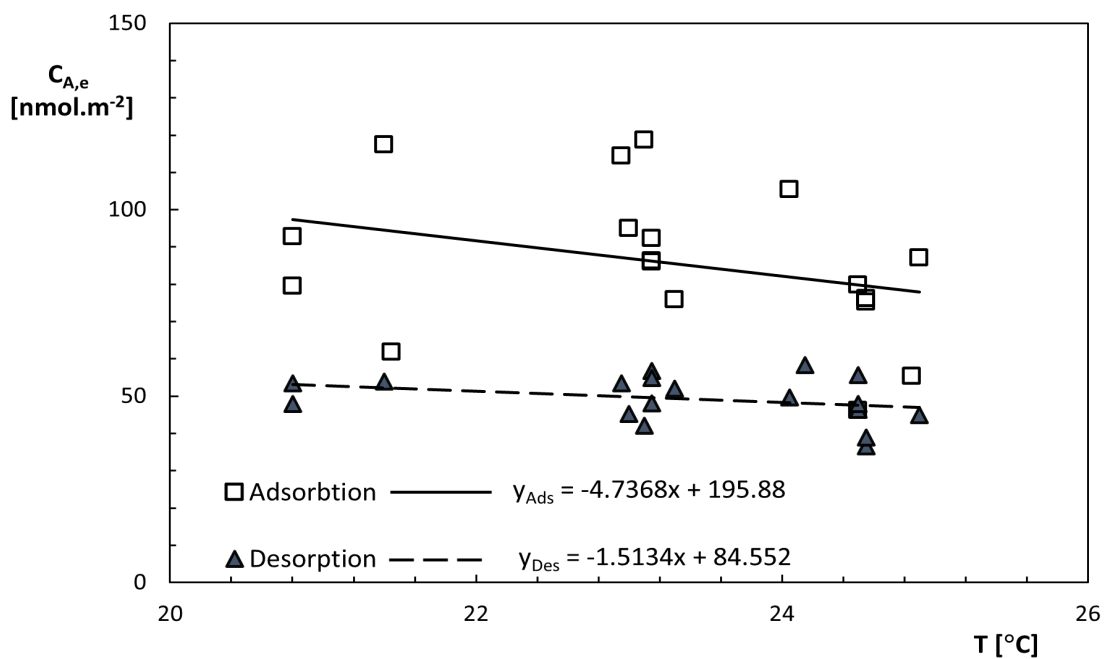


Figure 4.11: Sensitivity of adsorbed and desorbed amount per unit area of the Copper pipe on temperature.

Sensitivity on the equilibrium constant for the Copper was performed, and the sensitivity coefficient for temperature was calculated to be  $-12.1 \text{ } \mu\text{m}\cdot\text{K}^{-1}$  as the slope of the linear regression curve on the adsorption data set and  $-4.192 \text{ } \mu\text{m}\cdot\text{K}^{-1}$  on the desorption data set as depicted in Figure 4.12.

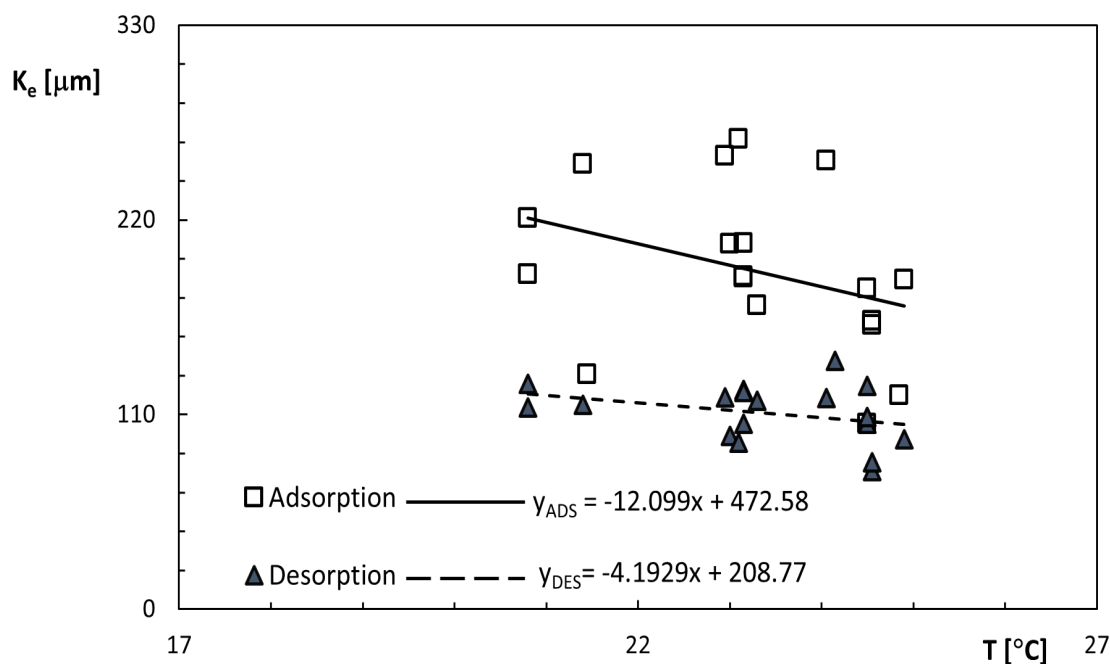


Figure 4.12: Sensitivity of equilibrium constant  $K_e$  with Copper pipe on temperature.

### 4.3.2 Sensitivity with pressure

The mean of maximum and minimum ambient pressure observed during the experiment added the mean of pressure drop with and without the test pipe were considered as of the average pressure along the test pipe. A sensitivity coefficient of  $-139 \text{ nmol}\cdot\text{m}^{-2}\cdot\text{MPa}^{-1}$  for the pressure Figure 4.13 as the slope of the linear regression curve on the adsorption dataset for data corrected for temperature bias and  $483 \text{ nmol}\cdot\text{m}^{-2}\cdot\text{MPa}^{-1}$  for desorption data set were calculated. The dependency of adsorbed amount on pressure was higher than that of desorption due to the fact that the gradient (driving force as concentration) for adsorption increases with the increases in temperature, while for desorption, the gradient (concentration) remain unchanged as the pressure of the air is increasing and not the VOCs. Both the data sets were also corrected for the pressure bias at 1 bar, as reported in Table 4.9. The variability of the experimental data was reduced for both temperature and pressure corrections from 23% to 18% for the adsorption data set and from 12% to 9% for the desorption data set.

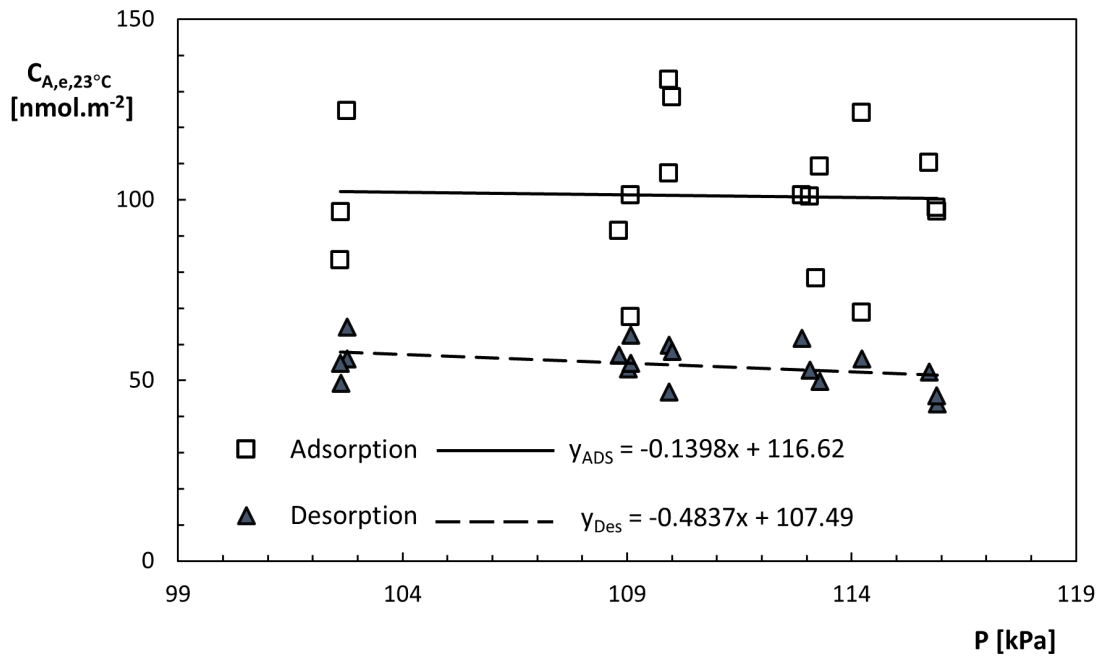


Figure 4.13: Sensitivity of adsorbed amount per unit area of the Copper pipe on pressure. The data set was corrected for temperature bias at  $23^{\circ}\text{C}$ .

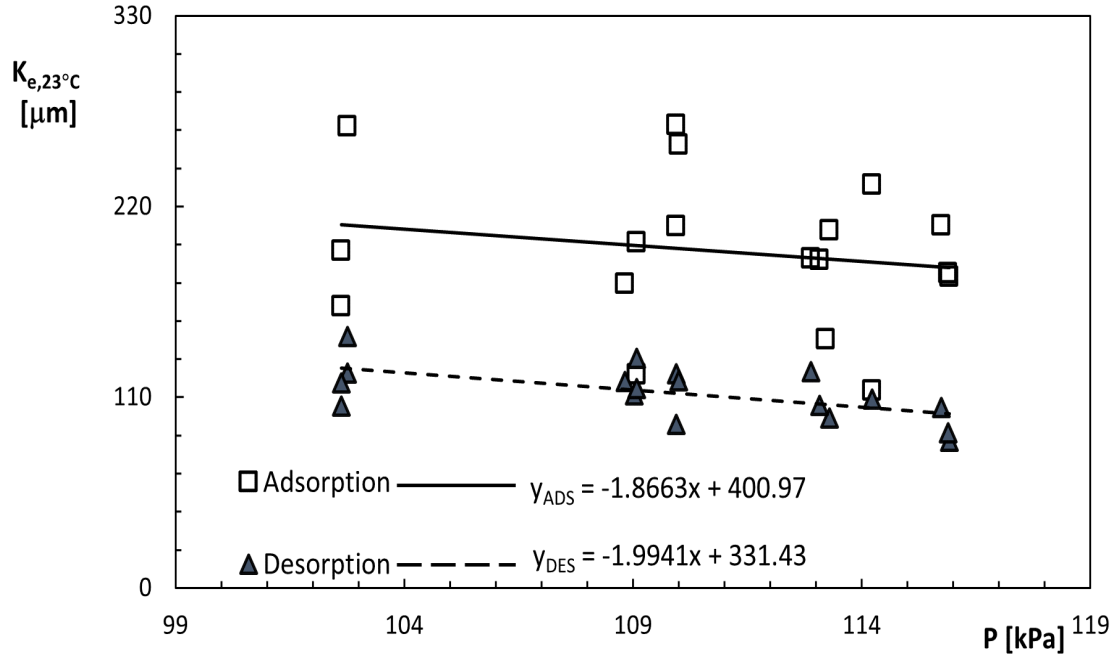


Figure 4.14: Sensitivity of equilibrium constant  $K_e$  with Copper pipe on pressure. The data set was corrected for temperature bias at  $23^{\circ}\text{C}$ .

The slope of the linear regression for the equilibrium constant Figure 4.14 on the adsorption dataset gives the value of the sensitivity coefficient, which is  $1866 \mu\text{m}\cdot\text{MPa}^{-1}$ . Likewise, with the similar approach for the desorption data set, this is calculated as  $1990 \mu\text{m}\cdot\text{MPa}^{-1}$ . The correction at 1 bar pressure was also performed on both datasets. Reduction in the variability of experimental data for both temperature and pressure on adsorption data set was observed from 24% to 19% and on desorption dataset from 14% to 9%, as reported in Table 4.9.

The adsorption and desorption are compared for analyzing the reversibility of the interactions. The difference between the amounts of Acetone that disappeared (adsorbed) and appeared (desorbed) was calculated to be  $33.9 \text{ nmol}\cdot\text{m}^{-2}$  as the difference of the mean values corrected for the temperature and pressure biases and  $35 \text{ nmol}\cdot\text{m}^{-2}$  as the mean of the differences measured in each test. While the difference of the equilibrium constant calculated for adsorption and desorption is  $82.3 \mu\text{m}$  calculated as the difference of the average and  $84 \mu\text{m}$  calculated as the mean of the difference for every experiment. These differences are significant and lie outside the experimental variability, and thus, the whole population for adsorption and desorption is considered as separate populations.

Table 4.9: Areic amount adsorbed and desorbed per unit area ( $C_{A,e}$ ) and Equilibrium constant with Copper pipe

	$C_{A,e}$ $\text{nmol}\cdot\text{m}^{-2}$	$\sigma\%$ —	$\sigma_{,23^\circ\text{C},1\text{bar}}$ $\text{nmol}\cdot\text{m}^{-2}$	$\sigma_{\%,23^\circ\text{C},1\text{bar}}$ —	$K_e$ , $\mu\text{m}$	$\sigma\%$ —	$K_{e,23^\circ\text{C},\text{cbar}}$ $\mu\text{m}$	$K_{e,23^\circ\text{C},1\text{bar}}$ —
Adsorption	85.8	23%	88.4	21%	191.5	24%	214.4	19%
Desorption	49.2	12%	54.5	10%	110.8	14%	132	9%
Both	67.5	35%	71.5	30%	151.2	35%	173.2	30%

Figure 4.15 and Figure 3.7 show the plot of average values grouped at 5 different Reynolds number ( $Re$ ) for  $C_{A,e}$  and  $K_e$  respectively.  $Re$  was always lower than 60, so a laminar regime in the test pipes. A slope of  $0.226 \text{ nmol}\cdot\text{m}^{-2}$  was calculated by linear regression on the mean values for the adsorption dataset and  $0.0533 \text{ nmol}\cdot\text{m}^{-2}$  by linear regression on the mean values for the desorption data set.

The dependency on equilibrium constant  $K_e$  by Reynolds number is calculated as the slope of linear regression (Figure 4.16) for adsorption data set  $0.533 \mu\text{m}$  and  $0.053 \mu\text{m}$  for desorption data set. The deviation from the mean value was lower than variability on the whole range of  $Re$ . In conclusion, the effect of  $Re$  on the adsorption phenomenon on the pipe wall is negligible.

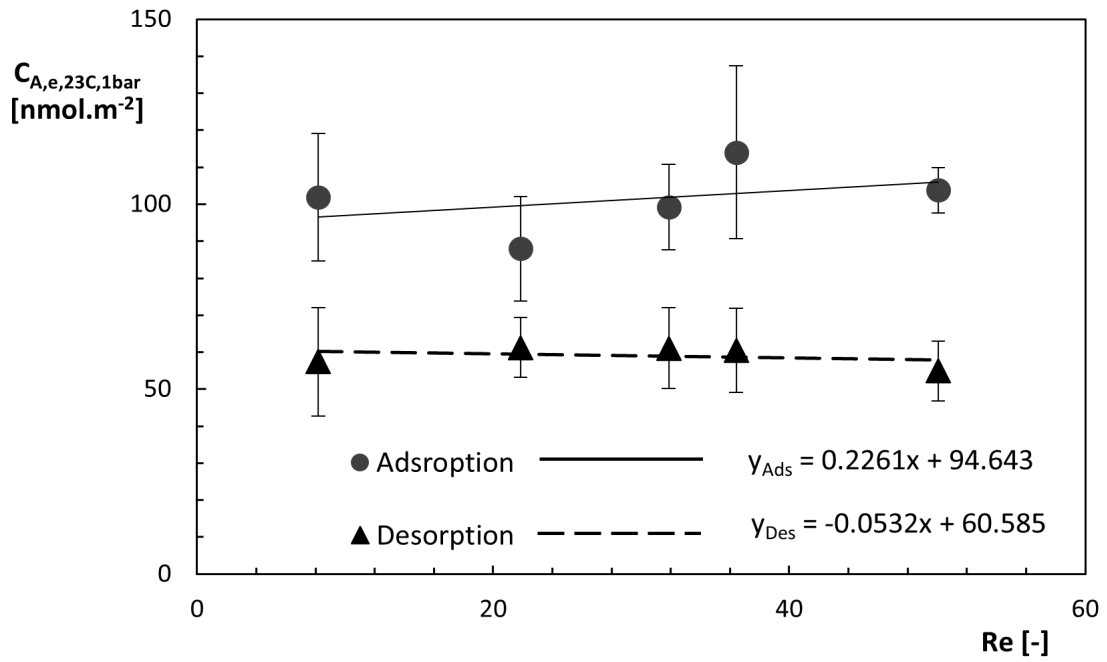


Figure 4.15: Sensitivity of adsorbed and desorbed amount per unit area of Copper on Reynolds number. Values corrected at 23 °C, 1 bar, and grouped on  $Re$ .

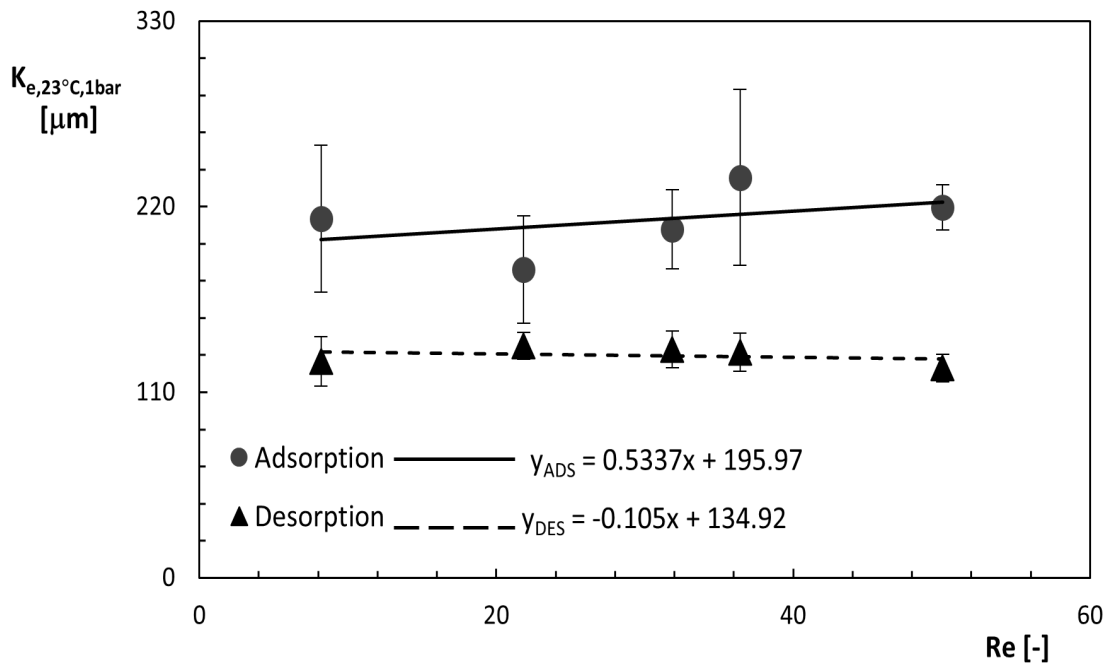


Figure 4.16: Sensitivity of Equilibrium constant with Copper pipe on Reynolds number. Values corrected at 23 °C, 1bar, and grouped on  $Re$ .

The dependency of the adsorbed amount and equilibrium constant on the contact time is shown in Figure 4.17, and Figure 4.18 as a function of average values grouped at 5 different residence times. Contact time ranged between 0.4 and 1 minute. A slope of  $1.70 \text{ nmol}\cdot\text{m}^{-2}\cdot\text{min}^{-1}$  was calculated by linear regression on mean values of the adsorption data and  $0.499 \text{ nmol}\cdot\text{m}^{-2}\cdot\text{min}^{-1}$  by linear regression on the mean values for desorption data set. The effect of residence time on the adsorbed amount per unit area is not completely clear due to the limited range of residence time and the role of other factors, but, in any case, this effect is very limited for both adsorption and desorption.

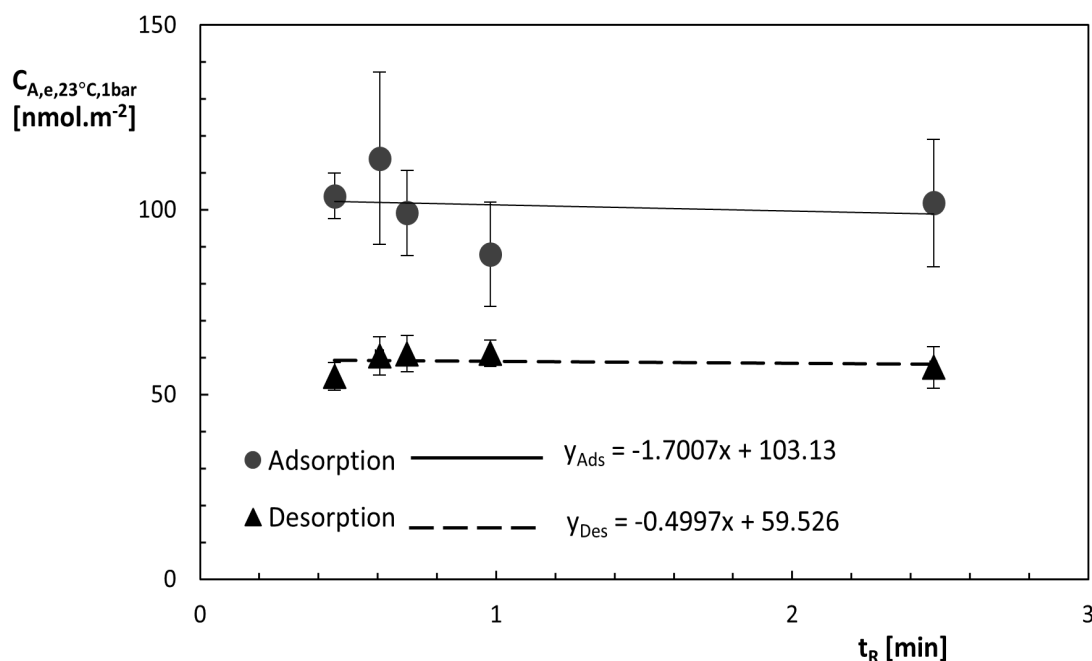


Figure 4.17: Sensitivity of adsorbed amount per unit area of Copper on residence time. Values corrected at  $20^\circ\text{C}$ , 1bar and grouped on  $\tau_R$ .

The slope of equilibrium constants means values plotted against residence time for adsorption data set was calculated to be  $3.972 \mu\text{m}\cdot\text{min}^{-1}$  and  $1.05 \mu\text{m}\cdot\text{min}^{-1}$  for desorption data set. The effect of residence time on the adsorbed amount per unit area and equilibrium constant is limited; however, due to the limited range of residence time and the role of other factors, it can be further investigated.



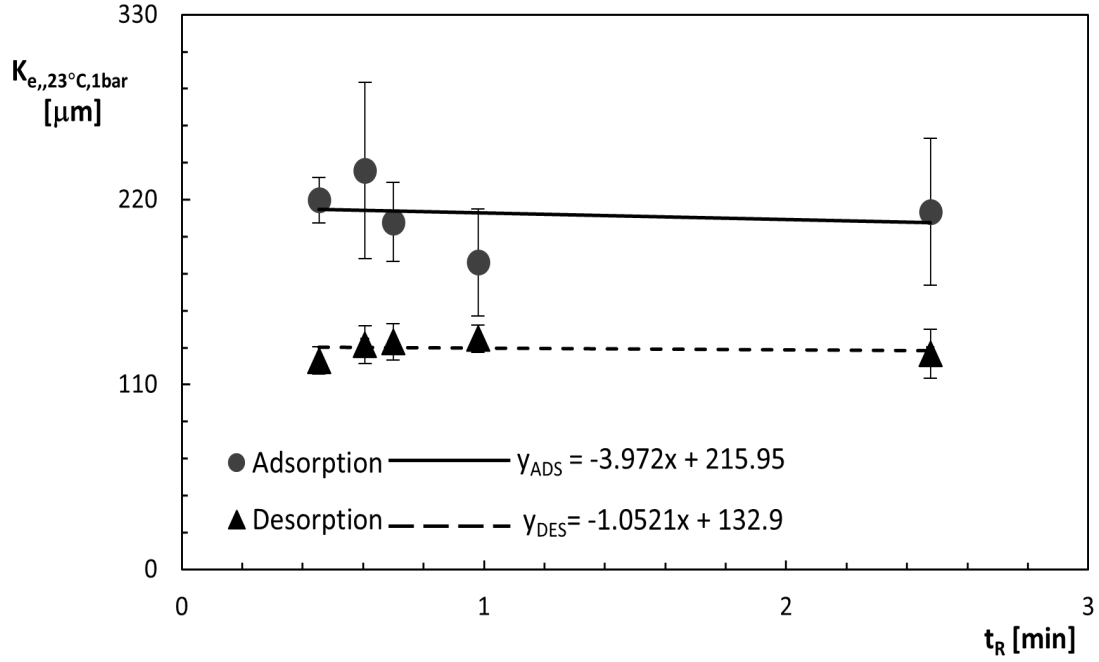


Figure 4.18: Sensitivity of Equilibrium constant with Copper pipe on residence time. Values corrected at 23 °C, 1bar and grouped on  $\tau_R$ .

### 4.3.3 Reproducibility and accuracy with Copper pipe

The uncertainty budget is applied to every single experiment in order to verify the confidence level in every single measurement. The combined uncertainty budget for accuracy of  $C_{A,e}$  and for  $K_e$  are computed from the uncertainty of the input quantities that have been determined from the information available or the performed measurements [13]. The budget for the most conservative experiment with high value of uncertainty is reported in Table 4.10 for  $C_{A,e}$  and Table 4.11 for  $K_e$ . In both of the cases, the accuracy of measurand  $C_{A,e}$  was less than 19% and less than 32% for  $K_e$ .

Table 4.10: Uncertainty budget for  $C_{A,e}$  for most conservative experiment on Copper pipe.

$\mathbf{X}$	$\mathbf{x}$	$[\mathbf{X}]$	$\mathbf{u} = \mathbf{u}(\mathbf{x})$	$\mathbf{u}/\mathbf{x}$	$\mathbf{c} = \partial \mathbf{K}_e / \partial \mathbf{x}_i$	$SI$
$\chi_{Voc}$	10	$\mu \text{ mol} \cdot \text{mol}^{-1}$	1	10.00%	8.67E + 00	63.0%
$q_{v,g}^o$	24	$\text{Sml} \cdot \text{min}^{-1}$	1.00	4.17%	3.61E + 00	10.94%
$I_{ads}$	0.54	min	0.059	10.91%	1.86E + 02	100.0%
$I_{des}$	0.07	min	0.036	50.00%	-1.86E + 02	38.0%
L	11.12	m	0.34	3.06%	-7.80E + 00	5.89%
D	1.651	mm	0.0108	0.65%	-5.25E + 01	0.27%
$C_{A,e}$	86.69	$\text{nmol} \cdot \text{m}^{-2}$	16.13	18.61%		

 Table 4.11: Uncertainty budget for  $K_e$  for most conservative experiment on Copper pipe

$\mathbf{X}$	$\mathbf{x}$	$[\mathbf{X}]$	$\mathbf{u} = \mathbf{u}(\mathbf{x})$	$\mathbf{u}/\mathbf{x}$	$\mathbf{c} = \partial \mathbf{K}_e / \partial \mathbf{x}_i$	$SI$
$q_{v,g}^o$	24	$\text{Sml} \cdot \text{min}^{-1}$	1	4.17%	8.20	2.57%
$I_{ads}$	0.54	min	0.059	10.91%	421.20	23.47%
$I_{des}$	0.073	min	0.036	50.00%	-421.20	8.92%
L	11.12	m	0.34	3.06%	-17.69	1.38%
D	1.65	mm	0.0108	0.65%	-119.13	0.06%
T	24.5	$^{\circ}\text{C}$	2.0	8.16%	0.66	0.07%
$P_{atm}$	98.36	kPa	0.1	0.10%	-182.71	12.76%
$dP_{wc}$	11	kPa	0.28	2.61%	-182.71	100.00%
$K_e$	196.69	$\mu\text{m}$	62.49	31.77%		

Reproducibility was calculated as the standard deviation of the mean. The standard deviation of the mean of the dataset corrected for temperature and pressure has a value around 21% for  $C_{A,e}$  considering the adsorption data set and 10% considering the desorption data set. While for the equilibrium constant, the reproducibility 19% on the adsorption data set and 9% on the desorption data set. In any of the above cases, the reproducibility is limited considering adsorption and desorption as separate data sets. For considering adsorption and desorption as a unique population, the reproducibility is more than 30% for both  $C_{A,e}$  and  $K_e$ . However, the adsorbed and desorbed are different datasets because of significant irreversible interactions on the pipe wall of the Copper. A poorer reproducibility is expected with materials without coating and having potential permeation.

## 4.4 Adsorption and desorption measured with electropolished Stainless steel pipe

The methodology for the quantification of aeric amount adsorbed and Equilibrium constant was extended on electropolished Stainless steel (later addressed as "Stainless steel" only) with 1/4" internal diameter. Tests were performed at different physical conditions that are reported in Table 4.12.

Table 4.12: Number of experiments on Stainless steel, pipe lengths and test condition ranges (residence time, temperature, pressure, and Reynolds number).

Sample	N Ads.	N Des.	L m	$t_R$ min	T °C	P kPa	Re –
Stainless steel	10	10	3	0.45 – 3.0	24 – 27	105 – 114	5 – 35

The adsorbed amount was quite different than that of the desorbed amount, and the data cannot be considered unique for both desorption and adsorption. The number of VOCs adsorbed over the surface was always higher than the number of desorbed VOCs. All the data for adsorption and desorption were considered separately as a unique population with respect to temperature and pressure dependency of interaction phenomena. Welch statistical t-tests reject the hypothesis that all data for adsorption and desorption belong to a unique population with a confidence of 100%.

### 4.4.1 Sensitivity with temperature

Due to the limited number of experiments over a narrow range of temperature, the sensitivity coefficient on temperature was not completely clear. However, a sensitivity coefficient  $-139.79 \text{ nmol}\cdot\text{m}^{-2}\cdot\text{K}^{-1}$  was calculated for the temperature (Figure 4.19) as the slope of the linear regression curve on the adsorption data set and  $109.25 \text{ nmol}\cdot\text{m}^{-2}\cdot\text{K}^{-1}$  for the desorption dataset. A slope is greatly affected by the range of temperature, while here, with this small range of temperature  $4^\circ\text{C}$  there was a negligible change after temperature correction. The data set reported in Table 3.12 was corrected to a specific temperature of  $25^\circ\text{C}$ . The variability due to temperature correction was reduced from 14% to 11% for the adsorption dataset, while for desorption, the variability was reduced from 15% to 12%.

For Equilibrium constant, the sensitivity coefficient was calculated through the slope of linear regression on the adsorption dataset (Figure 4.20), which is  $-414.21 \text{ }\mu\text{m}\cdot\text{K}^{-1}$  and for desorption, it is  $201.83 \text{ }\mu\text{m}\cdot\text{K}^{-1}$ . The reported datasets were corrected to a specific temperature of  $25^\circ\text{C}$  (inside the range of temperature), as reported in Table 4.13. The variability was improved from 15% to 10% for adsorption data set and from 14 to 12% for desorption data sets.

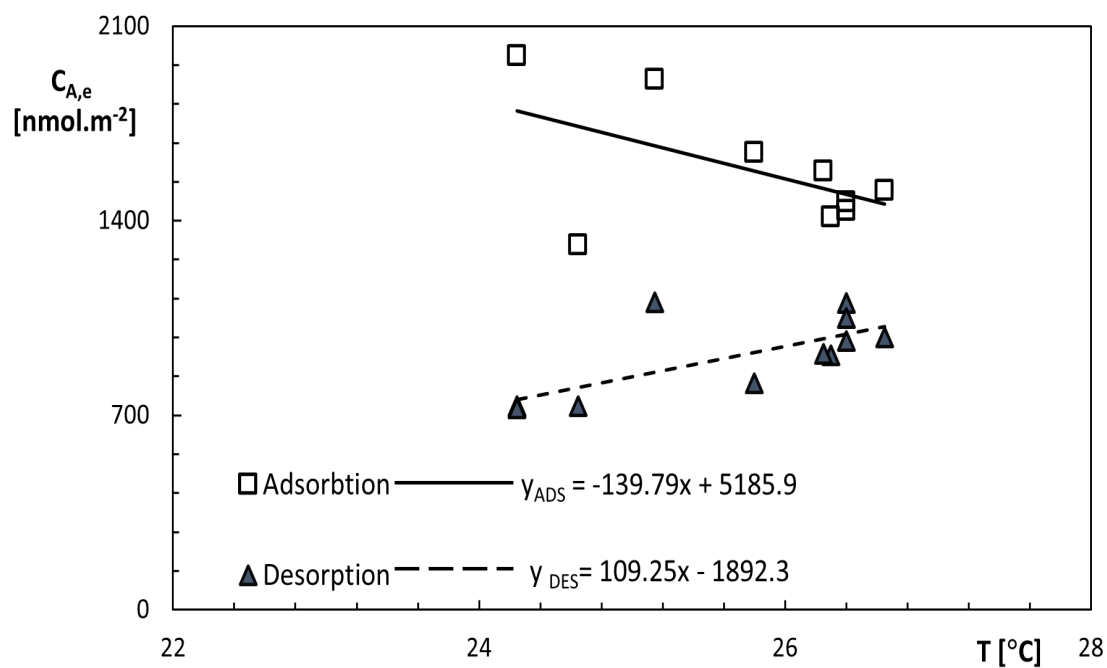


Figure 4.19: Sensitivity of adsorbed amount per unit area  $C_{A,e}$  with Stainless steel pipe on temperature.

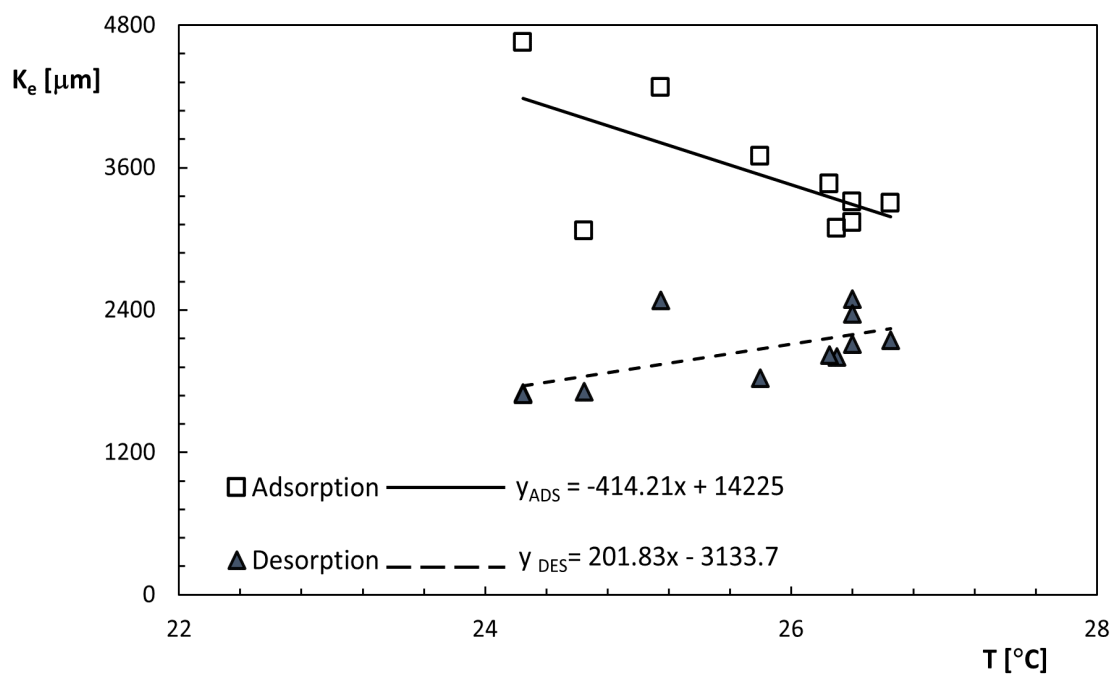


Figure 4.20: Sensitivity of Equilibrium constant  $K_e$  with Stainless steel pipe on temperature.

#### 4.4.2 Sensitivity with pressure

The sensitivity coefficient of as the slope of the linear regression curve on the whole dataset for the dataset was calculated. The corrected data for temperature was also corrected for the pressure bias. As the range of pressure was small 15kPa there was very little impact after correction. The sensitivity coefficient had a value  $10635 \text{ nmol}\cdot\text{m}^{-2}\cdot\text{MPa}^{-1}$  for the adsorption dataset and  $540.09 \text{ nmol}\cdot\text{m}^{-2}\cdot\text{MPa}^{-1}$  for the desorption dataset as reported both in Figure 4.21. The variation was remaining the same for both adsorption and desorption datasets due to the very small impact of correction due to pressure. However, the variation was reduced after correction for both temperature and pressure from 14% to 11% for the adsorption data set and from 15% to 12% for the desorption dataset.

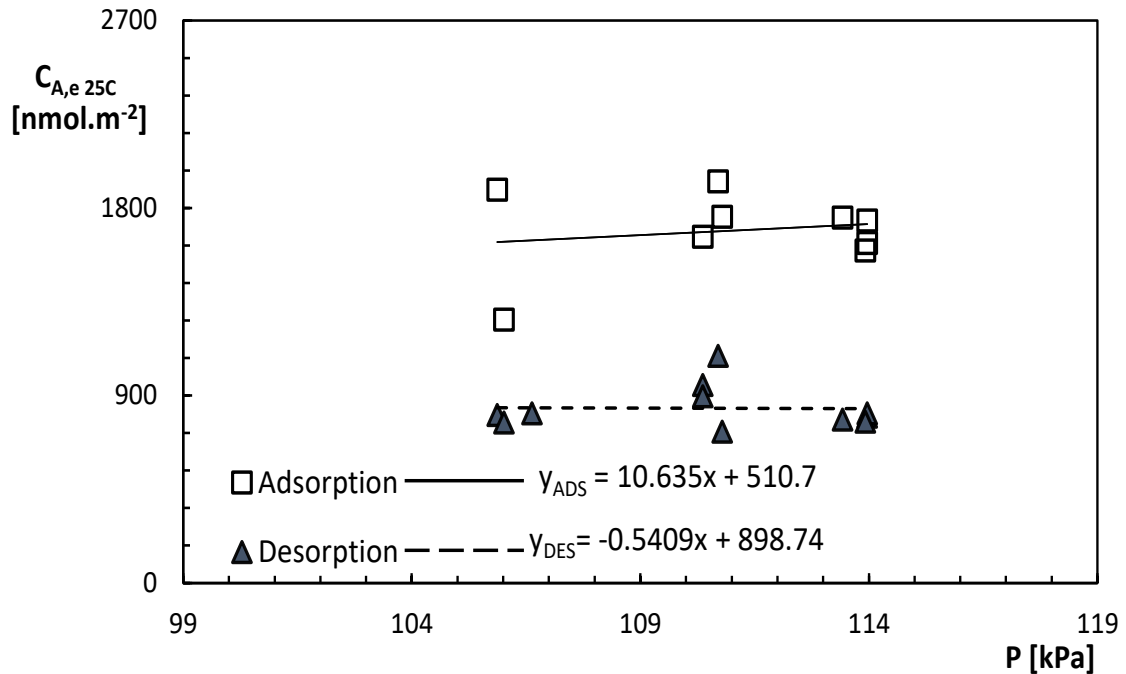


Figure 4.21: Sensitivity of adsorbed amount per unit area ( $C_{A,e}$ ) of Stainless steel pipe on pressure.

The sensitivity coefficient for equilibrium constant was calculated for adsorption and desorption datasets as shown in Figure 4.22; the values are  $18690 \mu\text{m}\cdot\text{MPa}^{-1}$  for adsorption data set, and  $-5510 \mu\text{m}\cdot\text{MPa}^{-1}$  for the desorption data set. The correction for pressure biased was made, and the variation was reduced after correction for both temperature and pressure from 15% to 11% for adsorption and from 14% to 11% for the desorption dataset.

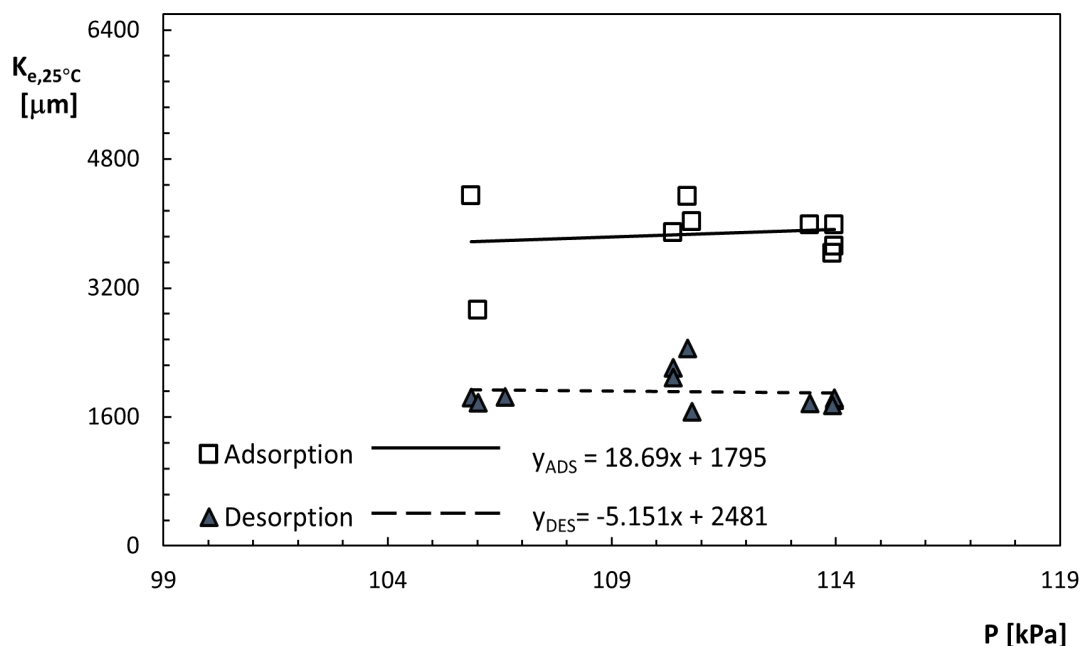


Figure 4.22: Sensitivity of Equilibrium constant  $K_e$  with Stainless steel pipe on pressure.

The reversibility of the interactions is analyzed by comparing the adsorption and desorption. The difference between the amounts of Acetone adsorbed on the surface of the test pipe and desorbed in the second part of the test was calculated to be  $741 \text{ nmol}\cdot\text{m}^{-2}$  as the difference of the mean values corrected for the temperature and pressure biases and  $751 \text{ nmol}\cdot\text{m}^{-2}$  as the mean of the differences measured in each run. The difference between the equilibrium constant calculated from adsorption and desorption data sets is  $1698 \text{ }\mu\text{m}$  calculated as the difference of the means and  $1721 \text{ }\mu\text{m}$  calculated as the mean of the differences. These differences are significant and lie outside the experimental variability, which indicates the two different phenomena during adsorption and desorption. Considering adsorption and desorption datasets as one population will worsen the reproducibility, as reported in Table 4.13. Thus the whole population for adsorption and desorption should be considered as a separate dataset.

The average values of the adsorbed amount per unit area grouped at three different Reynolds numbers ( $Re$ ) are plotted in Figure 4.23. The ( $Re$ ) always lower than 40 and remains in the laminar regime. A slope of  $2.15 \text{ nmol}\cdot\text{m}^{-2}$  was calculated by linear regression on the mean values of the adsorption dataset and  $0.945 \text{ nmol}\cdot\text{m}^{-2}$  by linear regression on the mean values of the desorption dataset.

In the case of Equilibrium constant, the values of  $Re$  still remained below 40,

Table 4.13: Areic amount adsorbed and desorbed per unit area ( $C_{A,e}$ ) and  $K_e$  with Stainless steel pipe

	$C_{A,e}$ nmol · m <sup>-2</sup>	$\sigma\%$ —	$\sigma_{,25^\circ\text{C},1\text{bar}}$ nmol · m <sup>-2</sup>	$\sigma_{\%,25^\circ\text{C},1\text{bar}}$ —	$K_e$ , $\mu\text{m}$	$\sigma\%$ —	$K_{e,25^\circ\text{C}1\text{bar}}$ $\mu\text{m}$	$K_{e,25^\circ\text{C},1\text{bar}}$ —
Adsorption	1584.8	14%	1574.2	11%	3554.5	15%	3869.8	11%
Desorption	913.4	15%	833.2	12%	2049.8	14%	1912.1	11%
Both	1215.6	31%	1166.7	34%	2726.9	31%	2793.1	33%

keeping it in the laminar regime. Value of slope through linear regression on adsorption dataset as shown in Figure 4.24 was 5.012  $\mu\text{m}$  and on the desorption dataset, it was 3.083  $\mu\text{m}$ . In conclusion, the effect of  $Re$  on Acetone adsorbed per unit area and Equilibrium constant obtained from both adsorption and desorption data sets are very limited; however, it is not completely clear due to the very narrow range of  $Re$  and the limited number of experiments.

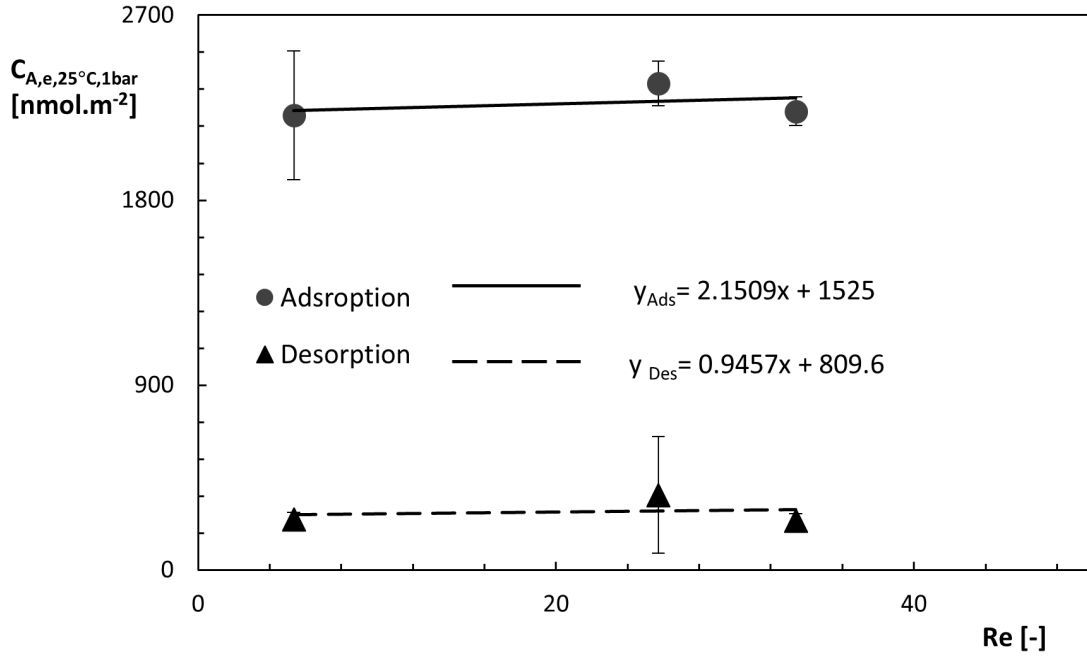


Figure 4.23: Sensitivity of adsorbed amount per unit area of Stainless steel pipe on Reynolds number.

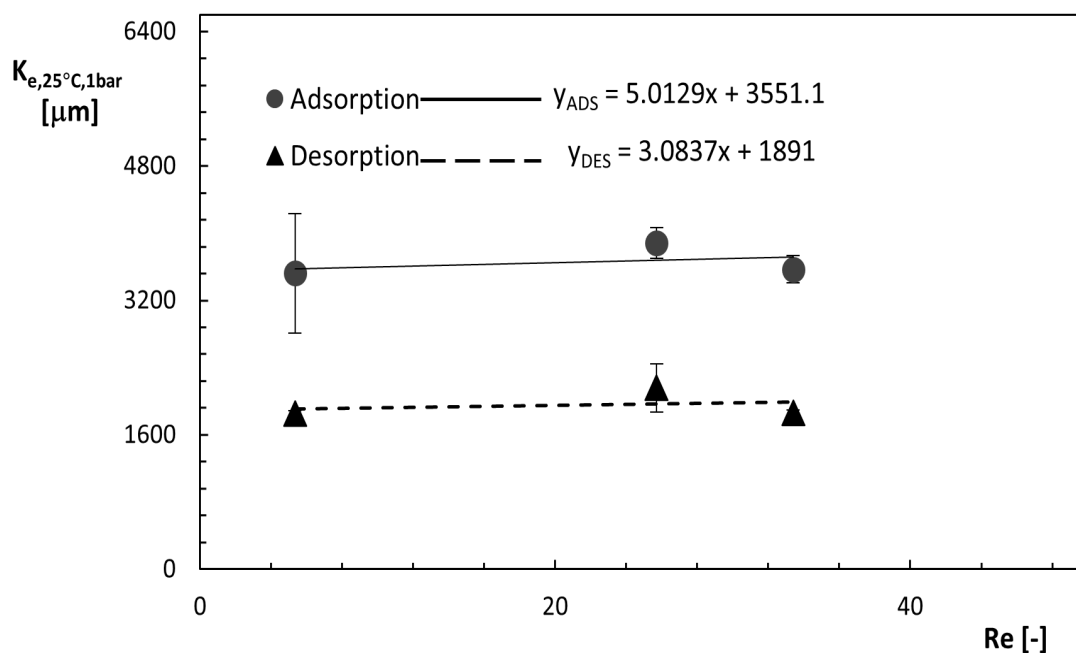


Figure 4.24: Sensitivity of Equilibrium with Stainless steel pipe on Reynolds number.

The dependency of the adsorbed amount on the contact time is shown in Figure 4.25 as a function of average values grouped at three different residence times. Contact time ranged between 0.5 and 3.5 minutes. The slope calculated by linear regression on the mean values of the adsorption data is  $-34.59 \text{ nmol}\cdot\text{m}^{-2}\cdot\text{min}^{-1}$  and by linear regression on the mean values of desorption data is  $-0.652 \text{ nmol}\cdot\text{m}^{-2}\cdot\text{min}^{-1}$ . The effect of residence time on the adsorbed amount per unit area is not completely clear due to the limited number of experiments and the role of other factors, but, in any case, this effect is very limited.

In the calculation of the Equilibrium constant, the dependency on the residence time is evident in Figure 4.27. Slope calculated by linear regression for adsorption and desorption dataset were  $-80.283 \text{ }\mu\text{m}\cdot\text{min}^{-1}$  and  $-11.662 \text{ }\mu\text{m}\cdot\text{min}^{-1}$ , respectively. Due to the lesser number of experiments and the effect of other factors, the role of residence time is negligible.



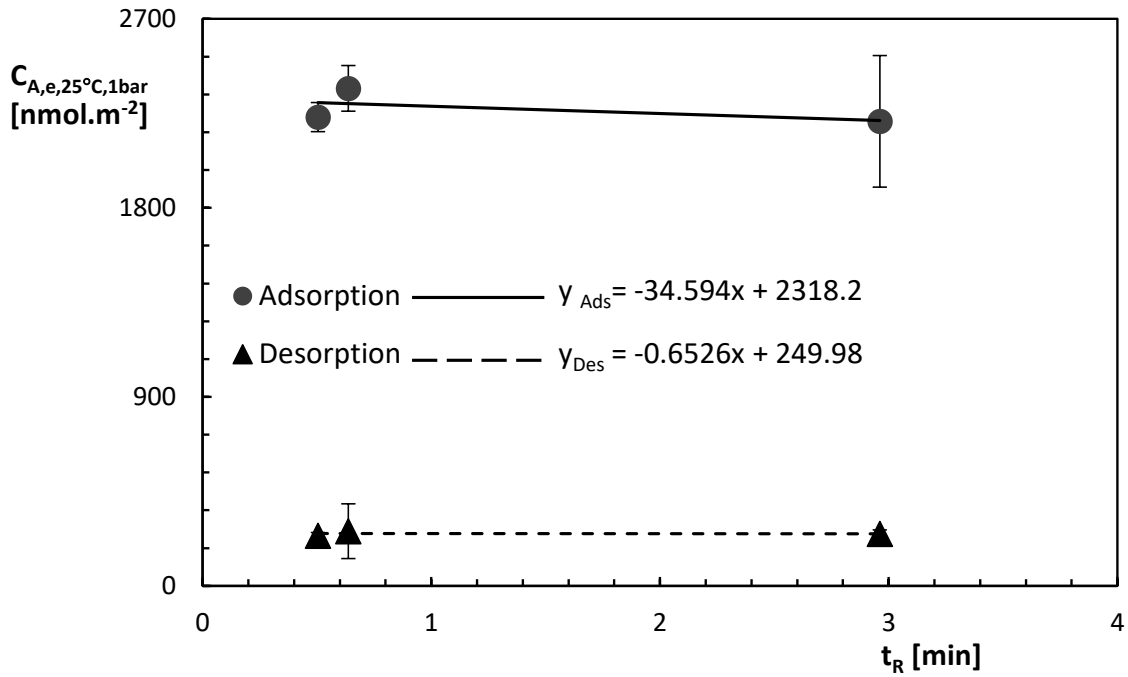


Figure 4.25: Sensitivity of adsorbed amount per unit area of Stainless steel pipe on residence time.

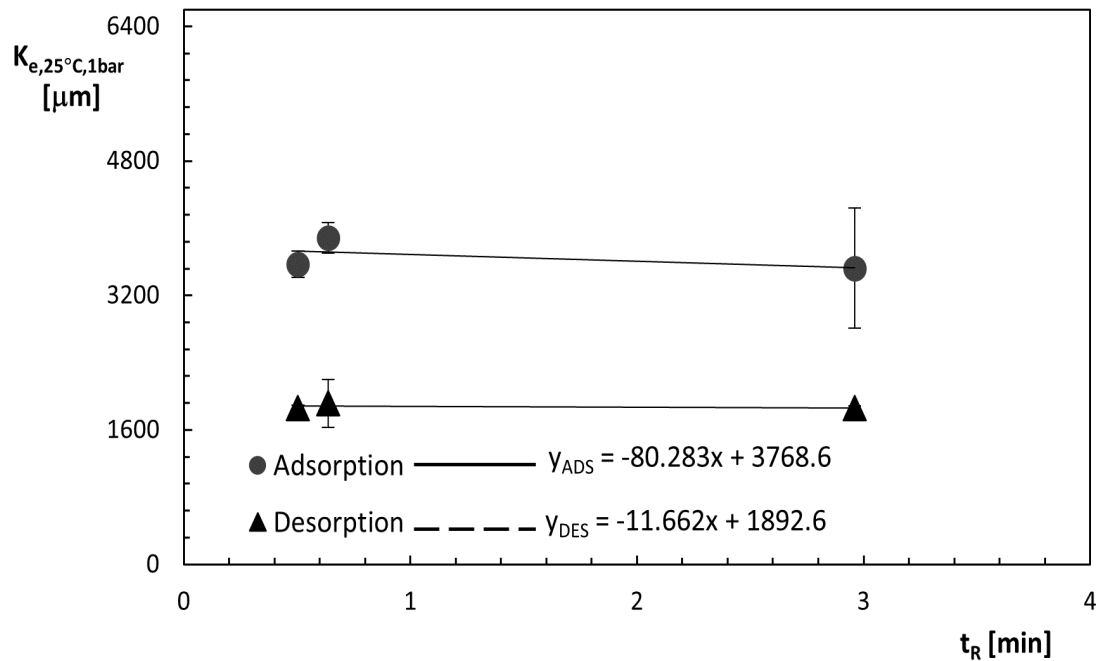


Figure 4.26: Sensitivity of Equilibrium constant with Stainless steel pipe on residence time.

### 4.4.3 Reproducibility and accuracy with Stainless steel pipe

The uncertainty budget is applied to every single experiment in order to verify the confidence level in every single measurement. The combined uncertainty of the measurand  $C_{A,e}$  and  $K_e$  are computed from the uncertainty of the input quantities that have been determined from the information available or the performed measurements [13]. The accuracy of measurand  $C_{A,e}$  was 11.41%. As this can be seen from Table 4.14, the most critical parameter, in this case, is the molar fraction having the Sensitivity Index (SI) of 100%. The budget for the most conservative experiment having higher uncertainty is reported in Table 4.14 for  $C_{A,e}$  and Table 4.15 for  $K_e$ . In the case of an equilibrium constant, the most critical parameter is pressure indicated in the table as  $P_{atm}$  having the Sensitivity Index 100%. While the accuracy of measurand  $K_e$  was 14.08%.

Table 4.14: Uncertainty budget for  $C_{A,e}$  for most conservative experiment on Stainless steel pipe

<b>X</b>	<b>x</b>	<b>[X]</b>	<b>u = u(x)</b>	<b>u/x</b>	<b>c = ∂Ke/∂xi</b>	<b>SI</b>
$\chi_{Voc}$	10	$\mu\text{mol} \cdot \text{mol}^{-1}$	1	10.00%	1.98E + 02	100.0%
$q_{v,g}^o$	77	$\text{Sml} \cdot \text{min}^{-1}$	1.00	1.30%	2.57E + 01	1.69%
$I_{ads}$	2.49	min	0.100	4.01%	7.97E + 02	16.3%
$I_{des}$	0.02	min	0.010	65.02%	-7.97E + 02	0.2%
L	3	m	0.1	3.33%	-6.59E + 02	11.11%
D	4.572	mm	0.04572	1.00%	-4.32E + 02	1.00%
$C_{A,e}$	1976.0	$\text{nmol} \cdot \text{m}^{-2}$	225.51	11.41%		

Table 4.15: Uncertainty budget for  $K_e$  for most conservative experiment on Stainless steel pipe

<b>X</b>	<b>x</b>	<b>[X]</b>	<b>u = u(x)</b>	<b>u/x</b>	<b>c = ∂Ke/∂xi</b>	<b>SI</b>
$q_{v,g}^o$	77	$\text{Sml} \cdot \text{min}^{-1}$	1	1.30%	57.50	2.01%
$I_{ads}$	2.494	min	0.100	4.01%	1786.22	19.43%
$I_{des}$	0.015	min	0.010	65.02%	-1786.22	0.19%
L	3.0	m	0.1	3.33%	-1475.73	13.26%
D	4.572	mm	0.0457	1.00%	-968.32	1.19%
T	25.15	C	2	7.95%	14.84	0.54%
$P_{atm}$	99.8	kPa	0.1	0.10%	-4052.25	100.00%
$dP_{wc}$	11	kPa	0.1	0.92%	-4052.25	100.00%
$K_e$	4427.18	$\mu\text{m}$	623.35	14.08%		

For both adsorption and desorption datasets for  $C_{A,e}$  and  $K_e$  the reproducibility calculated as the standard deviation ( $\sigma$ ) over the raw datasets, and corrected for

temperature and pressure are reported in Table 4.13. The reproducibility is improved by correction of temperature and pressure. There was a very little change after correction due to limited range of pressure.

## 4.5 Adsorption and desorption measured with PFA pipe

The methodology was extended to polymeric material Perfluoroalkoxy (PFA) polymer with 1/4" internal diameter. Tests were performed at different physical conditions that are reported in Table 4.16.

Table 4.16: Number of experiments with PFA, pipe lengths and test condition ranges (residence time, temperature, pressure, and Reynolds number).

Sample	N Ads.	N Des.	L m	$t_R$ min	T °C	P kPa	Re –
PFA	11	11	4.7	0.5 – 3.5	24 – 35	106 – 113	6 – 39

The adsorbed and desorbed amounts were quite different, and the data cannot be considered unique for both desorption, adsorption, and even for the equilibrium constant. Welch statistical t-tests reject the hypothesis that all data for adsorption and desorption belong to a unique population with a confidence of 99%. The number of VOCs adsorbed over the surface measured was always higher than the number of measured desorbed VOCs. All the data for adsorption were considered as a unique population with respect to temperature and pressure dependency of interaction phenomena.

### 4.5.1 Sensitivity with temperature

The effect of temperature on the adsorbed and desorbed amount shows an opposite trend to the other materials like Sulfinert and steel. A number of tests were performed to predict the sensitivity coefficient on temperature within a temperature range 10 °C. From the adsorption data, a sensitivity coefficient  $2.65 \text{ nmol}\cdot\text{m}^{-2}\cdot\text{K}^{-1}$  was calculated for the temperature as the slope of the linear regression curve and  $5.59 \text{ nmol}\cdot\text{m}^{-2}\cdot\text{K}^{-1}$  for desorption data, as shown in Figure 4.27. The data are corrected for 26 °C temperature (the central point of the temperature range for many experiments) for both adsorption and desorption.

The sensitivity coefficient for the equilibrium constant was calculated by the slope of linear regression (Figure 4.28) on both the adsorption and desorption datasets. For adsorption, the value was  $7.494 \text{ }\mu\text{m}\cdot\text{K}^{-1}$  and for desorption, it was  $13.883 \text{ }\mu\text{m}\cdot\text{K}^{-1}$ .

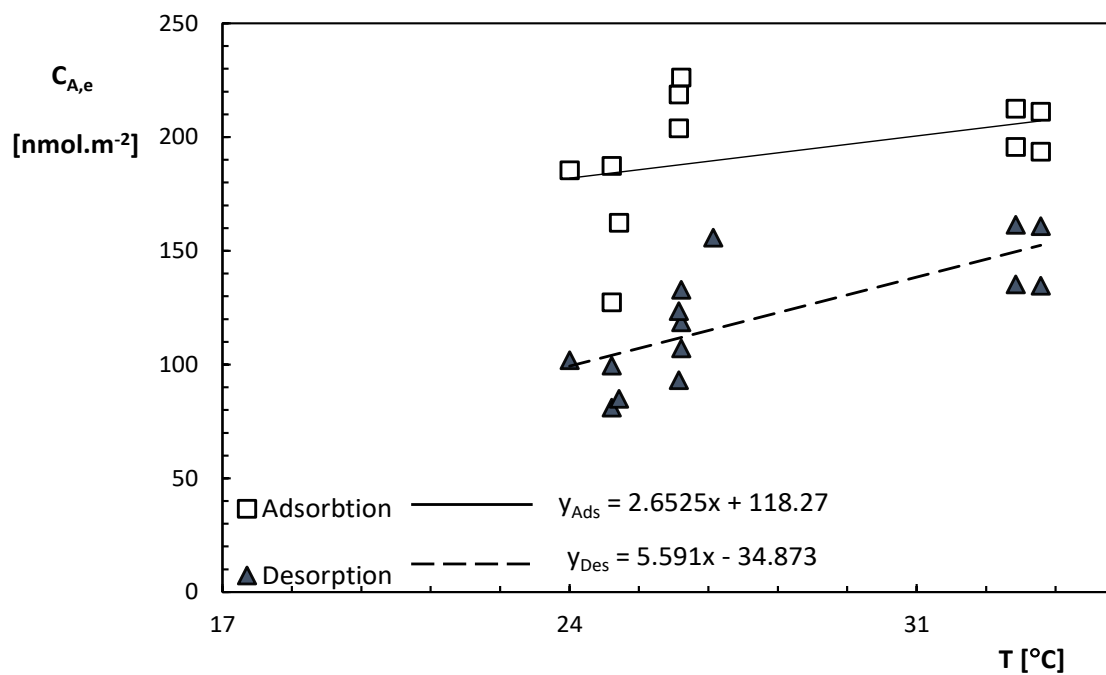


Figure 4.27: Sensitivity of adsorbed amount per unit area of PFA pipe on temperature.

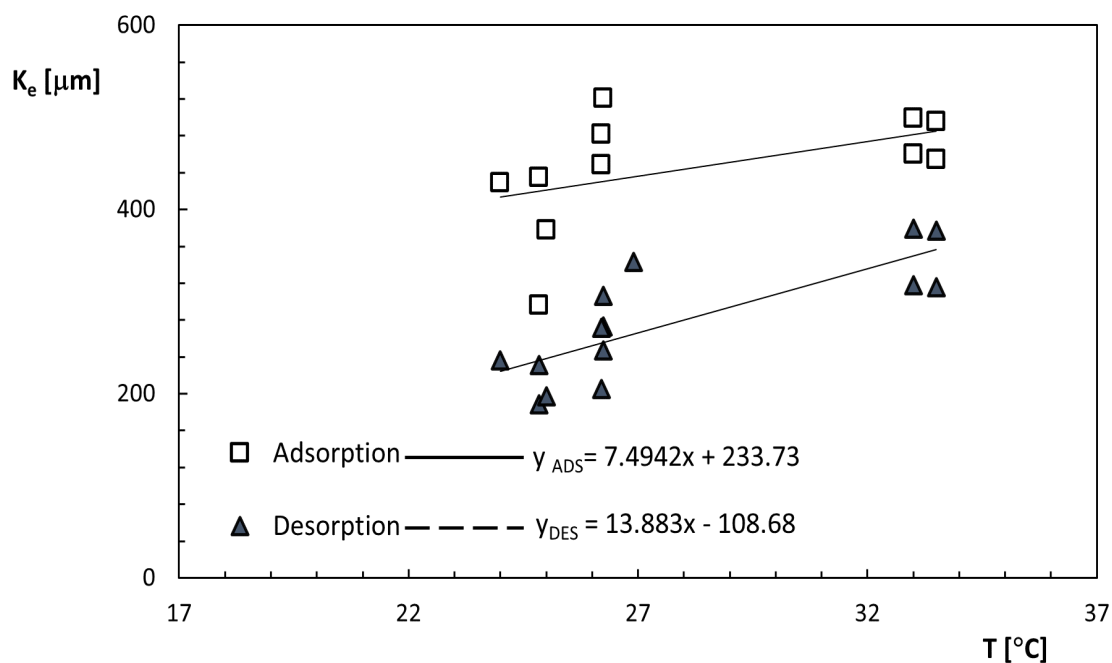


Figure 4.28: Sensitivity of Equilibrium constant with PFA pipe on temperature.

When correction was applied to the temperature, there was an improvement in reproducibility observed from 14% to 13% for adsorption dataset of  $C_{A,e}$  and from 22% to 16% for desorption dataset of  $C_{A,e}$ , as indicated in Table 4.17. While for the Equilibrium constant  $K_e$ , the variability was improved from 14% to 12% for the adsorption dataset, and for desorption, it was improved from 22% to 15%.

## 4.5.2 Sensitivity with pressure

The sensitivity coefficient calculated as the slope of the linear regression curve (Figure 4.29) on the adsorption dataset is  $6026 \text{ nmol}\cdot\text{m}^{-2}\cdot\text{MPa}^{-1}$  and on the desorption dataset is  $3068 \text{ nmol}\cdot\text{m}^{-2}\cdot\text{MPa}^{-1}$ . While for the equilibrium constant, the sensitivity coefficient value for adsorption was  $9690 \text{ }\mu\text{m}\cdot\text{MPa}^{-1}$  and in case of desorption, it was  $4550 \text{ }\mu\text{m}\cdot\text{MPa}^{-1}$  as indicated in Figure 4.30. The data were also corrected for the pressure bias to a pressure 1.08 bar (the central value among the range). With the small range of pressure 11 kPa there was a significant reduction of variability. The total variability for both temperature and pressure was reduced from 14% to 11% for the adsorbed amount and from 22% to 19% on the desorbed amount. While for the equilibrium constant, the total reproducibility was improved from 14% to 11% for the adsorption data set and from 22% to 15% for the desorption data set.

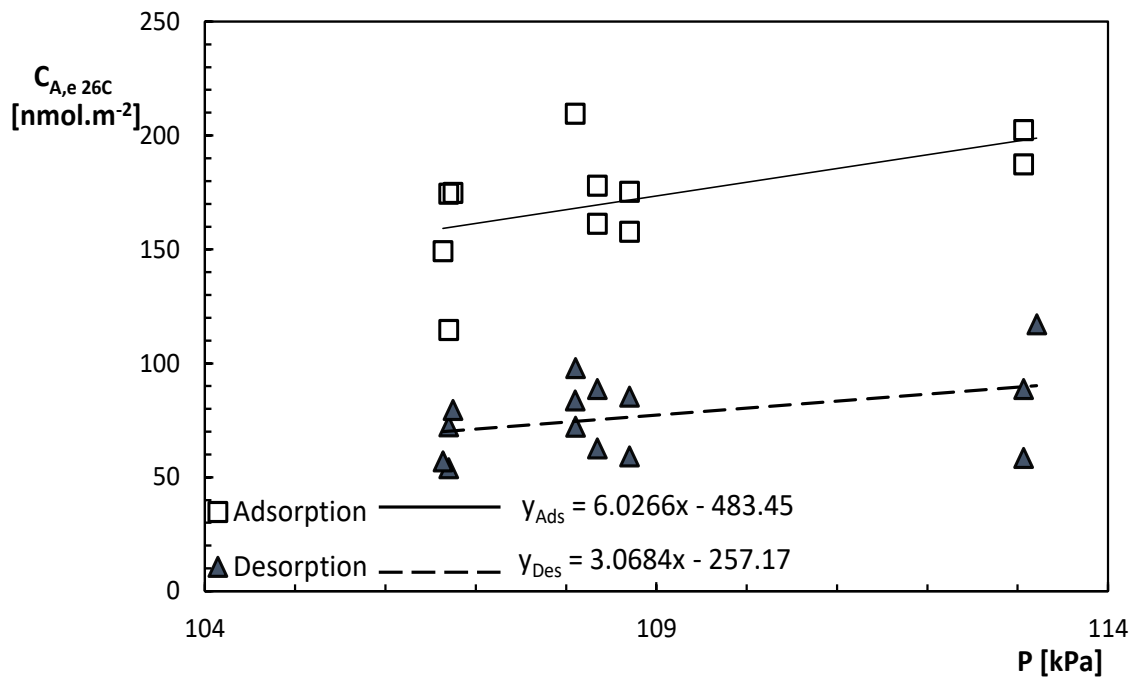


Figure 4.29: Sensitivity of adsorbed amount per unit area with PFA pipe on pressure.

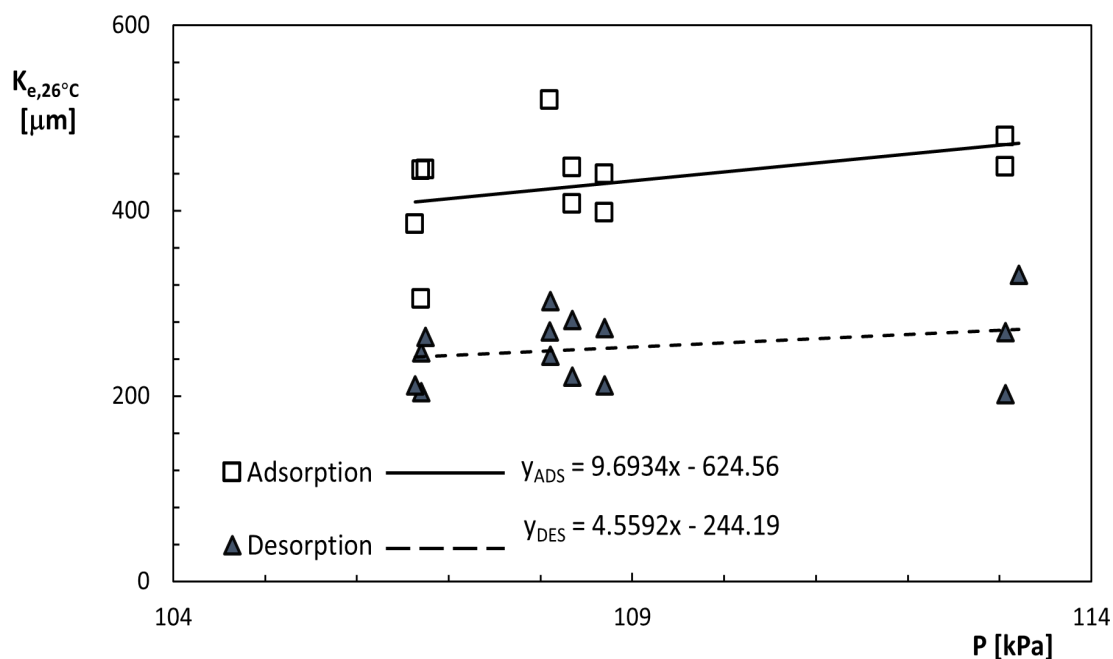


Figure 4.30: Sensitivity of Equilibrium constant  $K_e$  with PFA pipe on pressure.

The reversibility of the interactions was analyzed by comparing the adsorption and desorption. The difference between the amounts of Acetone adsorbed on the surface of the test pipe and desorbed in the second part of the test was calculated to be  $70.1 \text{ nmol}\cdot\text{m}^{-2}$  as the difference of the mean values corrected for the temperature and pressure biases and  $69.7 \text{ nmol}\cdot\text{m}^{-2}$  as the mean of the differences measured in each run. While the difference between equilibrium obtained from the adsorption dataset and desorption data set is  $174.1 \mu\text{m}$  calculated as the difference between means and  $106.92 \mu\text{m}$  calculated as the mean of the differences for every experiment. This difference is significant, and thus, the population for adsorption and desorption were considered as separate datasets, as reported in Table 4.17

Table 4.17: Areic amount adsorbed and desorbed per unit area ( $C_{A,e}$ ) and  $K_e$  with PFA pipe

	$C_{A,e}$ $\text{nmol}\cdot\text{m}^{-2}$	$\sigma\%$	$\sigma_{26^\circ\text{C},1.08\text{bar}}$ $\text{nmol}\cdot\text{m}^{-2}$	$\sigma_{\%,26^\circ\text{C},1.08\text{bar}}$	$K_e$ $\mu\text{m}$	$\sigma\%$	$K_{e,26^\circ\text{C},1.08\text{bar}}$ $\mu\text{m}$	$K_{e,26^\circ\text{C},1.08\text{bar}}$ $\mu\text{m}$
Adsorption	193.1	14%	183.3	11%	445.2	14%	422.3	11%
Desorption	120.8	22%	113.2	19%	277.8	22%	248.2	15%
Both	152.6	29%	144.1	28%	351	29%	324.8	30%

The average values of the adsorbed amount per unit area grouped at three different Reynolds numbers ( $Re$ ) are plotted in Figure 4.31. The ( $Re$ ) always

lower than 40 and remains in the laminar regime. A slope of  $0.104 \text{ nmol}\cdot\text{m}^{-2}$  was calculated by linear regression on all the mean values of adsorption data and  $1.3 \text{ nmol}\cdot\text{m}^{-2}$  for the desorption dataset. The dependence of desorption on the Reynolds number is more significant, while adsorption shows relatively constant behavior. These two lines overlapped on a certain value of Reynolds number, as depicted in Figure 4.31. Whereas, in the case of Equilibrium constant, the trend of both adsorption and desorption showed a similar dependence on the Reynolds number. Linear regression slope for the adsorption is  $0.2359 \mu\text{m}$  and for desorption it was  $0.2044 \mu\text{m}$  with no overlapping between two lines as displayed in Figure 4.32.

In conclusion, the effect of  $Re$  on Acetone adsorbed per unit area and Equilibrium constant is not significant, and the phenomenon does not affect the fluid dynamics to a greater extent.

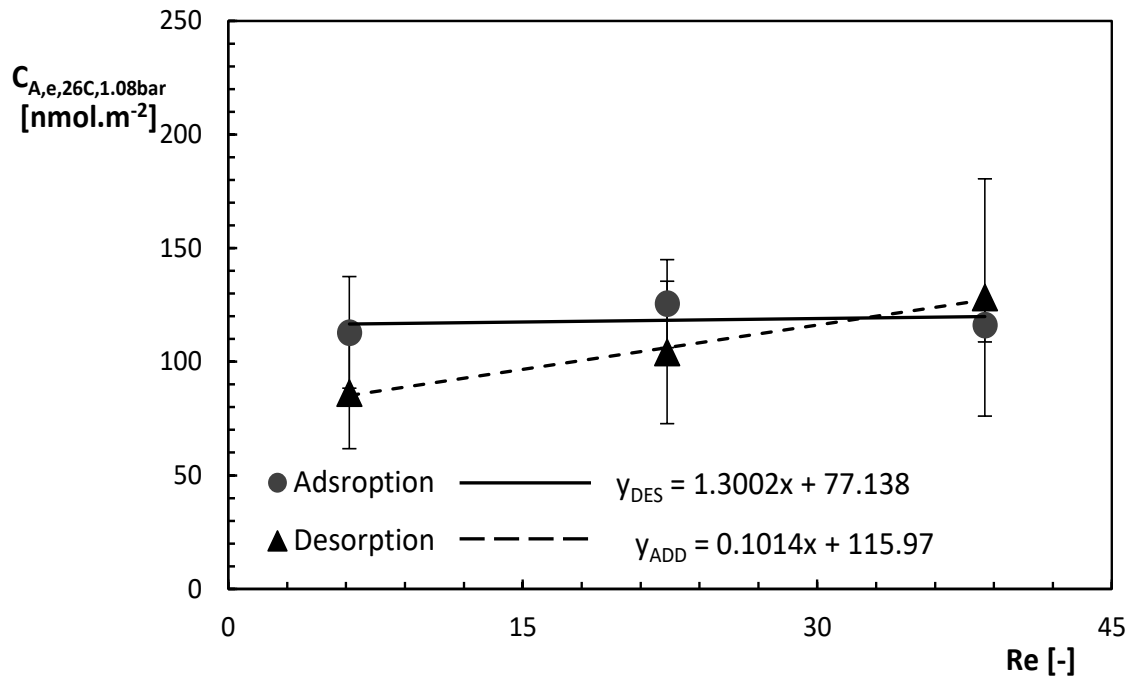


Figure 4.31: Sensitivity of adsorbed amount per unit area of PFA pipe on Reynolds number.

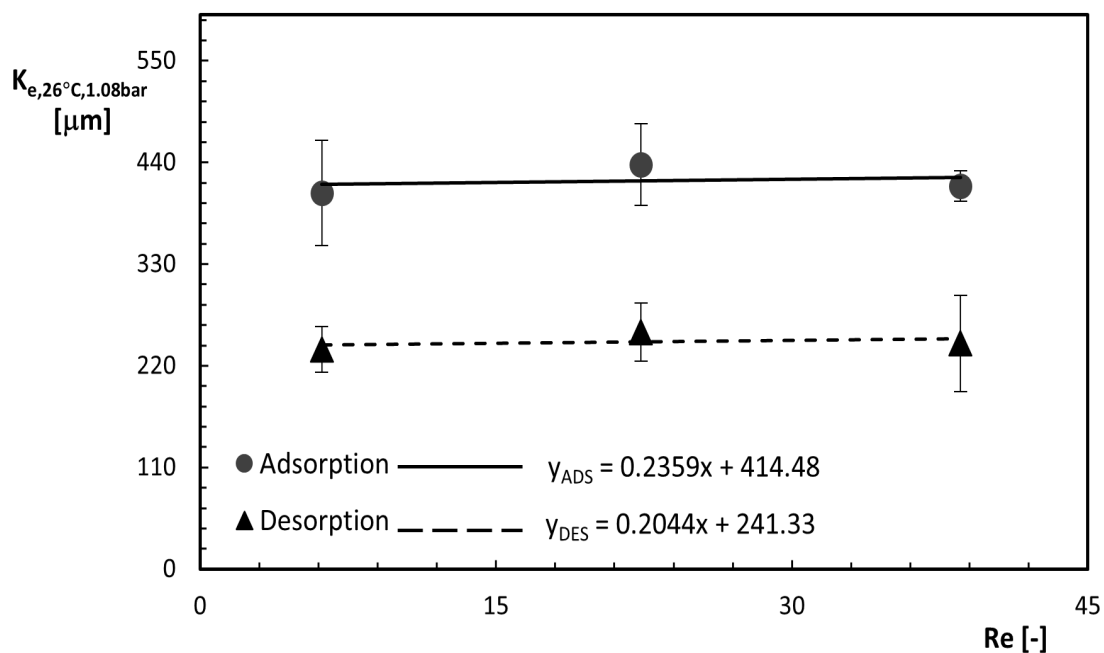


Figure 4.32: Sensitivity of Equilibrium constant with PFA pipe on Reynolds number.

The dependency of the adsorbed amount on the contact time is shown in Figure 4.33, and the dependency on the Equilibrium constant is shown in Figure 4.34 as a function of average values grouped at three different residence times. Contact time ranged between 0.5 and 3.5 minutes. The slope calculated by linear regression on the mean values of  $C_{A,e}$  on adsorption data is  $-2.614 \text{ nmol}\cdot\text{m}^{-2}\cdot\text{min}^{-1}$  and  $-12.125 \text{ nmol}\cdot\text{m}^{-2}\cdot\text{min}^{-1}$  for desorption data. While the slope of mean values of equilibrium constant on adsorption data set is  $6.28 \text{ }\mu\text{m}\cdot\text{min}^{-1}$  and on desorption data set is  $4.25 \text{ }\mu\text{m}\cdot\text{min}^{-1}$ . The effect of residence time on the adsorbed amount per unit area is not completely clear due to the limited number of experiments and the narrow range of residence time.



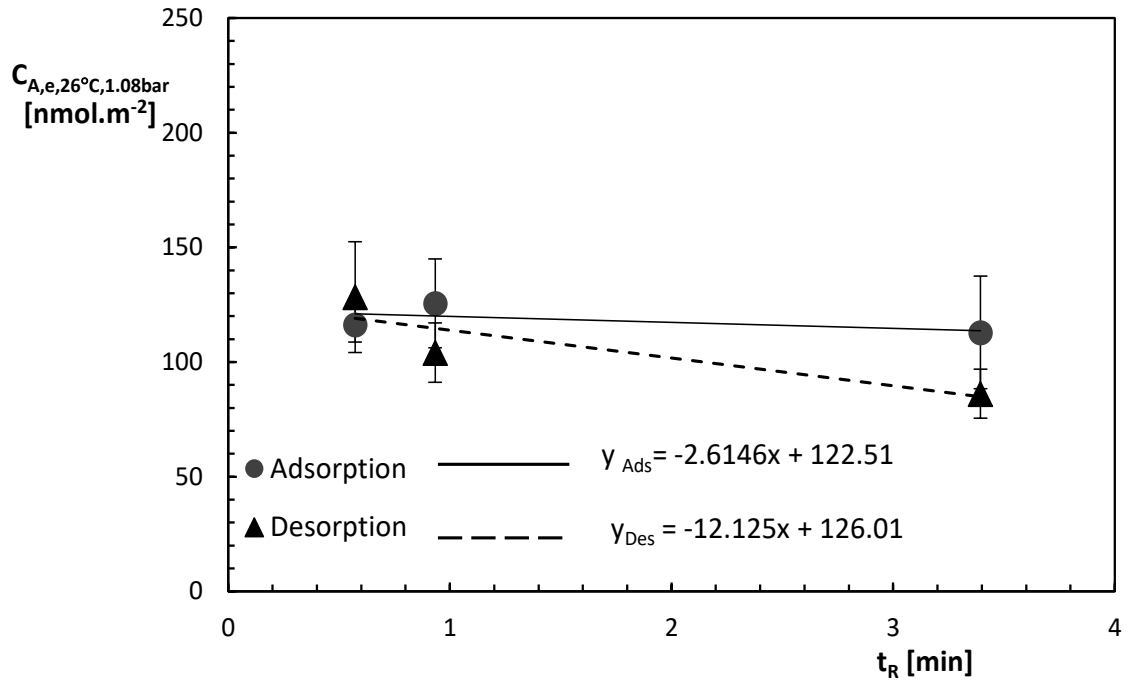


Figure 4.33: Sensitivity of adsorbed amount per unit area  $C_{A,e}$  of PFA pipe on residence time.

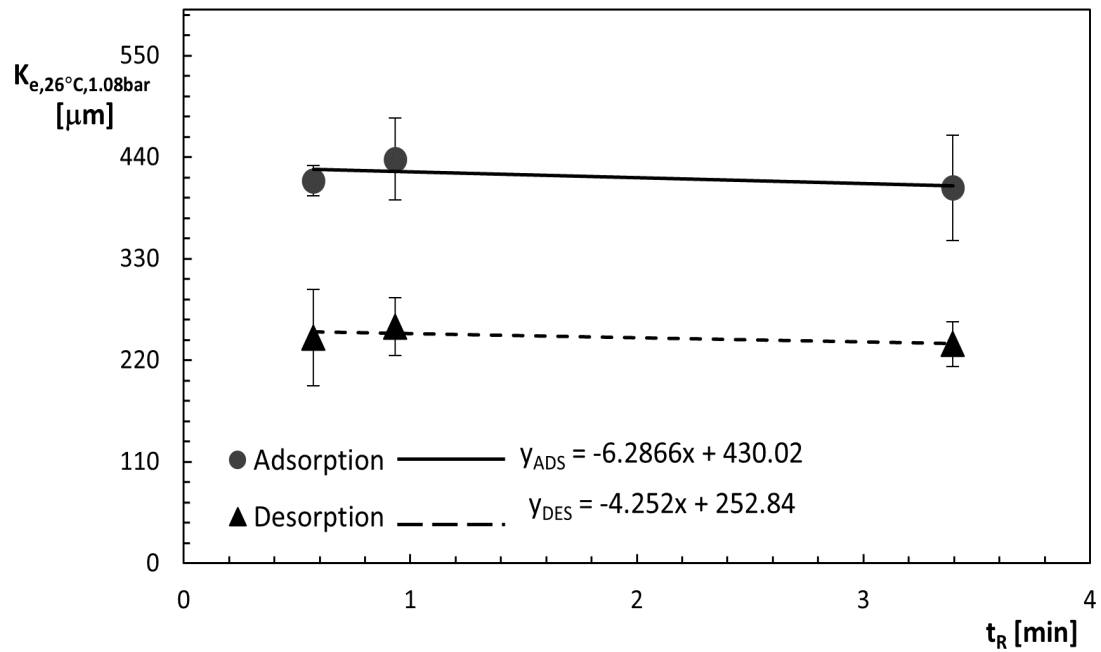


Figure 4.34: Sensitivity of Equilibrium constant  $K_e$  with PFA pipe on residence time.

### 4.5.3 Reproducibility and accuracy with PFA pipe

The uncertainty budget is applied to every single experiment in order to verify the degree of confidence in every single measurement. The accuracy of measurand  $C_{A,e}$  was 36.95% for the most conservative experiments with high value of uncertainty. As this can be seen from Table 4.18, the most critical parameter, in this case, is the integral of the adsorption part of the curve ( $I_{ads}$ ), having the Sensitivity Index (SI) of 100%. In the case of an Equilibrium constant, the most critical parameter is again integral of the adsorption part of the curve ( $I_{ads}$ ) in Table 4.19, having the Sensitivity Index 100%. While the accuracy of measurand  $K_e$  for the same experiments was 40.60%.

Table 4.18: Uncertainty budget for  $C_{A,e}$  for most conservative experiment on PFA pipe

<b>X</b>	<b>x</b>	<b>[X]</b>	<b>u = u(x)</b>	<b>u/x</b>	<b>c = ∂Ke/∂xi</b>	<b>SI</b>
$\chi_{Voc}$	10	$\mu\text{mol} \cdot \text{mol}^{-1}$	1	10.00%	10.6	8.2%
$q_{v,g}^o$	16	$\text{Sml} \cdot \text{min}^{-1}$	1.00	6.25%	6.65	3.20%
$I_{ads}$	1.14	min	0.30	26.24%	124	100.0%
$I_{des}$	0.28	min	0.01	4.12%	-124.00	0.20%
$L$	4.7	m	0.1	2.13%	-22.60	0.37%
$D$	3.903	mm	0.039	1.00%	-27.30	0.08%
$C_{A,e}$	106.43	$\text{nmol} \cdot \text{m}^{-2}$	39.33	36.95%		

Table 4.19: Uncertainty budget for  $K_e$  for most conservative experiment on PFA pipe

<b>X</b>	<b>x</b>	<b>[X]</b>	<b>u = u(x)</b>	<b>u/x</b>	<b>c = ∂Ke/∂xi</b>	<b>SI</b>
$q_{v,g}^o$	16	$\text{Sml} \cdot \text{min}^{-1}$	1	6.25%	15.45	3.20%
$I_{ads}$	1.143	min	0.30	26.24%	287.68	100.0%
$I_{des}$	0.284	min	0.012	4.12%	-287.68	0.15%
$L$	4.7	m	0.1	2.13%	-52.59	0.37%
$D$	3.90	mm	0.039	1.00%	-63.33	0.08%
$T$	24.9	C	2.0	8.03%	0.83	0.04%
$P_{atm}$	99.5	kPa	0.1	0.10%	-234.73	7.40%
$dP_{wc}$	7	kPa	0.18	2.49%	-234.73	23.97%
$K_e$	247.18	$\mu\text{m}$	100.36	40.60%		

Reproducibility was calculated as the standard deviation of the mean of the dataset with data corrected for temperature and pressure has a value of around

11% for  $C_{A,e}$  considering the adsorption data set and 19% considering the desorption data set. While for the equilibrium constant, the reproducibility 11% on the adsorption data set and 19% on the desorption data set, as reported in Table 4.17. In any of the above cases, the relative reproducibility is limited considering adsorption and desorption as separate data sets. For considering adsorption and desorption as a unique population, the reproducibility is more than 30% for both  $C_{A,e}$  and  $K_e$ . However, the adsorbed and desorbed are different datasets because of significant irreversible interactions on the pipe wall of the PFA and possible permeation.

## 4.6 Comparison and discussion

The methodology for quantification of mass adsorbed and desorbed during equilibrium was applied on four different pipes with two different diameters. All the pipes were expected to behave differently during the adsorption process due to different affinity towards VOCs.

Figure 4.35 shows the comparison of the curves for adsorption and desorption tests on all four materials. All the experiments were performed with a very small range of residence time but different flow rates. For Sulfinert®, the flowrate was  $35 \text{ Sml}\cdot\text{min}^{-1}$ , for Copper, the flowrate was  $24 \text{ Sml}\cdot\text{min}^{-1}$ , PFA  $58 \text{ Sml}\cdot\text{min}^{-1}$ , and for Stainless steel, the flowrate was  $77 \text{ Sml}\cdot\text{min}^{-1}$ . After one residence time, there was peak (rise of signal curve) evident for all materials except PFA. Due to the memory effect, the small spike due to the switch is overcome by the memory effect and cannot be observed. The rise of the curve was anticipated for PFA and delayed for stainless steel. For Copper, PFA, and Stainless steel, the stability was not achieved after 15 times of the residence time. While for Sulfinert, the stability is achieved completely 3 to 4 times of the residence time. In PFA, the signal during the fall of the curve maintains above the air signal, which depicts the memory release from the pipe during that period. In the desorption part of the curve, the signal for stainless steel is not reached to the VOC signal which is due to the high rate of irreversible losses. The same effect can be seen in PFA, where the irreversible losses are significant. The cleaning of the sulfinert was achieved after four times of the residence time, while for other materials, it takes more than 15 times for cleaning. In summary, the equilibrium of adsorption takes a longer time for PFA, and stainless steel, and the effect of irreversible losses and memory dominates the phenomenon.

The extent of the range of temperature, mainly due to the seasonal variations, was around  $14 \text{ }^\circ\text{C}$  for Sulfinert®,  $4 \text{ }^\circ\text{C}$  for Copper and  $3 \text{ }^\circ\text{C}$  for electropolished stainless steel, and  $12 \text{ }^\circ\text{C}$  for PFA. The correction of results was necessary to compare data for Sulfinert® and Copper. A sensitivity factor on temperature was calculated, and data were corrected for reference temperature (mainly the central

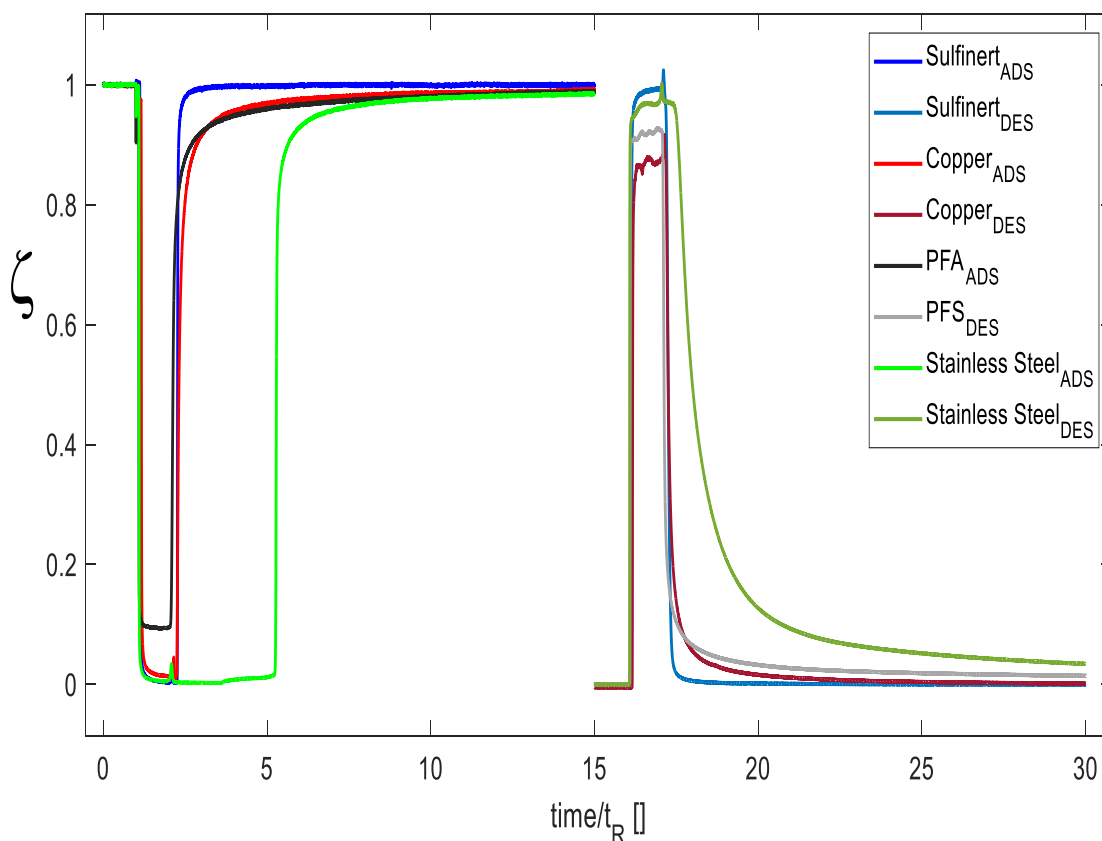


Figure 4.35: Comparing the concentration curves for different materials during adsorption and desorption test. The dim color represents the desorption.

point of the temperature range) 20°C for Sulfinert<sup>®</sup>, 23°C for Copper, 25°C for Stainless steel, and 26°C for PFA.

The extent of the range of pressure, mainly due to the pressure drop under different operational conditions, was around 30 kPa for Sulfinert<sup>®</sup> and 13 kPa for Copper and 10 kPa for Stainless steel, and 7 kPa for PFA. The correction was required for comparison of data; for Sulfinert<sup>®</sup> and Copper Stainless steel, the data were corrected to a reference pressure 1bar, while for PFA, the data were corrected to 1.08bar.

For Sulfinert<sup>®</sup>, the data for adsorption and desorption were considered as unique, and a common sensitivity coefficient was used for correction of whole data, while for Copper, Stainless steel, and PFA, the adsorption and desorption data sets were considered separately, and separate coefficient of temperature were considered. The dependency of temperature on desorption was higher than desorption, and it was evident for the Copper 4.11, Stainless steel (4.22, and PFA 4.27. It is due to the fact that the desorption process is enhanced by high temperature, and adsorption is enhanced by low temperature. The sensitivity on pressure shows a higher value

for adsorption and a lower value for desorption that can be seen in Figure 4.13 for Copper, Figure 4.21 for Stainless steel, and Figure 4.29 for PFA.

The dependency of the Equilibrium constant on temperature was lower than adsorbed amount; however, for all materials, a dependency was observed on temperature as well as pressure. The measured values of  $C_{A,e}$  and  $K_e$  are reported in Table 4.20 and compared for different materials.

Table 4.20: Areic amount adsorbed and desorbed ( $C_{A,e}$ ) and Equilibrium constant ( $K_e$ ) with reproducibility

		$C_{A,e,T,P}$ nmol·m <sup>-2</sup>	$\sigma, C_{A,e,T,P}$ nmol·m <sup>-2</sup>	$\sigma\%$	$K_{e,T,P}$ μm	$\sigma, K_{e,T,P}$ μm	$\sigma\%$
Sulfinert ®	Ads.	37.9	2.7	7%	76.6	4.3	6%
	Des.	28	4.8	17%	84.3	4.5	5%
Copper	Ads.	88.4	18.6	21%	214.4	41.5	19%
	Des.	54.5	5.3	10%	132	12	9%
S. steel	Ads.	1574.2	180.3	11%	3664	400.7	11%
	Des.	833.2	98.9	12%	1966.4	225.4	11%
PFA	Ads.	183.3	20.8	11%	422.3	48.3	11%
	Des.	113.2	21.4	19%	248.2	36.2	15%

A sensitivity of  $C_{A,e}$  and  $K_e$  on  $Re$  and contact time was performed for all materials in order to verify the effect of fluid dynamics and contact time on the phenomenon. As expected, the  $K_e$  for Sulfinert® and Copper does not depend on the fluid dynamic conditions ( $Re$ ) and the contact time and it has been validated by the given results.



# Chapter 5

## Estimation of irreversible losses and memory effect

Gases, when come into contact with solid surfaces, are subjected to reversible and irreversible losses. The irreversible losses are mainly due to the reaction with metallic pipes and permeation in polymeric materials. The mass reacted or permeate into the solid surface irreversibly per unit area per unit time is calculated as mass flux  $J$ . While for the memory effect, the mass release from unit area per unit time is calculated as release flux ( $M$ ). In both the case, the mass flux is calculated using the two different methods as explained in section 3.3 and 3.4. Experiments over different materials at different conditions, as reported in Table 5.1, were performed for both irreversibly reacted mass and release due to memory.

Table 5.1: Number of experiments and test condition ranges (temperature, pressure, and residence time).

	$N_{\text{exp}}$	T [°C]	P [kPa]	$t_{\text{R}}$ [min]
PFA	24	24.0 – 33.5	106.6 – 113.2	0.6 – 3.4
S. steel	18	24.3 – 27.0	105.9 – 114.0	0.5 – 3.0
Copper	14	23.0 – 27	107.6 – 110.5	0.3 – 0.6
Sulfinert®	10	22.0 – 27	102.9 – 109.6	0.4 – 2.4

### 5.1 Irreversible losses $J$

The estimation of irreversible losses in uncoated materials and polymeric materials is significant and cannot be ignored. Sulfinert® treated stainless is considered the most inert material for sampling VOCs, and very limited reactions are expected.

The mass irreversibly reacted to the walls of the pipe is calculated using two different approaches. Method A based on the difference of the signal of VOC in bypass and pipe was not easily applicable for coated materials like Sulfinert® as the difference was very small to observe. However, method B was working very well for all materials that allow us to measure the mass flux irreversibly reacted to the pipe and was considered as a representative approach in this research. The reacted amount per unit area per unit time ( $J$ ) was measured at different saturation, and the effect of saturation was evident. Figure 5.1 shows the effect of saturation over repeated experiments for the PFA pipe. Experiments were performed at  $58 \text{ Sml}\cdot\text{min}^{-1}$ . The area under the curve was reduced with saturation time that results in the reduction of calculated irreversible losses. The depletion of the signal was reduced to a minimum change of signal in the test pipe and bypass. At lower saturation, the equilibrium not yet reached, and the mass reacted due to equilibrium is calculated as bias to irreversible losses.

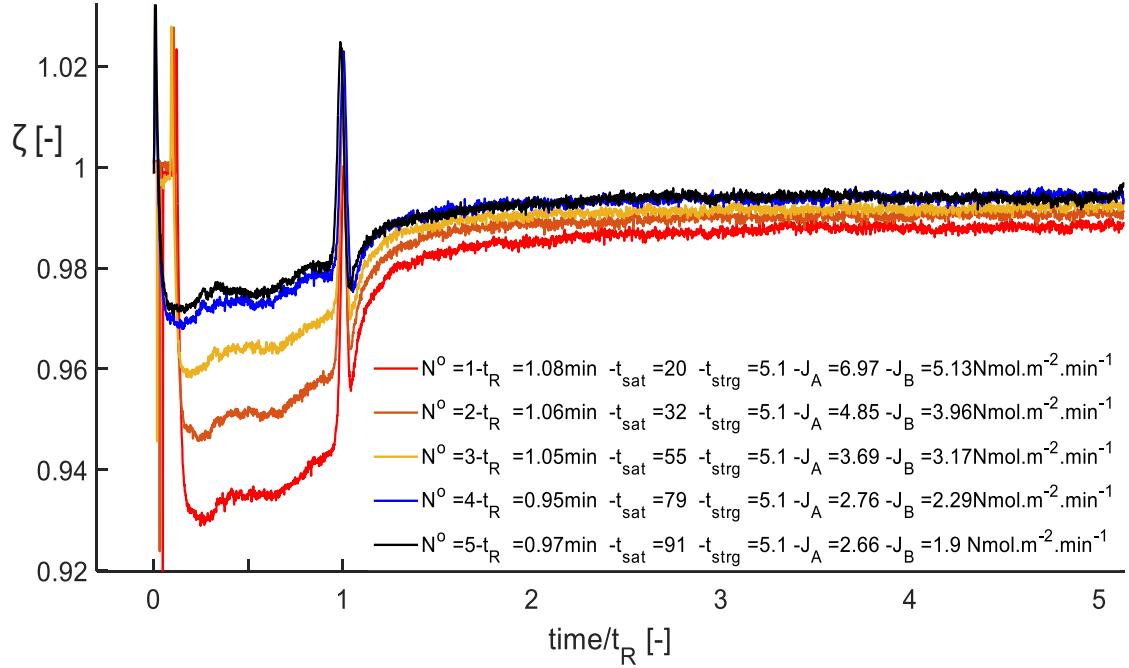


Figure 5.1: Signal of VOC in bypass and test pipe (PFA) at different saturation times. Red color shows less saturation while black shows more saturation time.

A dependency of saturation time was calculated as the slope of the linear line for both approach A and B, as shown in Figure 5.2 for PFA. A similar approach was applied for other materials. The value of slope for PFA was  $0.0456 \text{ nmol}\cdot\text{m}^{-2}\cdot\text{min}^{-1}$  for approach A data set and  $0.0329 \text{ nmol}\cdot\text{m}^{-2}\cdot\text{min}^{-1}$  for approach B data set. For electropolished stainless steel  $0.208 \text{ nmol}\cdot\text{m}^{-2}\cdot\text{min}^{-1}$  for approach A data set and  $0.0392 \text{ nmol}\cdot\text{m}^{-2}\cdot\text{min}^{-1}$  for approach B data set. For Copper the slope with



approach A dataset is  $0.005 \text{ nmol}\cdot\text{m}^{-2}\cdot\text{min}^{-1}$  and  $0.0164 \text{ nmol}\cdot\text{m}^{-2}\cdot\text{min}^{-1}$  with approach B data set. For Sulfinert®, the slope with approach A dataset is  $0.001 \text{ nmol}\cdot\text{m}^{-2}\cdot\text{min}^{-1}$  and  $0.014 \text{ nmol}\cdot\text{m}^{-2}\cdot\text{min}^{-1}$  with approach B data set.

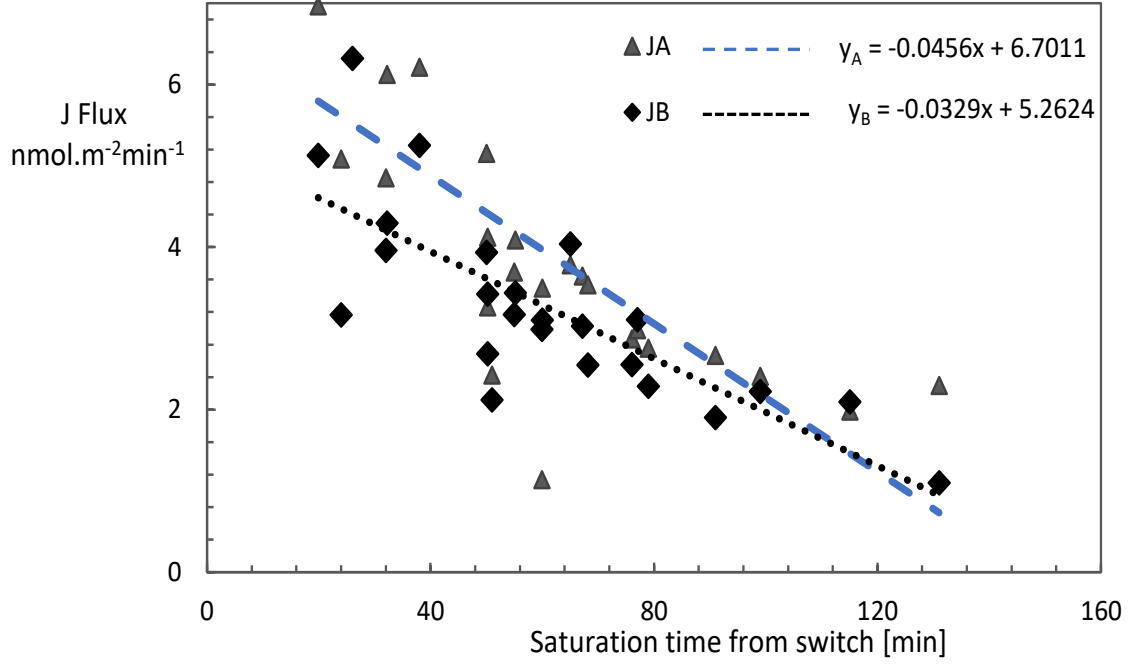


Figure 5.2: PFA, Sensitivity of irreversible reacted amount per unit area per unit time on saturation time.

The data with approach B was more reproducible and was consider the representative method in this work. All the data sets were corrected to a saturation of 60 min. The standard deviation of the data was reduced for PFA from 36% to 22% and for stainless steel from 40% to 34%, while for other materials, no significant changes were observed. It is because, for Sulfinert® and Copper, the values are very small with a higher standard deviation. The mean values and standard deviation of the data set before and after correction are reported in Table 5.2.

Table 5.2: Irreversible reacted flux ( $J$ ) for different materials raw data and corrected.

	$J$ $\text{nmol}\cdot\text{m}^{-2}\cdot\text{min}^{-1}$	$\sigma$ $\text{nmol}\cdot\text{m}^{-2}\cdot\text{min}^{-1}$	$\sigma\%$	$J_{1\text{hr saturation}}$ $\text{nmol}\cdot\text{m}^{-2}\cdot\text{min}^{-1}$	$\sigma\%$
PFA	3.24	1.16	36%	3.29	22%
Stainless Steel	3.31	1.31	40%	3.16	34%
Copper	1.48	0.25	17%	1.46	17%
Sulfinert®	0.17	0.05	33%	0.14	33%

The response signal of VOCs for different materials are shown in Figure 5.3. as expected, the Sulfinert® coated materials show lower interactions and a very small difference was observed between the signal of VOCs in the bypass and test pipe. The difference between the signal in bypass and test pipe was negligible for Copper; however, with method B (analysing the signal after a storage time), there was a significant loss observed that could be seen in Figure 5.3. A fluctuation of the signal was observed with electropolished stainless steel with more mass reacted over the surface.

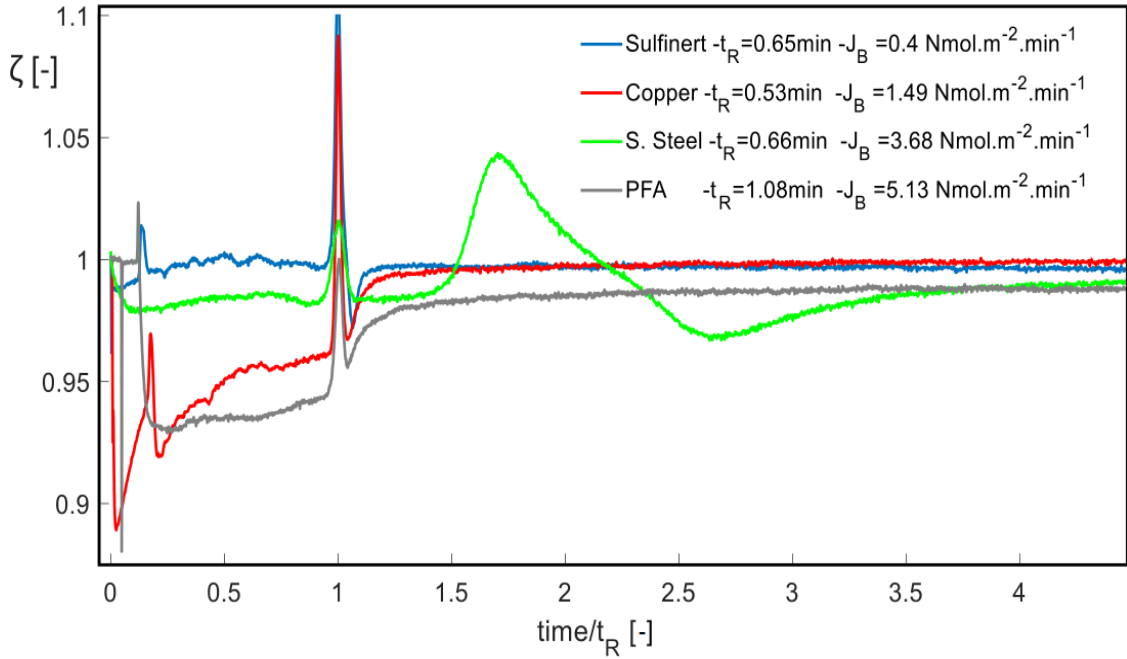


Figure 5.3: Signal of VOC in bypass and saturated test pipe during measurements for irreversible losses.

### 5.1.1 Sensitivity of reacted mass flux with temperature

Sensitivity of mass flux on temperature was performed with the available data. The temperature range was 9°C for PFA and 3°C for Stainless steel and Copper while 5°C for Sulfinert®. The sensitivity coefficient was calculated as linear slope over data corrected to 1hr saturation time as depicted in Figure 5.4. A sensitivity coefficient of 0.0298  $\text{nmol}\cdot\text{m}^{-2}\cdot\text{min}^{-1}\cdot\text{K}^{-1}$  for PFA and 0.478  $\text{nmol}\cdot\text{m}^{-2}\cdot\text{min}^{-1}\cdot\text{K}^{-1}$  for Stainless steel 0.168  $\text{nmol}\cdot\text{m}^{-2}\cdot\text{min}^{-1}\cdot\text{K}^{-1}$  on Copper and 0.0033  $\text{nmol}\cdot\text{m}^{-2}\cdot\text{min}^{-1}\cdot\text{K}^{-1}$  on Sulfinert®. due to limited range, no correction was made to the data for temperature.

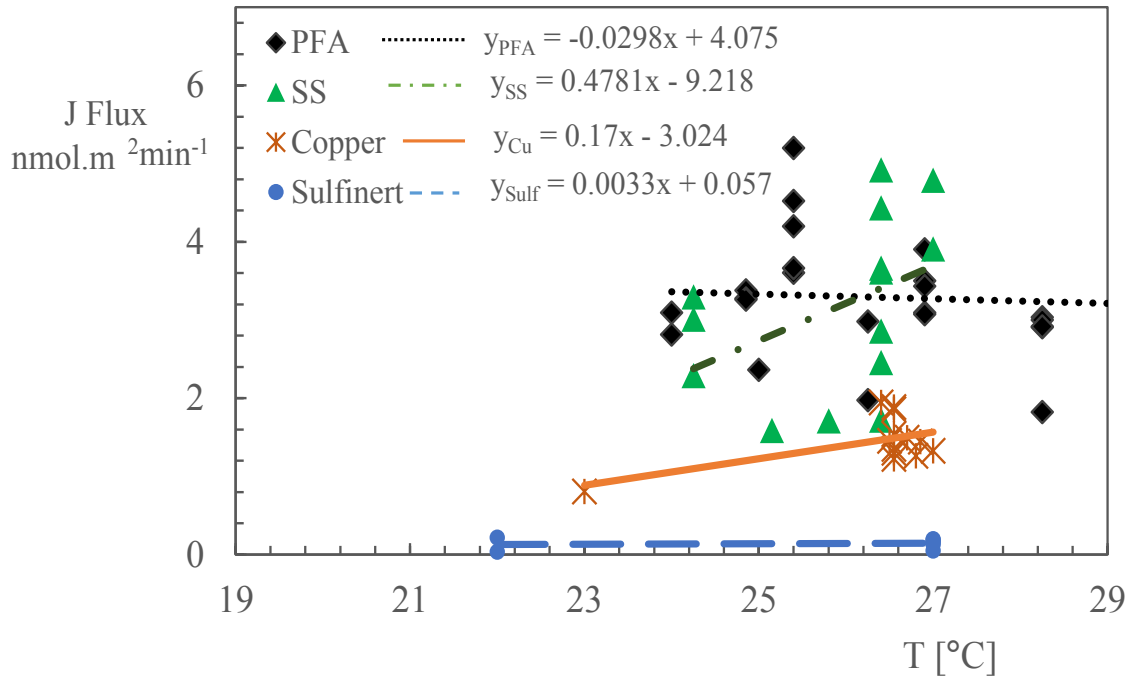


Figure 5.4: Sensitivity of irreversibly reacted mass flux on temperature for different materials.

### 5.1.2 Sensitivity of irreversibly reacted mass flux on pressure

Sensitivity of mass flux on pressure was performed with the available data. The pressure range was 7 KPa for PFA and Sulfinert® and 8 KPa for stainless steel while 4 KPa for Copper. The sensitivity coefficient was calculated as linear slope over data corrected to 1hr saturation time as depicted in Figure 5.5. A sensitivity coefficient of  $142 \text{ nmol}\cdot\text{m}^{-2}\cdot\text{min}^{-1}\cdot\text{MPa}^{-1}$  for PFA and  $043.4 \text{ nmol}\cdot\text{m}^{-2}\cdot\text{min}^{-1}\cdot\text{MPa}^{-1}$  for Stainless steel  $11.2 \text{ nmol}\cdot\text{m}^{-2}\cdot\text{min}^{-1}\cdot\text{MPa}^{-1}$  on Copper and  $2.9 \text{ nmol}\cdot\text{m}^{-2}\cdot\text{min}^{-1}\cdot\text{MPa}^{-1}$  on Sulfinert®. Due to the limited range and limited no of experiments, the pressure correction had a negligible effect on data.

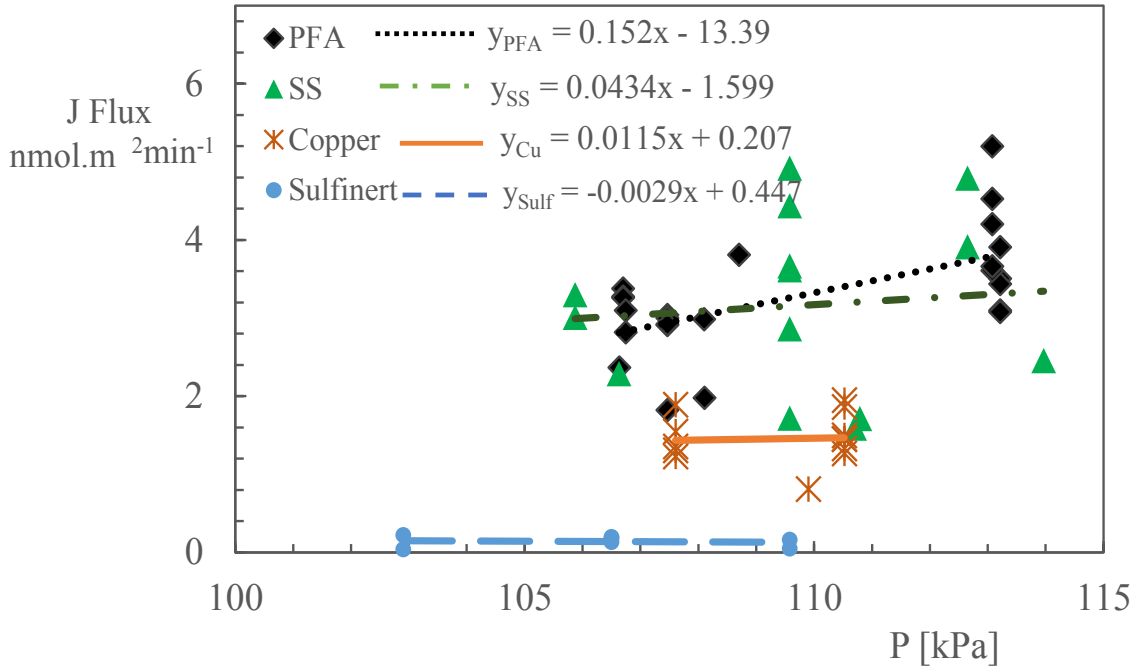


Figure 5.5: Sensitivity of irreversibly reacted mass flux on temperature for different materials.

## 5.2 Release flux due to memory effect

The memory effect of the pipes was estimated as the mass release from unit surface area per unit time ( $M$ ). The mass release due to memory effect from the walls of the pipe are calculated using two different approaches. Approach A based on the difference of the signal of VOC in bypass and pipe. Approach B as an average release over time. The released mass from unit area per unit time ( $M$ ) was measured at different cleaning times, and the effect is shown in Figure 5.6 over a repeated experiment for a PFA pipe. Experiments were performed at  $58 \text{ Sml}\cdot\text{min}^{-1}$ . The area under the curve was reduced with cleaning time that results in the reduction of calculated release mass. The rise of the signal was reduced to a minimum change of signal of air in test pipe and bypass. At lower cleaning, the equilibrium is not yet reached, and the mass reacted during the equilibrium is calculated as bias to memory release flux  $M$ .

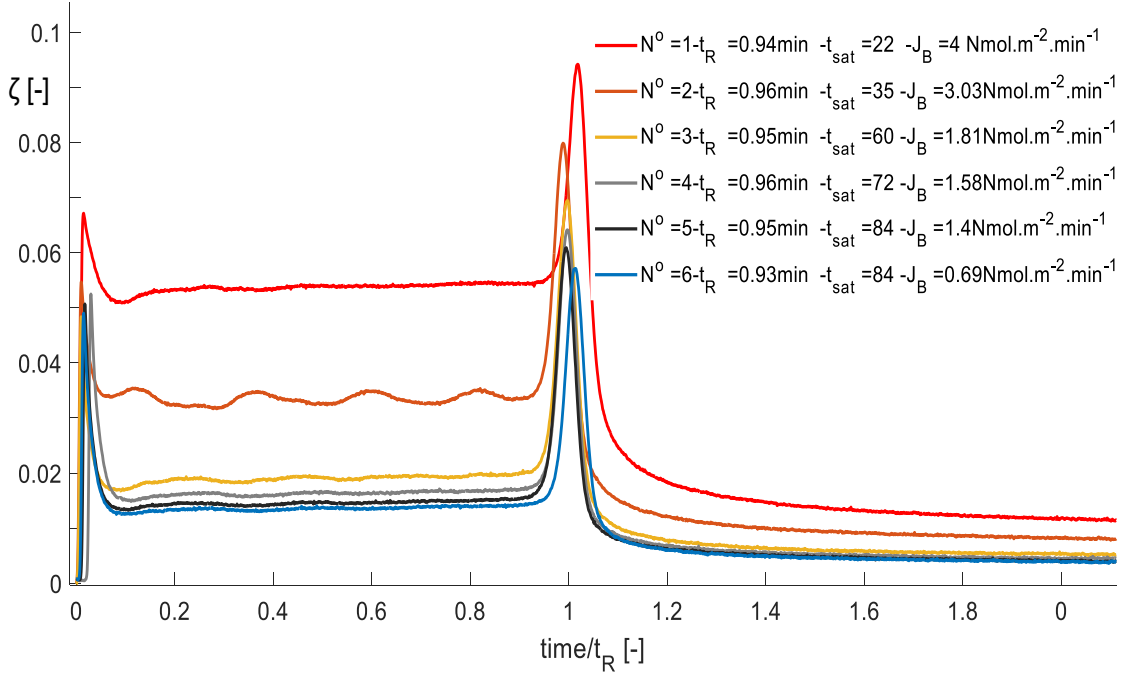


Figure 5.6: Signal of VOC in bypass and test pipe (PFA) at different cleaning time ( $t_{sat}$ ). Red colour shows less cleaning while black and blue shows more cleaning time.

The dependency of cleaning time was calculated as the slope of the linear line for both approach A and B that are depicted in Figure 5.7 for PFA. A similar approach was applied for other materials. The values of slope for PFA were  $0.0406 \text{ nmol}\cdot\text{m}^{-2}\cdot\text{min}^{-1}$  for approach A data set and  $0.0284 \text{ nmol}\cdot\text{m}^{-2}\cdot\text{min}^{-1}$  for approach B data set. For electropolished Stainless steel  $0.0586 \text{ nmol}\cdot\text{m}^{-2}\cdot\text{min}^{-1}$  for approach A data set and  $0.0458 \text{ nmol}\cdot\text{m}^{-2}\cdot\text{min}^{-1}$  for approach B data set. For Copper the slope with approach A dataset is  $0.0106 \text{ nmol}\cdot\text{m}^{-2}\cdot\text{min}^{-1}$  and  $0.0044 \text{ nmol}\cdot\text{m}^{-2}\cdot\text{min}^{-1}$  with approach B data set. For Sulfinert®, the slope with approach A dataset is  $0.0044 \text{ nmol}\cdot\text{m}^{-2}\cdot\text{min}^{-1}$  and  $0.0007 \text{ nmol}\cdot\text{m}^{-2}\cdot\text{min}^{-1}$  with approach B data set.

Similar to the irreversible reacted mass the approach B was consider the representative method in this work. The data were corrected to a saturation of 60 min for all the materials. The standard deviation of the data was reduced for PFA from 39% to 24% and for Stainless steel from 44% to 42% and from 22% to 17% for Copper, while for Sulfinert® no significant change was observed. The mean values and standard deviation of the data set before and after correction are reported in Table 5.3.

The response signal of air for different materials was following the opposite but the same trend as for VOCs (Figure 5.3) with upward curve. As expected, the Sulfinert® coated materials and Copper show lower release, and a very small

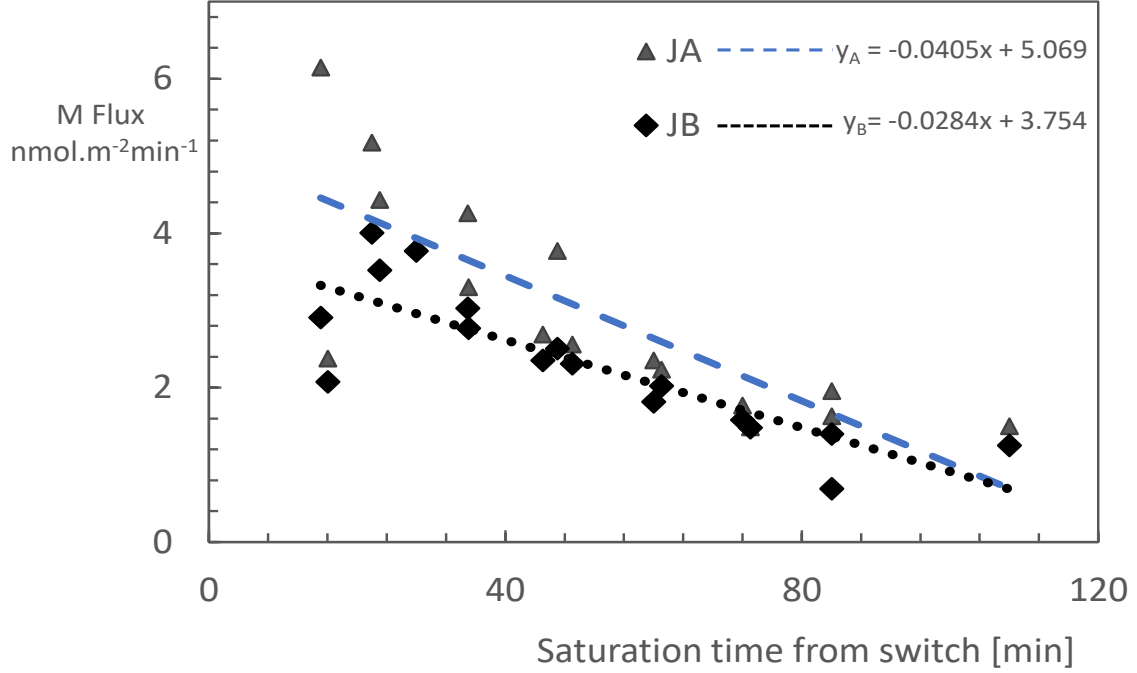


Figure 5.7: Sensitivity of release amount from unit area of PFA per unit time ( $M$ ) on saturation time.

Table 5.3: Release flux ( $M$ ) for different materials raw data and corrected.

	$M$ $\text{nmol} \cdot \text{m}^{-2} \cdot \text{min}^{-1}$	$\sigma$ $\text{nmol} \cdot \text{m}^{-2} \cdot \text{min}^{-1}$	$\sigma\%$	$M_{1\text{hr}} \text{ saturation}$ $\text{nmol} \cdot \text{m}^{-2} \cdot \text{min}^{-1}$	$\sigma\%$
PFA	2.32	0.90	39%	2.05	24%
Stainless Steel	3.44	1.53	44%	2.82	42%
Copper	0.66	0.14	22%	0.63	17%
Sulfinert®	0.17	0.05	27%	0.15	27%

difference was observed between the signal of VOCs in the bypass and test pipe. There was a negligible difference between the signal in the bypass and test pipe.

### 5.2.1 Sensitivity of released mass flux with temperature

Sensitivity of release mass flux on temperature was performed with the available data. The temperature range was  $9^\circ\text{C}$  for PFA and  $3^\circ\text{C}$  for Stainless steel and Copper while  $5^\circ\text{C}$  for Sulfinert®. The sensitivity coefficient was calculated as linear slope over data corrected to 1hr cleaning time as depicted in Figure 5.8. A sensitivity coefficient of  $0.108 \text{ nmol} \cdot \text{m}^{-2} \cdot \text{min}^{-1} \cdot \text{K}^{-1}$  for PFA and  $0.385 \text{ nmol} \cdot \text{m}^{-2} \cdot \text{min}^{-1} \cdot \text{K}^{-1}$  for Stainless steel  $0.03 \text{ nmol} \cdot \text{m}^{-2} \cdot \text{min}^{-1} \cdot \text{K}^{-1}$  on Copper and  $0.0175 \text{ nmol} \cdot \text{m}^{-2} \cdot \text{min}^{-1} \cdot \text{K}^{-1}$  on Sulfinert®. due to limited range, no correction

was made to the data for temperature.

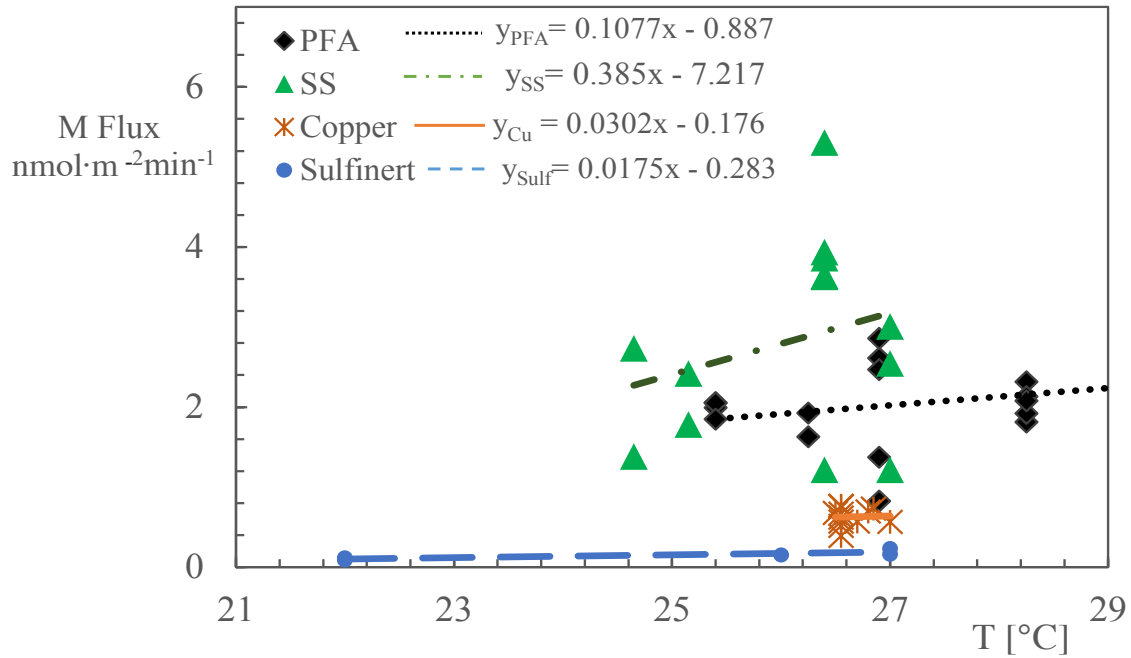


Figure 5.8: Sensitivity of release mass flux ( $M$ ) on temperature for different materials.

### 5.2.2 Sensitivity of released mass flux with Pressure

Sensitivity of mass flux on pressure was performed with the available data. The pressure range was 7 KPa for PFA and Sulfinert® and 8 KPa for stainless steel while 4 KPa for Copper. The sensitivity coefficient was calculated as linear slope over data corrected to 1hr cleaning time as depicted in Figure 5.9. A sensitivity coefficient of  $10 \text{ nmol}\cdot\text{m}^{-2}\cdot\text{min}^{-1}\cdot\text{MPa}^{-1}$  for PFA and  $121 \text{ nmol}\cdot\text{m}^{-2}\cdot\text{min}^{-1}\cdot\text{MPa}^{-1}$  for Stainless steel  $16.2 \text{ nmol}\cdot\text{m}^{-2}\cdot\text{min}^{-1}\cdot\text{MPa}^{-1}$  on Copper and  $25.5 \text{ nmol}\cdot\text{m}^{-2}\cdot\text{min}^{-1}\cdot\text{MPa}^{-1}$  on Sulfinert®. Due to the limited range and limited number of experiments, the pressure correction had a negligible effect on data.

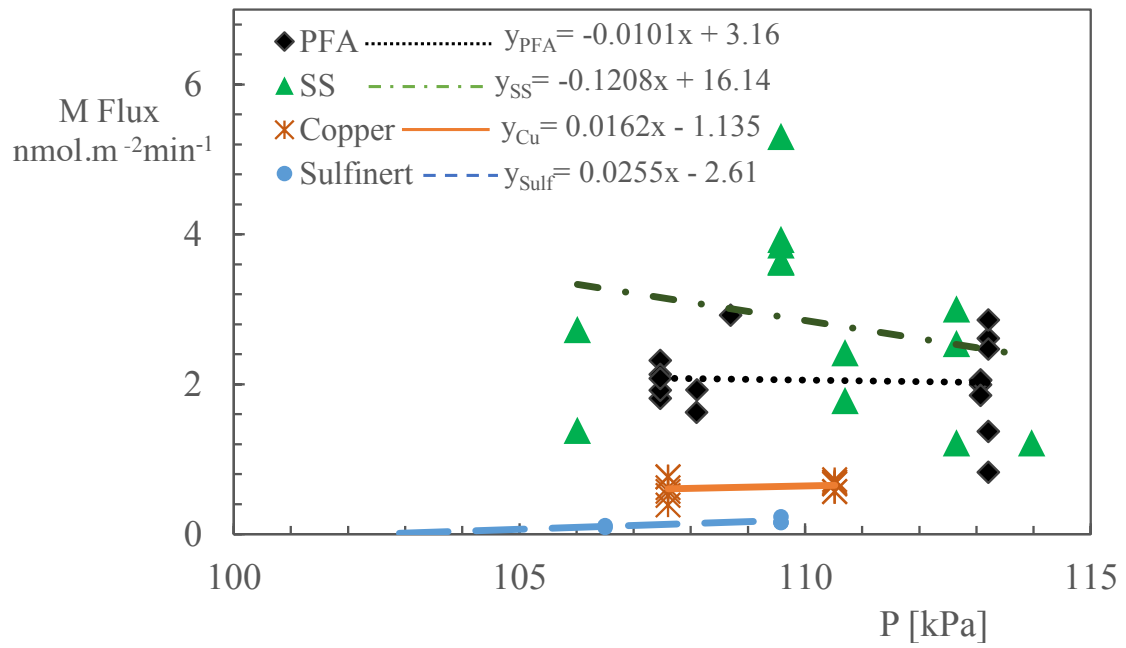


Figure 5.9: Sensitivity of released mass flux ( $M$ ) on pressure for different materials.



# Chapter 6

## Conclusion

The method for the quantification of different kind of interactions of VOCs with surfaces of commercially available pipes usually used for sampling of VOCs have been developed. The need for the accuracy of VOCs measurements at ppb to ppt level has always been stressed in many fields of life, from therapy monitoring to climate change monitoring and to indoor air quality. A key topic is the quantification of the amount of losses that can be considered as a bias for the measurement of the amount of VOC. The methods proposed here are the experimental quantification of interactions that reaches an equilibrium between a gas mixture and a pipe wall, irreversible losses, and release due to memory. Even if the actual quantification is at ppm level, due to the available VOC mixture source and the available detector (FID), the methods are applicable in principle to lower concentration levels depending on the availability of a mixture source and a detector. The ppm level assures a good reproducibility and has insights to lower levels if the interaction mechanisms remain the same as expected.

The 4-ways valves are really effective in switches giving a limited disturbance on pressure and signal and minimize the surface area in the bypass. The use of a capillary tube as a pressure drop device allows reducing the pressure difference in the pipe and bypass. Sonic nozzles allowed good stability to the flow rates working being independent on the discharge pressure. Still, the effect of temperature on the sonic nozzle changes the flow rate by changing the density of the flowing gas. The control of temperature and pressure was not critical and was really very broad. However, the estimation of average temperature and pressure inside the test pipe was effective for the calculation of the biases during the measurements. The Major source of uncertainty is the integral of the signal, and a stable signal with less fluctuation helps in reducing the uncertainty for adsorbed amount while for equilibrium constant, the pressure fluctuation during the experiment has a significant index of 100%. Working at high pressure reduces the signal fluctuation and also reduces the relative difference of pressure drop in test pipe and bypass.

The method for quantification of equilibrium constant  $K_e$  was applied to four

different materials of different characteristics at different physical condition. The reproducibility of the method for calculation of the adsorbed and desorbed amount per unit area and equilibrium constant were tested in more detail for Sulfinert®. A long pipe was tested as a whole and then cut into three different samples of the same length in order to investigate the reproducibility and measure the difference between different samples of the pipe. The difference between the amount adsorbed and desorbed was measurable for all the materials except Sulfinert®. due to its inert coating allows almost all the materials to reproduce during desorption. The reproducibility of the amount adsorbed and desorbed was higher for Sulfinert® 5% and 6%, respectively, and lower for Copper 19% and 9% due to reaction on the surface of the wall of Copper.

The dynamic of the phenomenon can be analyzed based on the rate of reaction at which equilibrium occurs. In polymeric materials, the irreversible losses due to permeation are significant and can be measured as mass per unit area per unit time ( $J$ ) is measured to quantify these losses.

The memory effect of the pipe plays a role during repeated use of pipe and is estimated as a mass release from unit area per unit time, i.e., release rate ( $M$ ). The methods for irreversible losses ( $J$ ) and release due to memory ( $M$ ) were applied in detail for PFA pipe and electropolished Stainless steel, and the effect of saturation time, temperature, pressure were analyzed in order to consider the effect as bias.

The methods were able to compare different materials and scenarios in order to investigate competition between substances. Good control of the temperature and pressure during the experiments will allow us to have a stable flow and signal. These methods were able to measure the interactions, and differentiate the response of different materials at ppm level. This work is aimed to fix a starting point of a quantitative method for the measurement of reversible interactions, irreversible interactions, and memory effect before applying the method to the low amount of substance fraction. The proposed quantitative method for measurement of interactions in sampling lines to offer reliable data to calculate the biases affecting VOC measurements.

In future work, these methods can be extended to lower amount of substance (ppb) with a PTR-MS as a detector, with acetone, methanol, and ethanol as VOCs and at different levels of moisture, in order to calculate the biases during measurement of VOCs. However, the measurement at low level requires more attentions to the biases during the measurements. The method can be used to compare the response of different materials that are usually used for sampling at trace level and can be applied to different applications.

# Bibliography

- [1] “A WMO/GAW Expert Workshop on Global Long-term Measurements of Volatile Organic Compounds”. In: (2007).
- [2] John L Adgate et al. “Outdoor, indoor, and personal exposure to VOCs in children”. In: *Environmental health perspectives* 112.14 (2004), pp. 1386–1392.
- [3] Yekbun Adiguzel and Haluk Kulah. “Breath sensors for lung cancer diagnosis”. In: *Biosensors and Bioelectronics* 65 (2015), pp. 121–138.
- [4] Laurent Akesso et al. “Deposition parameters to improve the fouling-release properties of thin siloxane coatings prepared by PACVD”. In: *Applied surface science* 255.13-14 (2009), pp. 6508–6514.
- [5] Stacey E Anderson et al. “Evaluation of the contact and respiratory sensitization potential of volatile organic compounds generated by simulated indoor air chemistry”. In: *Toxicological Sciences* 97.2 (2007), pp. 355–363.
- [6] Karine Arrhenius, Andreas Fischer, and Oliver Bükler. “Methods for sampling biogas and biomethane on adsorbent tubes after collection in gas bags”. In: *Applied Sciences* 9.6 (2019), p. 1171.
- [7] Kenneth B Balmer. “Auger surface line scan to evaluate element segregation in and chelant passivation of a 316L weld”. In: *Pharmaceutical Engineering* 15.3 (1995).
- [8] Patrick H Banes. “Passivation understanding and performing procedures on austenitic stainless steel systems”. In: *Pharm. Eng.* 10 (1990), pp. 41–46.
- [9] Gary Barone. *Silicon-based decorative coatings*. US Patent App. 11/981,772. Apr. 2009.
- [10] Gilvan Barroso et al. “Polymeric and ceramic silicon-based coatings—a review”. In: *Journal of materials chemistry A* 7.5 (2019), pp. 1936–1963.
- [11] Robert Benesch, Malik Haouchine, and Tracey Jacksier. “The stability of 100 ppb hydrogen sulfide standards”. In: *Analytical chemistry* 76.24 (2004), pp. 7396–7399.

- [12] Jonathan A Bernstein et al. “The health effects of nonindustrial indoor air pollution”. In: *Journal of Allergy and Clinical Immunology* 121.3 (2008), pp. 585–591.
- [13] Iec BIPM et al. *Evaluation of measurement data—guide to the expression of uncertainty in measurement. Joint Committee for Guides in Metrology (JCGM 100: 2008, GUM 1995 with minor corrections)*. 2008.
- [14] Paul J Brewer et al. “Breakthrough in Negating the Impact of Adsorption in Gas Reference Materials”. In: *Analytical chemistry* 91.8 (2019), pp. 5310–5315.
- [15] Andrew S Brown et al. “Final report on CCQM-K93: Preparative comparison of ethanol in nitrogen”. In: *Metrologia* 50.1A (2013), p. 08025.
- [16] AF Budzynski. “Electrochemical honing-studies on shape precision of holes being processed”. In: *Proceedings of the 8th International Symposium for Electromachining (ISEM-8), Moscow, Russia*. 1986.
- [17] Fanis Buljubasic and Gerhard Buchbauer. “scent of human diseases: a review on specific volatile organic compounds as diagnostic biomarkers”. In: *Flavour and Fragrance Journal* (2015).
- [18] Balaras C.a. et al. “Risk Assessment in Relation to Indoor Air Quality. Report No. 22.” In: 2000.
- [19] Christopher D Cappa et al. “Simulating secondary organic aerosol in a regional air quality model using the statistical oxidation model—Part 2: Assessing the influence of vapor wall losses”. In: *Atmospheric Chemistry and Physics* 16.5 (2016), pp. 3041–3059.
- [20] Shaojie Chen, Longzhe Jin, and Xuexi Chen. “The effect and prediction of temperature on adsorption capability of coal/CH<sub>4</sub>”. In: *Procedia Engineering* 26 (2011), pp. 126–131.
- [21] Zhilin Chen et al. “An open-walled ionization chamber appropriate to tritium monitoring for glovebox”. In: *Review of Scientific Instruments* 81.7 (2010), p. 073302.
- [22] James G Crump and John H Seinfeld. “Turbulent deposition and gravitational sedimentation of an aerosol in a vessel of arbitrary shape”. In: *Journal of Aerosol Science* 12.5 (1981), pp. 405–415.
- [23] M Datta and D Landolt. “Fundamental aspects and applications of electrochemical microfabrication”. In: *Electrochimica acta* 45.15-16 (2000), pp. 2535–2558.

- [24] Gianluigi De Gennaro et al. “Indoor and outdoor monitoring of volatile organic compounds in school buildings: Indicators based on health risk assessment to single out critical issues”. In: *International Journal of Environmental Research and Public Health* 10.12 (2013), pp. 6273–6291.
- [25] Alessia Demichelis et al. “Molar fraction stability in dynamic preparation of reference trace gas mixtures”. In: *IET Science, Measurement & Technology* 10.5 (2016), pp. 414–419.
- [26] Benjamin L Deming et al. “Measurements of delays of gas-phase compounds in a wide variety of tubing materials due to gas–wall interactions”. In: *Atmospheric Measurement Techniques* 12.6 (2019), pp. 3453–3461.
- [27] MT Duffy and Werner Kern. “Chemical vapor deposition of aluminum oxide films from organo-aluminum compounds”. In: *RCA Review* 31.4 (1970), pp. 754–770.
- [28] Richard R Eley. “Rheology in coatings, principles and methods”. In: *Encyclopedia of Analytical Chemistry: Applications, Theory and Instrumentation* (2006).
- [29] I Elmi et al. “Development of ultra-low-power consumption MOX sensors with ppb-level VOC detection capabilities for emerging applications”. In: *Sensors and Actuators B: Chemical* 135.1 (2008), pp. 342–351.
- [30] Jennifer Englert et al. “Preparation and analysis of zero gases for the measurement of trace VOCs in air monitoring”. In: *Atmospheric Measurement Techniques* 11.6 (2018), pp. 3197–3203.
- [31] Cyprian Fijało et al. “Devices for the production of reference gas mixtures”. In: *Critical reviews in analytical chemistry* 46.5 (2016), pp. 361–373.
- [32] “Final Publishable JRP Summary for ENV56 KEY-VOCs Metrology for VOC indicators for air pollution and climate change”. In: 2014–2017.
- [33] H Scott Fogler. *Essentials of Chemical Reaction Engineering: Essenti Chemica Reactio Engi*. Pearson Education, 2010.
- [34] Keng Yuen Foo and Bassim H Hameed. “Insights into the modeling of adsorption isotherm systems”. In: *Chemical engineering journal* 156.1 (2010), pp. 2–10.
- [35] Ronald C Geib. “Calibration Standard Gases Are Key to Reliable Measurements”. In: *Spec. Gas Rep* (2005).
- [36] Kai-Uwe Goss. “The air/surface adsorption equilibrium of organic compounds under ambient conditions”. In: *Critical Reviews in Environmental Science and Technology* 34.4 (2004), pp. 339–389.

- [37] Kai-Uwe Goss. “The air/surface adsorption equilibrium of organic compounds under ambient conditions”. In: *Critical Reviews in Environmental Science and Technology* 34.4 (2004), pp. 339–389.
- [38] Franklin R Guenther et al. “International Comparison CCQM-K41: Hydrogen sulfide in nitrogen”. In: *Metrologia* 44.1A (2007), p. 08004.
- [39] M Hakim et al. “Diagnosis of head-and-neck cancer from exhaled breath”. In: *British journal of cancer* 104.10 (2011), pp. 1649–1655.
- [40] Phil Harris and Mike Pelligrini. “Mass Transport in Sample Transport lines Adsorption Desorption Effects and their Influence on Process Analytical Measurements”. In: *Proceedings of the 56th ISA Analytical Division Symposium, Paper S*. Vol. 11. 2011.
- [41] Takeshi Hattori. “Chemical contamination control in ULSI wafer processing”. In: *AIP Conference Proceedings*. Vol. 550. 1. American Institute of Physics. 2001, pp. 275–284.
- [42] Takeshi Hattori et al. *Ultraclean surface processing of silicon wafers: secrets of VLSI manufacturing*. Springer Science & Business Media, 2013.
- [43] H Hocheng and PS Pa. “The application of a turning tool as the electrode in electropolishing”. In: *Journal of Materials Processing Technology* 120.1-3 (2002), pp. 6–12.
- [44] Michael Horsfall Jnr and Ayebaemi I Spiff. “Effects of temperature on the sorption of Pb<sup>2+</sup> and Cd<sup>2+</sup> from aqueous solution by *Caladium bicolor* (Wild Cocoyam) biomass”. In: *Electronic Journal of Biotechnology* 8.2 (2005), pp. 43–50.
- [45] Yuanlong Huang et al. “Unified Theory of Vapor–Wall Mass Transport in Teflon-Walled Environmental Chambers”. In: *Environmental science & technology* 52.4 (2018), pp. 2134–2142.
- [46] L Gregory Huey et al. “CIMS measurements of HNO<sub>3</sub> and SO<sub>2</sub> at the South Pole during ISCAT 2000”. In: *Atmospheric Environment* 38.32 (2004), pp. 5411–5421.
- [47] James F Hunter et al. “Comprehensive characterization of atmospheric organic carbon at a forested site”. In: *Nature Geoscience* 10.10 (2017), pp. 748–753.
- [48] JP Joly et al. “Temperature-programmed desorption (TPD) of water from iron, chromium, nickel and 304L stainless steel”. In: *Vacuum* 59.4 (2000), pp. 854–867.
- [49] Kenji Kato et al. “Final report on key comparison APMP. QM-K4. 1: Ethanol in nitrogen”. In: *Metrologia* 45.1A (2007), p. 08007.

- [50] “Key reactive molecules as exhaled breath biomarkers for disease diagnostics and monitoring.” In: 2015.
- [51] Yong-Doo Kim et al. “Final report on international key comparison APMP. QM-K41: 10  $\mu\text{mol/mol}$  hydrogen sulfide in nitrogen”. In: *Metrologia* 51.1A (2014), p. 08012.
- [52] Jordan E Krechmer et al. “Quantification of gas-wall partitioning in Teflon environmental chambers using rapid bursts of low-volatility oxidized species generated in situ”. In: *Environmental science & technology* 50.11 (2016), pp. 5757–5765.
- [53] Pawan Kumar et al. “Coordination polymers: opportunities and challenges for monitoring volatile organic compounds”. In: *Progress in Polymer Science* 45 (2015), pp. 102–118.
- [54] Becky SC Kwan. “Reading in preparation for writing a PhD thesis: Case studies of experiences”. In: *Journal of English for Academic Purposes* 8.3 (2009), pp. 180–191.
- [55] Irving Langmuir. “The adsorption of gases on plane surfaces of glass, mica and platinum.” In: *Journal of the American Chemical society* 40.9 (1918), pp. 1361–1403.
- [56] Sangil Lee et al. “Determination of physical adsorption loss of primary standard gas mixtures in cylinders using cylinder-to-cylinder division”. In: *Metrologia* 54.6 (2017), p. L26.
- [57] Sangil Lee et al. “International key comparison CCQM-K94: 10  $\mu\text{mol/mol}$  dimethyl sulfide in nitrogen”. In: *Metrologia* 53.1A (2016), p. 08002.
- [58] Xiaoxi Liu et al. “Effects of gas-wall interactions on measurements of semivolatile compounds and small polar molecules”. In: *Atmospheric Measurement Techniques* 12.6 (2019), pp. 3137–3149.
- [59] John J Mahle et al. *Ultra Low Concentration Adsorption Equilibria*. Tech. rep. SOLDIER and BIOLOGICAL CHEMICAL COMMAND ABERDEEN PROVING GROUND MD, 2006.
- [60] A Malek and S Farooq. “Comparison of isotherm models for hydrocarbon adsorption on activated carbon”. In: *AIChE Journal* 42.11 (1996), pp. 3191–3201.
- [61] Aiko Matsunaga and Paul J Ziemann. “Gas-wall partitioning of organic compounds in a Teflon film chamber and potential effects on reaction product and aerosol yield measurements”. In: *Aerosol Science and Technology* 44.10 (2010), pp. 881–892.
- [62] Warren Lee McCabe, Julian Cleveland Smith, and Peter Harriott. *Unit operations of chemical engineering*. Vol. 5. McGraw-hill New York, 1993.

- [63] P. McMurry and D. Grosjean. “Gas and aerosol wall losses in Teflon film smog chambers.” In: *Environmental science technology* 19 12 (1985), pp. 1176–82.
- [64] HelvéCio C Menezes, Leiliane CA Amorim, and Zenilda L Cardeal. “Sampling and analytical methods for determining VOC in air by biomonitoring human exposure”. In: *Critical reviews in environmental science and technology* 43.1 (2013), pp. 1–39.
- [65] Magdalena Michulec et al. “Analytical techniques used in monitoring of atmospheric air pollutants”. In: *Critical reviews in analytical chemistry* 35.2 (2005), pp. 117–133.
- [66] Burnaby Munson. “Chemical ionization mass spectrometry: theory and applications”. In: *Encyclopedia of Analytical Chemistry: Applications, Theory and Instrumentation* (2006).
- [67] JA Neuman et al. “Study of inlet materials for sampling atmospheric nitric acid”. In: *Environmental Science & Technology* 33.7 (1999), pp. 1133–1136.
- [68] JB Nowak et al. “A chemical ionization mass spectrometry technique for airborne measurements of ammonia”. In: *Journal of Geophysical Research: Atmospheres* 112.D10 (2007).
- [69] Demetrios Pagonis et al. “Effects of gas–wall partitioning in Teflon tubing and instrumentation on time-resolved measurements of gas-phase organic compounds”. In: *Atmospheric measurement techniques* 10.12 (2017), pp. 4687–4696.
- [70] A Parthasarathi and HL Fraser. “The annealing of vacancy defects in  $\beta$ -NiAl I. Vacancy loop growth in as-grown single crystals annealed in ultra-high vacuum”. In: *Philosophical Magazine A* 50.1 (1984), pp. 89–100.
- [71] S Penkett et al. “WMO/GAW Expert workshop on global long-term measurements of nitrogen oxides and recommendations for GAW nitrogen oxides network.” In: (2011).
- [72] Robert E Phillips. “What is electrochemical grinding and how does it work”. In: *Carbide and Tool Journal* 18 (1986), pp. 12–14.
- [73] JR Pierce et al. “Constraining particle evolution from wall losses, coagulation, and condensation-evaporation in smog-chamber experiments: optimal estimation based on size distribution measurements”. In: *Aerosol Science and Technology* 42.12 (2008), pp. 1001–1015.
- [74] B Rappenglück et al. “The first VOC intercomparison exercise within the Global Atmosphere Watch (GAW)”. In: *Atmospheric Environment* 40.39 (2006), pp. 7508–7527.



- [75] Stefan Reimann et al. “Deliverable 3.17. Updated Measurement Guideline for NO<sub>x</sub> and VOCs”. In: ().
- [76] George C Rhoderick et al. “Stability of gaseous volatile organic compounds contained in gas cylinders with different internal wall treatments”. In: *Elementa: Science of the Anthropocene* 7 (2019).
- [77] Ralph M Riggin. *Compendium of methods for the determination of toxic organic compounds in ambient air*. Tech. rep. Battelle Columbus Labs., OH (USA), 1984.
- [78] Michael Roberts, Michael Reiss, and Grace Monger. *Advanced biology*. Nelson Thornes, 2000.
- [79] JtA Roels. *Energetics and kinetics in biotechnology*. Elsevier Biomedical Press, 1983.
- [80] JtA Roels. *Energetics and kinetics in biotechnology*. Elsevier Biomedical Press, 1983.
- [81] Daryl Roll et al. “Current methodologies and chemistries utilized in effective passivation procedures”. In: *Proceedings of Interphex 96* (1996), pp. 134–141.
- [82] Sabrina Rovelli et al. “VOCs measurements in residential buildings: quantification via thermal desorption and assessment of indoor concentrations in a case-study”. In: *Atmosphere* 10.2 (2019), p. 57.
- [83] Soledad Rubio and Dolores Perez-Bendito. “Recent advances in environmental analysis”. In: *Analytical chemistry* 81.12 (2009), pp. 4601–4622.
- [84] Yannick Saalberg and Marcus Wolff. “VOC breath biomarkers in lung cancer”. In: *Clinica Chimica Acta* 459 (2016), pp. 5–9.
- [85] Koichiro Saga and Takeshi Hattori. “Influence of Surface Organic Contamination on the Incubation Time in Low-Pressure Chemical Vapor Deposition”. In: *Journal of the Electrochemical Society* 144.9 (1997), p. L253.
- [86] G Sassi, A Demichelis, and Maria Paola Sassi. “Uncertainty analysis of the diffusion rate in the dynamic generation of volatile organic compound mixtures”. In: *Measurement Science and Technology* 22.10 (2011), p. 105104.
- [87] G Sassi, A Demichelis, and MP Sassi. “Air flow rate thermal control system at low pressure drop”. In: *Flow Measurement and Instrumentation* 35 (2014), pp. 44–47.
- [88] Guido Sassi, Bilal Alam Khan, and Maricarmen Lecuna. “Reproducibility of the Quantification of Reversible Wall Interactions in VOC Sampling Lines”. In: *Atmosphere* 12.2 (2021), p. 280.
- [89] Guido Sassi et al. “Preparation of standard VOC mixtures for climate monitoring”. In: *International Journal of Environmental Analytical Chemistry* 95.13 (2015), pp. 1195–1207.

- [90] Sandford Sillman. “Overview: Tropospheric ozone, smog and ozone-NO<sub>x</sub>-VOC sensitivity”. In: *Treatise on Geochemistry* (2003).
- [91] Lurdes IB Silva, Teresa AP Rocha-Santos, and AC Duarte. “Comparison of a gas chromatography-optical fibre (GC-OF) detector with a gas chromatography-flame ionization detector (GC-FID) for determination of alcoholic compounds in industrial atmospheres”. In: *Talanta* 76.2 (2008), pp. 395–399.
- [92] Lurdes IB Silva et al. “Carbon nanotube field-effect transistor detector associated to gas chromatography for speciation of benzene, toluene, ethylbenzene, (o-, m- and p-) xylene”. In: *Journal of Chromatography A* 1216.37 (2009), pp. 6517–6521.
- [93] Darlene L Slusher et al. “A thermal dissociation–chemical ionization mass spectrometry (TD-CIMS) technique for the simultaneous measurement of peroxyacyl nitrates and dinitrogen pentoxide”. In: *Journal of Geophysical Research: Atmospheres* 109.D19 (2004).
- [94] Anjali Srivastava. “Issues in VOC monitoring and reporting”. In: *Linnaeus Eco-Tech* (2007), pp. 525–532.
- [95] Anjali Srivastava and Dipanjali Majumdar. “Monitoring and reporting VOCs in ambient air”. In: *Air quality monitoring, assessment and management* 1 (2011).
- [96] “Standard Classification of Insulating Coatings for Electrical Steels by Composition, Relative Insulating Ability and Application”. In: *ASTM Standard* (2008–18).
- [97] Jan E Szulejko, Yong-Hyun Kim, and Ki-Hyun Kim. “Method to predict gas chromatographic response factors for the trace-level analysis of volatile organic compounds based on the effective carbon number concept”. In: *Journal of separation science* 36.20 (2013), pp. 3356–3365.
- [98] Chiharu Takahashi et al. “Final report on key comparison APMP. QM-K4 of ethanol in air”. In: *Metrologia* 40.1A (2003), p. 08008.
- [99] *University of Torino, Meteorological station of the Department of Physics*. <http://www.meteo.dfg.unito.it/tutti>. Accessed: 2018-2021.
- [100] R Vecchi et al. “Organic and inorganic sampling artefacts assessment”. In: *Atmospheric Environment* 43.10 (2009), pp. 1713–1720.
- [101] Adriaan MH van der Veen et al. “International comparison CCQM-K46: Ammonia in nitrogen”. In: *Metrologia* 47.1A (2010), p. 08023.
- [102] Sarah Riddle Vogt and Cristian Landoni. “Approaches to airborne molecular contamination assessment”. In: *Metrology, Inspection, and Process Control for Microlithography XXV*. Vol. 7971. International Society for Optics and Photonics. 2011, p. 79712I.

- [103] MG Walls et al. “In situ observation of the oxidation and reduction processes on Fe-Cr alloys”. In: *Journal of Vacuum Science & Technology A: Vacuum, Surfaces, and Films* 14.3 (1996), pp. 1362–1367.
- [104] DKW Wang and CC Austin. “Determination of complex mixtures of volatile organic compounds in ambient air: an overview”. In: *Analytical and bioanalytical chemistry* 386.4 (2006), pp. 1089–1098.
- [105] GLOBAL ATMOSPHERE WATCH. “WMO Global Atmosphere Watch (GAW) Strategic Plan: 2008–2015”. In: (2011).
- [106] Olaf Wilke et al. “Investigations for the improvement of the measurement of volatile organic compounds from floor coverings within the health-related evaluation of construction products”. In: *Final Report for BAM: Federal Institute for Materials Research and Testing, Berlin, Germany* (2009).
- [107] G Yang et al. “Electropolishing of surfaces: theory and applications”. In: *Surface Engineering* 33.2 (2017), pp. 149–166.
- [108] Penglin Ye et al. “Vapor wall loss of semi-volatile organic compounds in a Teflon chamber”. In: *Aerosol Science and Technology* 50.8 (2016), pp. 822–834.
- [109] Geoffrey K Yeh and Paul J Ziemann. “Gas-wall partitioning of oxygenated organic compounds: measurements, structure–activity relationships, and correlation with gas chromatographic retention factor”. In: *Aerosol Science and Technology* 49.9 (2015), pp. 727–738.
- [110] Stefano Zampolli et al. “A supramolecular approach to sub-ppb aromatic VOC detection in air”. In: *Chemical communications* 27 (2007), pp. 2790–2792.
- [111] Jinsong Zhang et al. “A critical review on studies of volatile organic compound (VOC) sorption by building materials (RP-1097)”. In: *TRANSACTIONS-AMERICAN SOCIETY OF HEATING REFRIGERATING AND AIR CONDITIONING ENGINEERS* 108.1 (2001), pp. 162–174.
- [112] Jinsong Zhang et al. “A critical review on studies of volatile organic compound (VOC) sorption by building materials (RP-1097)”. In: *TRANSACTIONS-AMERICAN SOCIETY OF HEATING REFRIGERATING AND AIR CONDITIONING ENGINEERS* 108.1 (2001), pp. 162–174.
- [113] X Zhang et al. “Vapor wall deposition in Teflon chambers.” In: *Atmospheric Chemistry & Physics Discussions* 14.19 (2014).
- [114] Yaping Zhou and Li Zhou. “Fundamentals of high pressure adsorption”. In: *Langmuir* 25.23 (2009), pp. 13461–13466.

This Ph.D. thesis has been typeset by means of the  $\text{\TeX}$ -system facilities. The typesetting engine was  $\text{\pdfL\TeX}$ . The document class was `toptesi`, by Claudio Beccari, with option `tipotesi=scudo`. This class is available in every up-to-date and complete  $\text{\TeX}$ -system installation.